Monitoring Semivolatile Organic Compounds at 200m above ground in rural Netherlands using a Denuder Sampler combined with a Proton-Transfer-Reaction Mass Spectrometer

Author:Jessica Strickland
Supervisor: Dr. Rupert Holzinger

July 7, 2017

Abstract

Semivolatile Organic Compounds (SVOCs) are anthropogenically and naturally produced atmospheric compounds which can exist in both the gas and condensed phases. These compounds readily condense on surfaces and are therefore important in the context of organic aerosol formation which ultimately impacts radiative forcing and air quality. Unfortunately, the duality of these particles and their trace amounts make them difficult to investigate, but a new technique has been developed to collect and analyze SVOCs. In this project a Denuder Sampler (DS) is combined with a Proton Transfer Reaction Time of Flight Mass Spectrometer (PTR-ToF-MS) to facilitate deeper investigation of gas phase SVOCs.This setup provides the means to probe the atmosphere with great precision and it is possible to investigate the relatively unexplored realm of SVOCs. The performance of this setup was tested in a controlled lab setting as well as stationed in the rural Netherlands for field measurements. The setup was stationed at $200m$ atop the Cabauw Experimental Site for Atmospheric Research (CESAR) from September, 2016 – January, 2017. The full mass spectra revealed over 354 different compounds with charge-to-mass ratios within the range $m/z15 - 500$ Da. An analysis code was created in Python to convert the raw data to reflect what was physically in the atmosphere and to analyze the results. This paper includes an overall review of the performance of the new technique and the types of compounds found in rural Netherlands throughout the course of the field measurements.

Acknowledgments

I would like to start by thanking my supervisor Rupert Holzinger and rest of the PTR-MS subgroup for their help and always being available and eager to discuss my project over coffee. I also appreciate the hands-on guidance and assistance I received from Henk Snellen and Carina van der Veen. Additionally, I would like to acknowledge the help of Fred Bosveld, Henk Baltink, and Bas Henzig who aided my search for supplementary data with supplementary data. Finally I would like to thank my peers, friends, and especially my partner Truls for being my rock through this process.

Contents

1 Introduction

1.1 Atmospheric Semivolatile Organic Compounds (SVOCs)

With each breath, we inhale and exhale a relatively unknown variety of atmospheric compounds that influence air quality and atmospheric properties. For example, as shown in Figure 1, aerosols are the only radiative forcing agent that is expected to have a net cooling. However, the contribution of aerosols to climate change is the most uncertain forcing [1]. Organic compounds enter the atmosphere through natural and anthropogenic processes, but most emissions occur in the gaseous phase and are transformed into the condensed phase via atmospheric chemistry reactions. Many emitted compounds, such as Semi-volatile Organic Compounds (SVOCs), commonly exist in both the gas and condensed phase, which makes them interesting in the context of organic aerosol formation.

The partitioning of a compound between the gas and liquid phase depends on the liquid phase vapor pressure[1]. For example, Volatile Organic Compounds (VOCs, vapor pressure > 1Pa) are often found in the gas phase and are now known as essential components of tropospheric chemistry [2]. As VOCs participate in oxidizing reactions, the vapor pressure decreases as the intermolecular forces become stronger and these compounds can transform into organic aerosols or less volatile SVOCs. SVOCs have a significant influence in the reactive chemistry of the atmosphere, but they are also present and used in many products such as cosmetics, textiles, and varnishes and can enter the atmosphere via these sources. The global budget for secondary organic aerosol requires that up to 70% of the mass of emitted VOCs must be converted to the particle phase [3].

These SVOCs are typically heavier compounds than VOCs and have vapor pressures that enable them to exist in both the gas and condensed phase at room temperature ($10^{-9} - 10^{1}$ Pa at $25°C$, boiling points typically $< 300°C$) [4]. As temperature decreases or altitude increases, the vapor pressure decreases and SVOCs may condense on available nuclei. Due to the fact that SVOCs readily condense, they are interesting in the context of organic aerosol formation. Moreover, according to Hallquist et al. (2009), volatile precursors comprise approximately 70% of secondary organic aerosol mass with broad uncertainty [3]. Therefore, it is crucial to understand the life cycle of SVOCs. This research project is devised to shed light on the presence and properties of these relatively unexplored compounds.

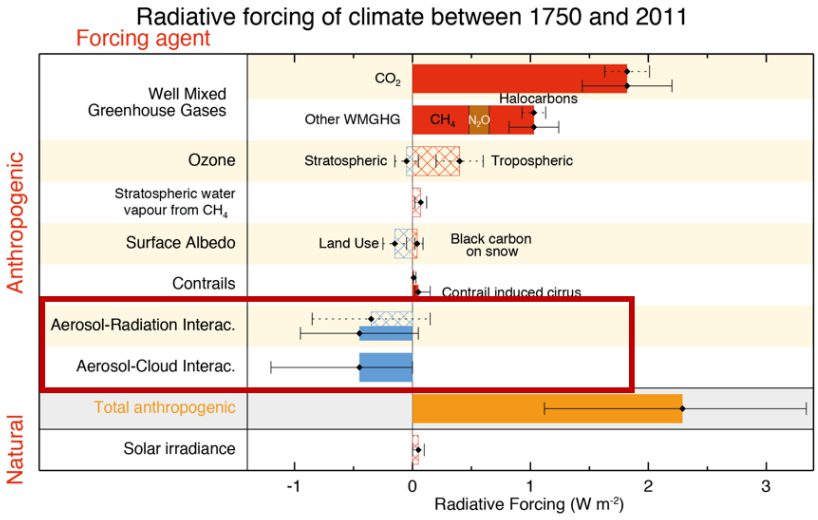

Figure 1: Bar chart from IPCC Fifth Assessment Report for Radiative Forcing (RF, hatched) and Effective Radiative Forcing (ERF, solid) for the period 1750–2011. Uncertainties (5 to 95% confidence range) are given for RF (dotted lines) and ERF (solid lines) [1].

[1] Vapor pressure is the pressure that a compound exerts in its gas phase compared to its condensed phase at equilibrium in a closed system at a certain temperature. A compound with a high vapor pressure is relatively more volatile.

1.2 Measuring SVOCs

Research of SVOCs is relatively lacking because they are difficult to detect and there are no recent, comprehensive atmospheric composition studies. Limited estimates suggest that $10^4 - 10^5$ different atmospheric organic species have been measured, which may only account for a fraction of the actual number, highlighting the importance of further investigation [2]. SVOCs are difficult to monitor because of their trace quantities and their readiness to condense. The Denuder Sampler (DS) is a new tool that has been designed to overcome the major challenges of low sensitivity and 'stickiness' of SVOCs. The DS is comprised of a series of denuders which are materials that can collect gas-phase particles. The DS design is described in detail in section 2.1. Two sections of the DS are constructed to collect SVOCs and the final section will collect VOCs. The fact that the DS can collect compounds with such a range in volatility is a great asset. The compounds are pre-concentrated in the DS before transferring the sample to a detector.

The detector used in this project is a Proton Transfer Reaction Time of Flight Mass Spectrometer (PTR-ToF-MS) which employs a hydronium ion source (TOF1000, resolution ~ 1200 FWHM[2]). This ionization technique requires no buffer gas which would dilute the pre-concentrated SVOCs. Also, the proton transfer reaction produces less fragmentation compared to traditional methods such as electron ionization. Overall, this detector provides on-line, real time measurements in a large mass range with a level of detection $< 1pptv$, allowing us to investigate these formerly undetectable particles. Full mass spectrums (charge-to-mass ratios, m/z) with corresponding volume mixing ratios are generated for analysis. Combining the DS with the PTR-ToF-MS allows us to probe a large range of masses and to embellish the current knowledge of SVOCs in the atmosphere.

1.3 SVOCs in rural Netherlands and project objectives

Investigating atmospheric constituents in different regions, such as a rural areas, is critical because organic compounds are strongly influenced by processes such as fossil fuel use and manufacturing, intensive agriculture, and biomass burning. The setup was stationed at the $200m$ level of the Cabauw Experimental Site for Atmospheric Research (CESAR, Cabauw Tower, Netherlands) from September 2016 - January 2017. The materials and setup are described in Section 2. The nature of this project was very exploratory because the DS is a new tool. The method of implementation is described in Section 3. The main objective is to characterize the performance of the DS and to analyze the SVOCs that are collected in rural Netherlands. A method is developed to retrieve volume mixing ratios of SVOCs in ambient air from the raw data while also attempting to address the impact of contamination (Section 4).

The project is split into two sets of experiments including controlled lab setting experiments (Section 5) and field measurements at the Cabauw experimental site (Section 6). In the lab setting, selected SVOCs are used to test the recovery of the DB1 denuder section and evaluate its ability to collect SVOCs. The lab experiments also involved investigating the impact of fragmentation. After the DS is shown to effectively catch SVOCs in the lab setting, the performance of each denuder section is examined as a time evolution of field measurements. The analysis of SVOCs in rural Netherlands answers questions such as what mass ranges and ion groups are present, what influence do different meteorological conditions have on SVOCs, and what can we learn about the partitioning of the organic species over time. Partitioning is investigated using supplementary data collected at the CESAR, such as meteorological conditions and Organic Aerosol (OA) measurements at $5m$. Overall, the present study tests and evaluates the performance of this new SVOC collecting technique and delineates possible reference values for SVOC investigations into a rural air profile.

[2]full width at half maximum: an expression of the mass resolution $m/\Delta m$

2 Materials and Setup

The Denuder Sampler (DS) and Proton Transfer Reaction Time of Flight Mass Spectrometer (PTR-ToF-MS) are stationed at the Cabauw Experimental Site for Atmospheric Research (CESAR) KNMI-mast. This tower is situated on a polder ($0.7m$ below mean sea level) in a rural part of the Netherlands (51.971°N, 4.927°E) that is shown in Figure 2. Real-time data is collected from the measurements which take place at the $200m$ level. The instruments are controlled remotely using *Teamviwer* (Version 12, 2016[3]), however, the site was visited occasionally for maintenance.

Figure 2: Cabauw Experimental Site for Atmospheric Research (CESAR), KNMI-mast Cabauw tower, in the Netherlands.

The $200m$ level is an interesting altitude because of the changing height of the boundary layer depending on insolation and meteorological conditions. The variation is clear in Figures 3. A large temperature range (−5°C to $30°C$) and high wind speeds (up to $110km/hr$) are common at this location and height. This auxiliary meteorological data was collected at $200m$ during the time period September 2016 - February 2017 using the CESAR Database [5]. The setup, including the PTR-ToF-MS and DS, is contained within a large box providing protection from the elements (Figure 3). The box is insulated and equipped with ventilation that is initiated when the temperature rises above 20°, reaching maximum ventilation at $25°C$.

An open metal column with an air flow rate of $500L/min$ is attached to the outside of the box. The DS accesses air from this column via tubing that penetrates small hole (see red box in figure 3). Undesirable wall losses are minimized by using a short and high flow inlet. The components of the setup are illustrated more clearly in the schematic, figure 7.

[3]Developed by TeamViewer GmbH, this software is compatible with Mac, Linux, Windows and most mobile devices

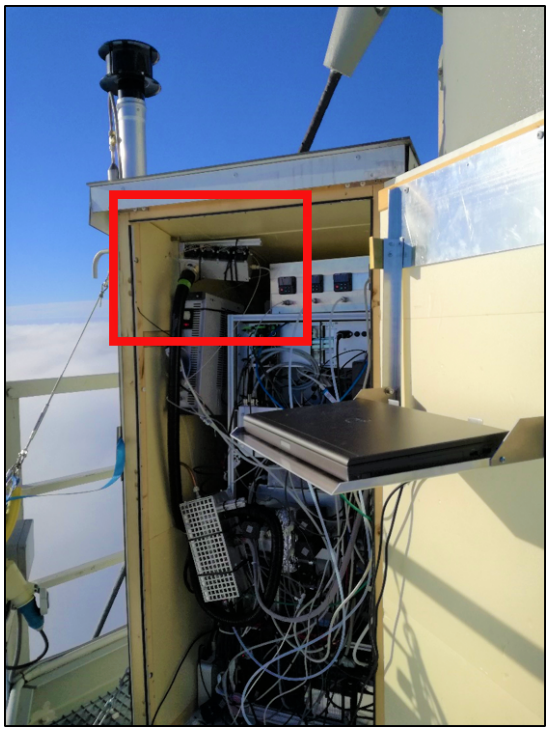

(a) Setup in position for sampling. Lifted condensation level is below $200m$ and DS is not sampling from the boundary layer.

(b) Setup is removed from the insulating box for maintenance. Boundary layer is expected to be well mixed.

Figure 3: The setup including the PTR-ToF-MS and DS is pictured here at the $200m$ level of the CESAR tower. The DS is indicated by the red box. The height of the boundary layer is different in both pictures, indicated by the cloud height

2.1 Denuder Sampler (DS)

The DS is the part of the setup which samples air and collects compounds. Semivolatile Organic Compounds are difficult to monitor because they exist in low concentrations and are eager to condense. The DS is a relatively new instrument designed to overcome these challenges while also having the ability to collect VOCs as well. The DS has four sections, illustrated in figure 4, which are $3cm$ long with an outer diameter (OD) of $4mm$. The first section consists of the standard Polyether ether ketone (PEEK) material which is also used in the tubing of the setup. Ideally, no compounds are detected from this section. The next two sections are designed to catch SVOCs. These sections consist of an assemblage of micro-channels called a denuder. These two denuder sections have micro channels with an Inner Diameter (ID) of $80\mu m$ which are coated with dimethylpolysiloxane (Agilent DB-1 Column). While sampling, air will be pulled through the microchannels as laminar flow and gas-phase SVOCs will collide and condense on the walls of the DB1 material while aerosols and VOCs do not condense and will continue to the next section. Ideally, all SVOCs will collect in the first DB1 section. The fourth section is a denuder designed to collect the VOCs. This denuder is activated charcoal (Mast Carbon, UK) with larger, and thus fewer, microchannels (ID: $800\mu m$). After sampling, the DS sections are heated successively ($T = 150 - 170°C$) causing the condensed organic compounds in each section to evaporate sequentially . During this time, the flow in the DS is switched to provide nitrogen that will transfer the thermally desorbed compounds to the PTR-ToF-MS via the flow. Transfer lines are heated to avoid re-condensation. Fans are activated to cool the sections when they are not being heating. The multiple functions of the DS, such as the heating, cooling and flow direction and rate, are controlled via a denuder automation sequence which was adjusted throughout the project.

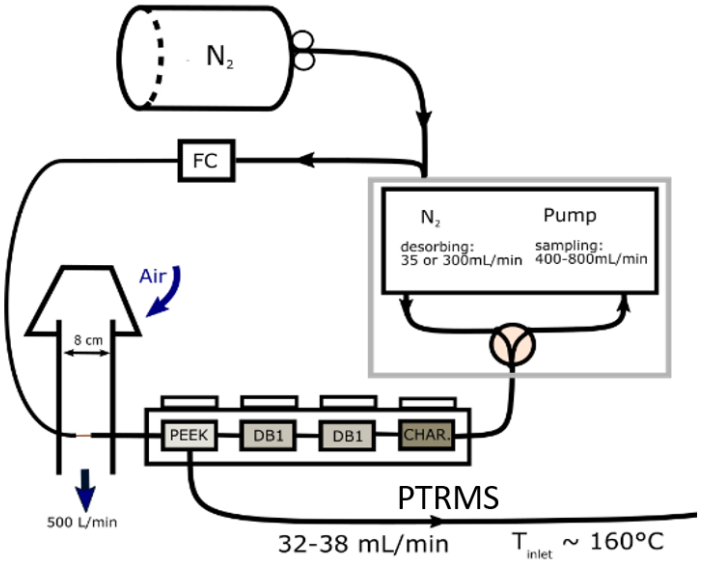

Figure 4: Schematic representation for DS. Heating elements and fans control the temperature of the four sections: PEEK tubing, DB1 denuders, and charcoal denuder. The flow can be set to pump, pulling air through the sections, or set to nitrogen which is used to transfer desorbed compounds to the PTR-ToF-MS.

2.2 Proton Transfer Reaction Time of Flight Mass Spectrometer (PTR-ToF-MS)

After collection, compounds are sent to a detector and this section discusses the function and features of the PTR-ToF-MS which provide the level of sensitivity and precision required for SVOCs analysis. The PTR-ToF-MS was developed in 1995 at the Institut für Ionenphysik in Innsbruck, Austria and is based on using a hydronium ion source (H_3O+) to donate a proton to the organic compounds for detection [6]. The high precision measurement capabilities of the PTR-ToF-MS are necessary for investigating different isobars[4]. By using a PTR-MS coupled with a TOF1000 instrument, it is possible to monitor trace SVOCs (volume mixing ratios as low as $0.01 ppb$) because the sample will not require a buffer gas due to the chemical properties of the ion source. Also, the real-time analysis capability of this detector is an asset for our field measurements. Investigating temporal changes in atmospheric composition is challenging using conventional methods, such as gas chromatography, which are limited to longer time scales.

[4]Isobars are compounds with the same nominal mass but different exact masses as the result of different molecular formulae and the mass effect of different atoms

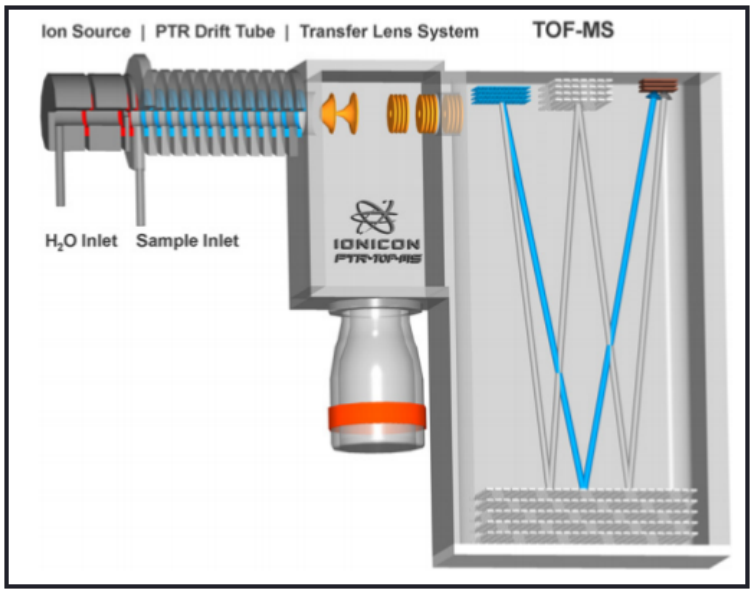

Figure 5: Schematic of the PTR-ToF-MS detector, consisting of the hollow cathode ion source, the proton transfer reaction drift tube, the transfer lens system and the reflection time of flight mass spectrometer [7].

2.2.1 Ion source

The hydronium ions (H_3O^+, m/z 19.018 Da) used to ionize sample compounds are produced in the hollow cathode using a liquid water source (flow rate of 5sccm) see Figure 5). In this region of the PTR-ToF-MS, free electrons are repelled and a mix of positive and negative ions is maintained as an electronically neutral (net), relatively high density plasma ($10^{10} - 10^{11} cm^{-3}$). The neutral H_2O molecules are ionized by electron collisions to produce hydronium ions. The hollow cathode current controls the amount of ionization by adjusting the potential which influences the plasma [5]. The hydronium ions are produced at a purity of at least 99.5% [6]. However, other ions such as O_2^+ and NO^+, can be present if the flow of H_2O is too low and the low pressure can allow the flow to go backwards. A high density ion source is ideal for measuring trace gases such as SVOCs and impurities, such as O_2^+ complicate measurements because they can also react with the sampled compounds. Therefore, these source ions should be maximized while restricting the amount of interfering ions such as O_2^+. The ratio O_2^+/H_3O^+ was minimized such that it is $< 5\%$. By tuning the voltages that control sensitivity for extraction from ion source to drift tube, it is possible to improve this ratio [6].

2.2.2 Drift tube reaction chamber

Hydronium ions enter the adjacent drift tube section where the proton transfer reactions will take place. The sample, transferred from the DS, is injected into the drift tube with the high density hydronium ions. The source ions have a mean drift velocity which is controlled by the drift tube electric field strength. The source ions collide with the organic sample compounds (R), donating a proton if energetically permitted.

$$H_3O^+ + R \xrightarrow{k} RH^+ + H_2O \tag{1}$$

The reaction rate constant for the proton transfer reaction is $k \sim 10^{-9} cm^3/s$ [6]. At the end of this reaction section, the density of product ions (RH^+) is given by 2.

$$[RH^+] = [H_3O^+]_0(1 - e^{-k[R]t}) \approx [H_3O^+]_0[R]kt \tag{2}$$

[5] The hollow cathode current was maintained at 3mA or the entire duration of the project

[6] In this project the variables U_s and U_{so} were adjusted. By decreasing U_{so} to $45V$, H_3O^+ was increased and O_2^+ was reduced. However, if U_{so} is decreased too much, the amount of hydronium decreases as well.

where $[H_3O^+]_0$ is the ion source in absence of reactant neutrals and the reaction time, t, is the time H_3O^+ required for the ions to traverse the length of the drift tube [6]. The ion detection system measures count rates of the source and product ions (RH^+). Finally, $[R]$ can be determined via Equation 2, using the amount of product and source ions and the reaction time. High sensitivity requires a high quantity of product ions relative to the compounds provided by the sample ([R]) which can be achieved maintaining a high density of source ions. Furthermore, a high sensitivity is achieved because the sample does not need to be diluted with an additional buffer gas (i.e. helium). The sample can be analyzed directly because the proton affinity of water is such that the hydronium ions will not donate a proton to the abundant non-organic compounds in air. The proton affinity of water is $7.22eV$ and reactions with organic compounds (typically $7-9eV$) are typically slightly exoergic [6]. This property makes the proton transfer reaction method ideal for low concentration compounds, such as SVOCs.

The exoergicity of the proton transfer reactions is low enough that the breakup of neutrals is less common compared to other traditional methods such as electron ionization [8]. However, parent ion fragmentation with undetectable neutral products can occur if the collision energy during the proton transfer reaction is too high. Therefore, the electric field strength in the drift tube (E) and corresponding energy of the hydronium ions must be selected with this in mind. Notwithstanding, E must also be kept sufficiently high to limit the loss of hydronium ions through water clusters formation ($H_3O(H_2O)_2$, m/z 55.054 Da) via association reactions (Equation 3). A lower density of source ions hinders the detection sensitivity.

$$H_3O^+ + H_2O + M \rightarrow H_3O^+ \cdot H_2O + M \tag{3}$$

The reaction rate for water cluster formation has a strongly negative energy dependence. Therefore, if E is too low water clusters will form, decreasing the amount of hydronium ions available, but also complicating measurements by reacting with organics. At higher energies, collisional breakup can reduce the amount of water clusters and the electric field can be adjusted considering these reactions. Applying different electric field strengths was explored in the controlled lab setting and will be discussed in section 5.2.

2.2.3 Time of flight reflection mass spectrometer

Finally, the ionized organic compounds are transferred to the Time of Flight (ToF) detector where the time it takes a compound to traverse the space will reveal its charge-to-mass ratio (m/z). After protonation, the ionized compounds (RH^+) enter the pulse extraction region via a transfer lens system. Here, the push and pull voltages responsible for pushing/pulling the ions into the mass spectrometer can be tuned to improve the balance of the ion beam so that it is unimpeded.The PTR-ToF-MS is ideal for monitoring SVOCs because the overall transmission relative to the primary ion increases with mass, in contrast to conventional methods of detection such as quadrupole mass spectrometer [7]. Upon entering the mass spectrometer, a section of the ion beam is pulsed by an electric field giving all of the compounds the same kinetic energy. Each extraction pulse generates a complete mass spectrum for the time interval/mass range chosen. The mass-to-charge ratios (m/z) can be determined by the time of flight. Time of Flight mass spectrometry eliminates the necessity of selecting a subset of ions to be monitored in a specific experiment and has a mass resolution which allows the separation of the most nominally isobaric ions.

3 Methods

3.1 Lab setting experiments

The performance of the DS was investigated by calculating the recovery of administered SVOCs of ranging volatility.To start each experimental run, the liquid solution containing the selected SVOC and Ethanol is inserted into the PEEK section of the DS via a constructed aluminum spoon. The entrance of the DS was modified to accommodate the experiments. Initially, any attachments were removed from the entrance and the secondary nitrogen flow tube was affixed to the DS entrance as shown in Figure 6. Two concerns were addressed during method development. The first challenge was to prevent an inflow of lab air so that any detected signal could be attributed to the isolated compound. The second challenge was minimizing solution loss through undesirable surface contact and implementation time length.

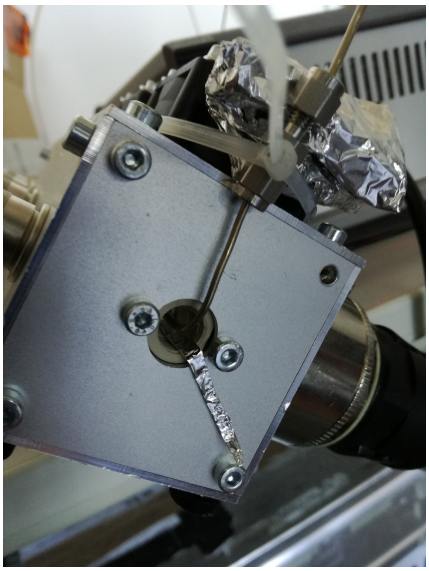

(a)

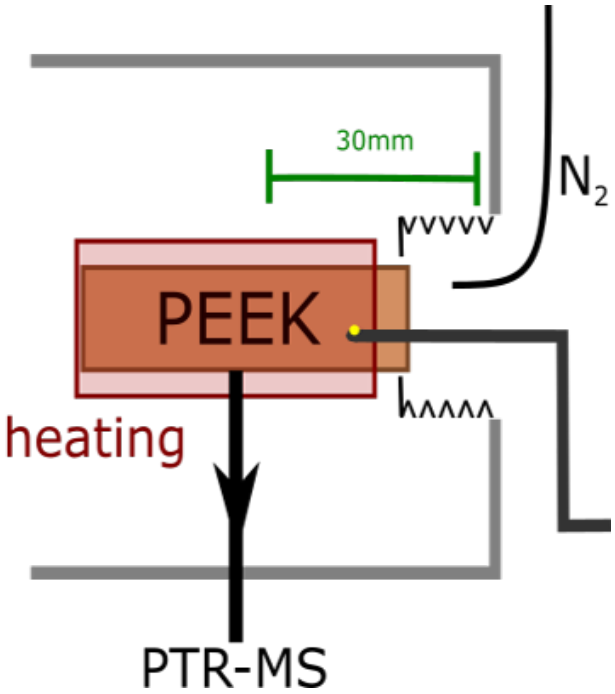

(b) Schematic side-view cross-section

Figure 6: Depicted here is the initial lab setup of the DS for performance tests. The DS entrance is modified to accommodate the secondary nitrogen flow and the liquid sample which is inserted using a constructed aluminum spoon

A 30-minute DS automation provides instruction for the DS to sample the inserted solution. After the automation is initiated, the solution is inserted into the DS. The sequence began with a flow in the pump direction (400 or $800 mL/min$) for six minutes. The PEEK section is heated ($150°C$ or $170°C$) during the last three minutes of sampling to ensure the SVOC evaporates entirely and is collected in the successive denuder sections. During sampling, the secondary nitrogen access is engaged, supplying a sufficient flow that has a rate that is slightly above the sampling DS pump flow rate to prevent lab air intrusion. After the compounds collect in the denuders, the sections of the DS are heated successively to thermally desorb the compounds and transfer them to the PTR-ToF-MS via a flow of nitrogen in the opposite direction ($\sim 40 or 300 mL/min$). During all stages, there is a flow of $32-38 mL/min$ towards the PTR-ToF-MS. Therefore, a small signal is expected during sampling and a higher signal is expected when the DB1 denuder section is heating. Automation adjustments, such as increasing the temperature of the section heating elements or changing the drift tube electric field strength, were made throughout the project to make improvements or to test different features.

3.2 Field measurement methods

Measurements were executed at the 200m level of the Cabauw tower using a repeating four-hour sequence of automation instructions which could be controlled remotely. The automation sequences control the various parts of the setup (see Figure 7) such as the components of the DS, the rotors, and the PTR-ToF-MS variables. All variables are displayed and can be altered in the *TOF2.3* software. The four-hour sequence changed slightly throughout the project but the key processes are the standard gas background, the zero flow blank, the nitrogen blank, and successive air sampling.

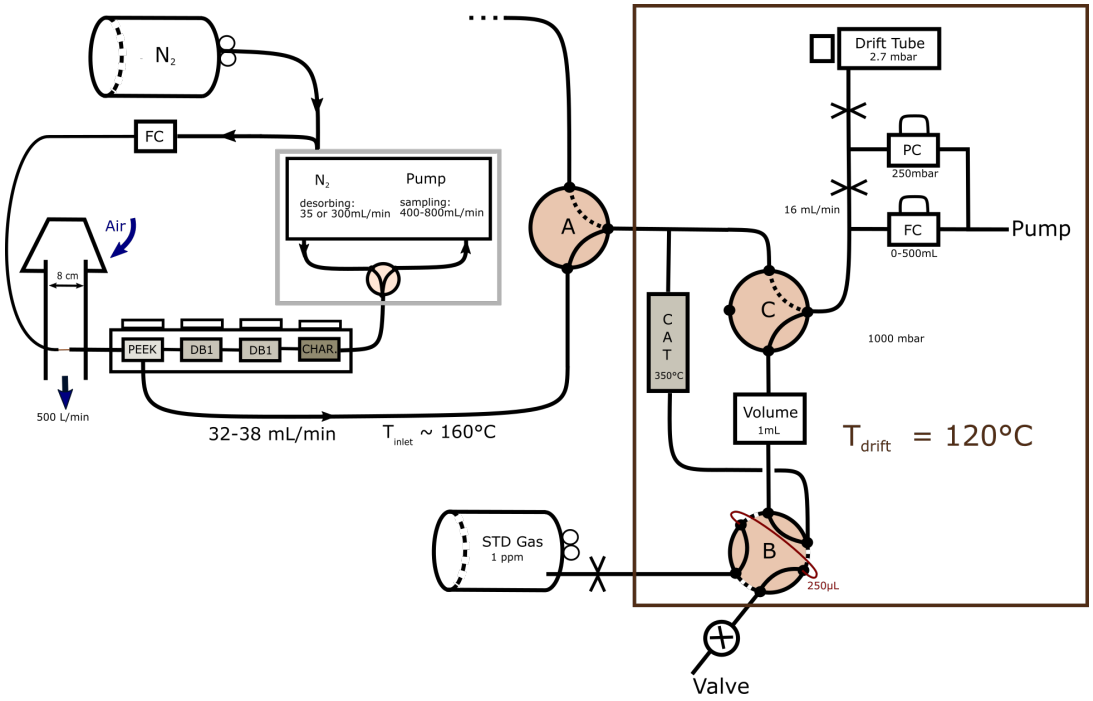

Figure 7: Schematic representation of the setup for the DS coupled with a PTR-ToF-MS. Three rotors (illustrated as A, B, and C) rotate to allow different flow paths. For instance, rotor B will control a standard gas (STD) background injection. The catalyst (CAT) and the mixing volume which are required for the standard gas background are also pictured. The current infrastructure includes the DS, but an aerosol inlet can also be equipped and accessed via rotor A. The four sections and fans of the DS are illustrated and the DS flow is controlled by the nitrogen gas and pump. Gas is transferred to the PTR-ToF-MS via rotor C and through channels controlled by capillaries (><), flow controllers (FC) and pressure controllers (PC), and pumps. The PC will adjust if resistance increases (i.e. via capillaries or residue buildup) ensuring that sufficient air will flow through.

3.2.1 Standard gas background

Each four-hour cycle begins with a standard gas background which is used to calibrate the instrumentation. The background provides results from known compounds and energy information that can be compared to actual samples to improve measurements. The standard gas background is controlled by automating Digital Output 1 (DO1) and shifting rotors B and C (Figure 7). First, air is sent to a catalyst which is heated to about $350°C$ and hydrocarbon-free 'zero' air is produced via $VOC \rightarrow CO_2 + H_2O$. This zero air retains a humidity that is closer to that of ambient air compared to other methods of filtering. Next, the zero air is transferred to the relatively large mixing volume ($1mL$) where it will be mixed with a small volume injection ($125\mu L$) of the standard gas. Finally, the diluted standard gas is sent to the PTR-ToF-MS via rotor C. Fragmentation within the drift tube can impact PTR-ToF-MS measurements by shifting a spectrum peak depending on the energy of the collision. The standard gas background can be used to create a corresponding mass transmission curve, which depicts the mass-dependent transmission factor for each of the standard gas charge-to-mass ratios. Development of a measurement standard has been addressed by R. Holzinger and others in reference [11]. The resulting mass-dependent efficiency

information can be applied to improve measurements by evaluating the impact of fragmentation for the known compounds.

3.2.2 DS automation sequence

After the standard gas background, the next steps in the four-hour cycle (excerpt shown in Figure 12) involve a repetition of a 25-minute DS sequence for performing blanks or sampling air. The DS automation begins with ten minutes of sampling with a flow rate of $800mL/min$ in the pump direction. During this time, SVOCs are expected to collide and condense on the surfaces of the DB1 material sections of the DS while other compounds proceed to the next section where VOCs collect in the charcoal section (see Figure 7). Then, the collected compounds are thermally desorbed by heating each section ($150°C$) successively for three minutes. Each preceding section remains heated to prevent re-condensation. During desorption, the compounds are transferred to the PTR-ToF-MS via a nitrogen flow opposite of the pump direction at a flow rate of either $35 - 40$ or $300mL/min$. This flow rate must be larger or equal to the inlet flow of the PTR-ToF-MS which was $\sim 35mL/min$. Next, all heating element temperatures are increased to $170°C$ for a cleaning stage to ensure that all compounds have been evaporated off. The fans are active when the elements are not heating and can reduce the temperature of each section from 170° to room temperature in less than 5 minutes. This sequence executed repeatedly and is adjusted slightly to perform two blanks.

A zero flow blank and a nitrogen blank are executed during the four-hour cycle. These blanks are compared to the air samples to determine whether compounds are veritably found in ambient air. These blanks can be used to identify and reduce the effects of contamination from the air sample data. The zero flow blank occurs after the standard gas background during the first execution of the DS automation sequence. During the ten minutes of sampling, the flow rate is set to zero in the pump direction but the PTR-ToF-MS inlet still has a small flow of $\sim 35mL/min$. After the zero flow sampling, the thermal desorption process begins and any compounds detected are expected to be contamination

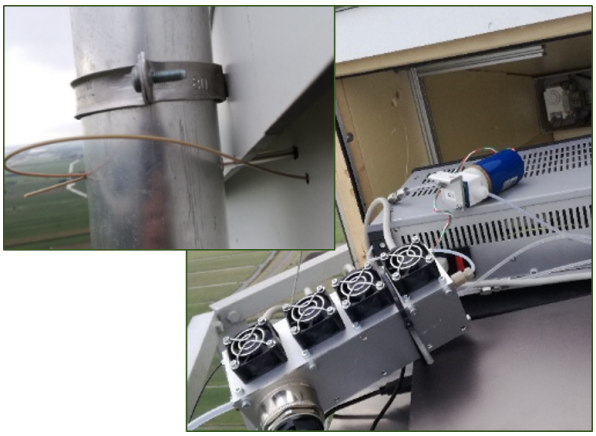

Figure 8: The flow controller (blue device) that provides a secondary access to the nitrogen is shown here. The nitrogen tube is placed in the sampling tube as shown in the expanded photo.

The nitrogen blank was introduced on October 8^{th}. This blank was developed in an attempt to better reflect contamination that is caused by the sampling flow which is absent during the zero flow blank. After the zero flow blank, the next DS automation samples ambient air, followed by the nitrogen blank. This blank is executed by activating a secondary access to the nitrogen, shown in Figure 8, via an instruction for Digital Output 7. Sufficient nitrogen ($800mL/min$) is provided at the entrance of the DS for 12 minutes, one minute before and after the ten minute sampling period. Therefore, no air enters the DS during sampling and any compounds detected during desorption are assumed to be from contamination. After this blank, the remainder of the four hour cycle is occupied by DS sequences which sample ambient air. The performance and comparison of the two blank methods are discussed in section 6.2.1.

4 Data Treatment

4.1 Overview

A method was developed to retrieve the volume mixing ratios of SVOCs in ambient air from the raw data produced by the PTR-ToF-MS. To start, the raw data files are processed in an IDL graphical interface called *PTRwid* [9]. From *PTRwid*, a comma separated value (.csv) type file is produced containing the concentrations ($60s$ averages), engineering data (if available), and optional categorizing index values. These files are then saved as text files (.txt) and imported into an analysis code (Python environment) that was developed to manipulate and analyze the data. For example, the volume mixing ratios produced when the DB1 denuder section is heating must be identified, stored and interpreted. Then, these values must be converted to be with respect to the ambient air instead of the DS nitrogen flow (details in Appendix section B.1). DS contamination was apparent throughout the project. Contamination is addressed by incorporating and subtracting two blanks: a zero flow blank and a nitrogen blank. Therefore, to determine if each mass is significant in air, a Student T-test (details in Appendix section B.2) is used to compare sample data to the results of two blank methods. Unfortunately, data treatment is complicated by periods missing engineering variables and entire gaps in data during periods with instrument or software issues.

4.2 Processing raw data in PTRwid

PTRwid is a user-friendly graphical interface initiated by code in an IDL environment that can be used to evaluate the full mass spectra and create a unified mass list associated with multiple files over long time periods. *PTRwid* requires minimal user input and is computation time-cost effective; however, the computation time is still large when considering long time series (Sept 2016 - January 2017: ~ 500 GB data). The PTR-ToF-MS produced a single mass spectrum every second[7] over several months. These spectra and the corresponding engineering variables can be displayed, processed, and exported in *PTRwid*. Additionally, extended processing was applied to the unified mass list. For instance, the engineering data can be used to apply categorizing index values to the averaged and merged data.

To identify the compounds and attribute the corresponding chemical formulas, the mass scale calibration matches with a library of ion masses. The time of flight bins are converted to mass bins by fitting the following equation [8]:

$$t_{\mathrm{TOF}} = a \cdot m^{ex} + t_0 \tag{4}$$

where t_{TOF} is the time of flight bin, m is the ion mass, and a, ex, t_0 are optimization parameters [9].

A section of the mass spectrum containing one identified peak is shown in Figure 9. Da is the unit Dalton[9]. Peaks are resolved using the derivative of the spectrum (*dSpec*), shown in the lower plot of Figure 9. A potential *Peak Start* is detected when *dSpec* is positive and exceeds 6 times the median value of the absolute value of *dSpec* in the neighboring range ($\pm 1Da$).

[7] The single spectrum is an average itself because there is a pulse every $25\mu s$ (max flight time) for $1.5\mu s$ (extraction time), so $1s/25\mu s = 40,000$ spectra.

[8] Three fit methods are used (see reference [9]) and the set that yields the most matches with the library compounds is chosen for subsequent analysis.

[9] The unit Dalton is the unified atomic mass unit which is approximately the mass of one nucleon and is numerically equivalent to $1g/mol$.

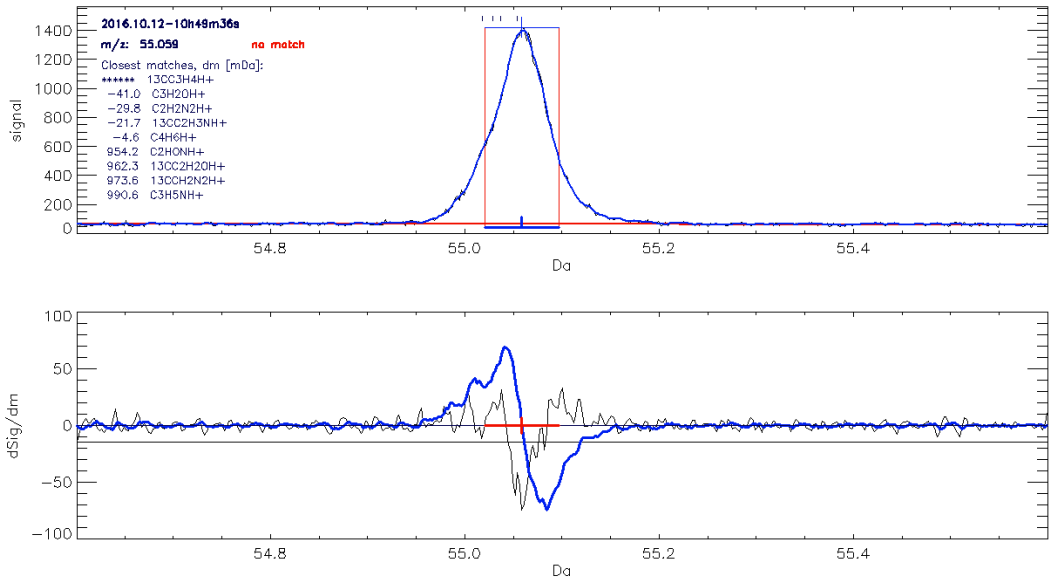

Figure 9: Upper plot: *PTRwid* output for a small portion of the spectrum (*Spec*), Lower plot: the derivative of the spectrum (*dSpec*). blue: Smoothed SumSpectrum, black: unsmoothed SumSpectrum [9]. The range from *Peak Start* to *Peak End* is indicated by blue horizontal line in the upper plot and the blue tick indicates the position of *Peak Max*. The small black ticks above the curve in the upper plot depict the closest mass matches, with chemical formulas listed on the left.

The potential matches for each compound were evaluated and the best matching chemical formula was attributed on the following criteria. Firstly, the match with the lowest standard deviation (mDa) concerning the peak shape and peak maximum is prioritized (see list in the left upper plot of Figure 9). However, if the closest match contained ^{13}C and violated the abundance relationship considering the signal of the ^{12}C version of the species, then the next best match was selected. Compound matches without nitrogen were prioritized as well. Unfortunately, some compounds have no suggested matches and likely belong to other groups such as metals or halogenated compounds.

Considering that a full spectrum is obtained every second, it is unlikely to retrieve mass peaks of the exact same value for a long time series. Sampling different air and changes in instrument operating conditions can yield different results. One list of masses for an entire time series can be created using the unified mass list option. The unified mass list can then be averaged, merged, and further processed. The concentration of each mass is displayed over the time series in extended processing. An example is shown in Figure 10. The data shown in Figure 10 have also been categorized (ind) using the available engineering data in *PTRwid*'s index option and 60-second averages are displayed in grayish blue. The index option is useful for identifying the stages and status of the instrumentation. For example, the index that was developed and applied in Figure 10 uses the sampling flow rate and fan status to identify when the individual sections of the DS are being heated. In this case, SVOCs are expected when index 101 is assigned because the first DB1 denuder section is being heated. Unfortunately, all of the engineering was not available from October 7^{th} to 16^{th}, 2016 and applying indexes became more difficult. A more robust index was developed and details of each index list are described in Appendix Section B.3. The final product is an exported (comma separated value) csv-type file for the entire time series considered which can be analyzed in other software with ease using the index value.

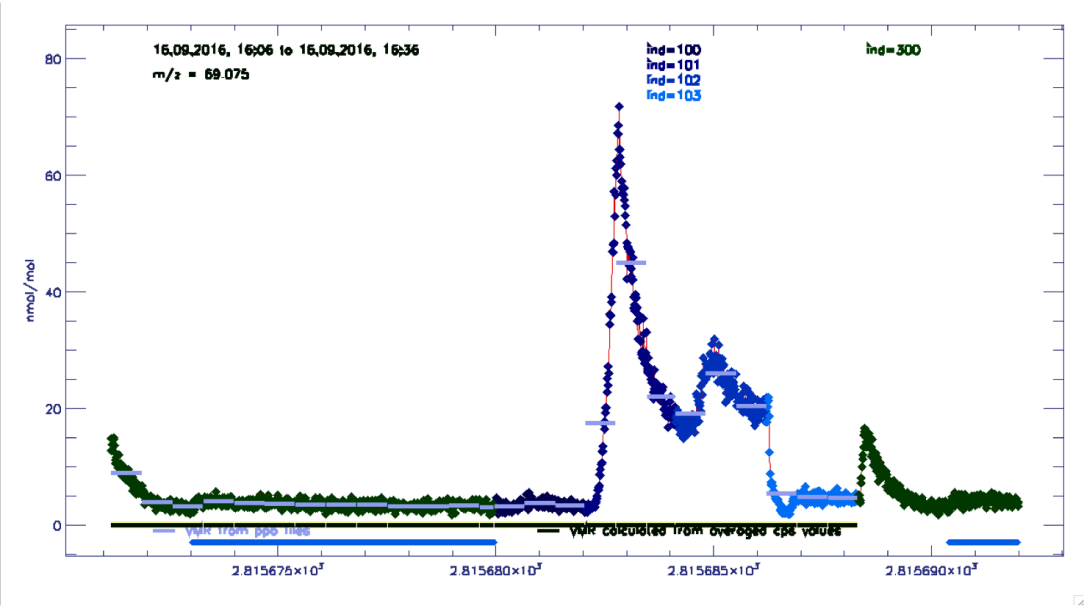

Figure 10: A 30 minute time series of $m/z69.075$ starting at 16:06 (GMT), September 16^{th}, 2016. 60-second averages are denoted by the greyish-blue bars. The first index from Section B.3 is applied: The gradient of blue corresponds to the signal from each DS section.

4.3 Interpreting volume mixing ratios during desorption

The next step in data treatment is interpreting the volume mixing ratios produced using *PTRwid*. Three 60-second averages correspond to the time when each individual section of the DS is heating and the signal during this time can be interpreted differently. The *PTRwid* export is imported into the Python analysis code and the index value for the entire time series for each mass is checked to identify if a DS section is heating. Any SVOCs are expected to be detected when either DB1 denuder section is heated. The volume mixing ratios of the compounds detected are stored; however, this information can be interpreted differently. The options considered included the average of the three values, the maximum value, or the value corresponding to the first minute - which may be reasonable assuming that the condensed SVOCs evaporate quickly. During the early stages of the field study, it became apparent that a significant amount of masses were detected in the second DB1 denuder section as well. Therefore, the addition of the first minute in both DB1 sections was also considered for interpreting SVOC results.

The results using each method of interpretation were compared by considering the amount of significant compounds detected in each DS section. Compounds were determined to be significant in air if the volume mixing ratio assigned was statistically different than the two blanks which do not sample ambient air. More specifically, significance was determined by comparing the sample to each blank using a Student T-test ($p < 0.05$). The results are displayed in Figures 11 and 11b and the details of the Student T-test can be found in the Appendix section B.2.

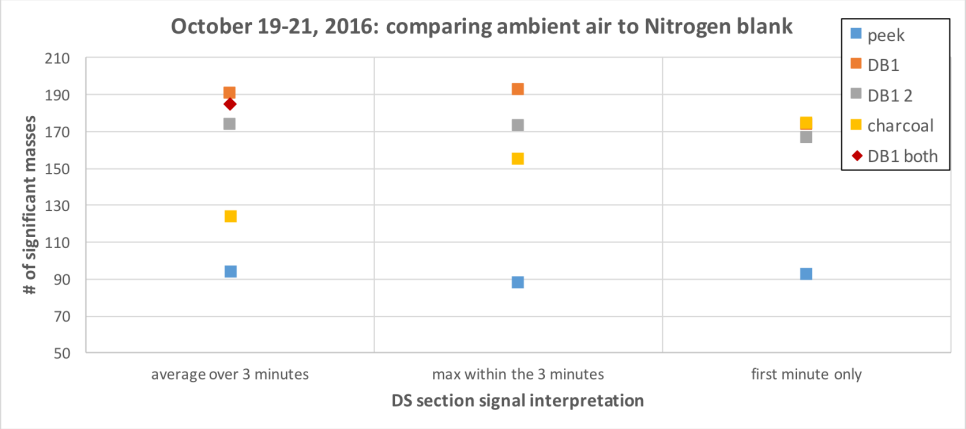

(a)

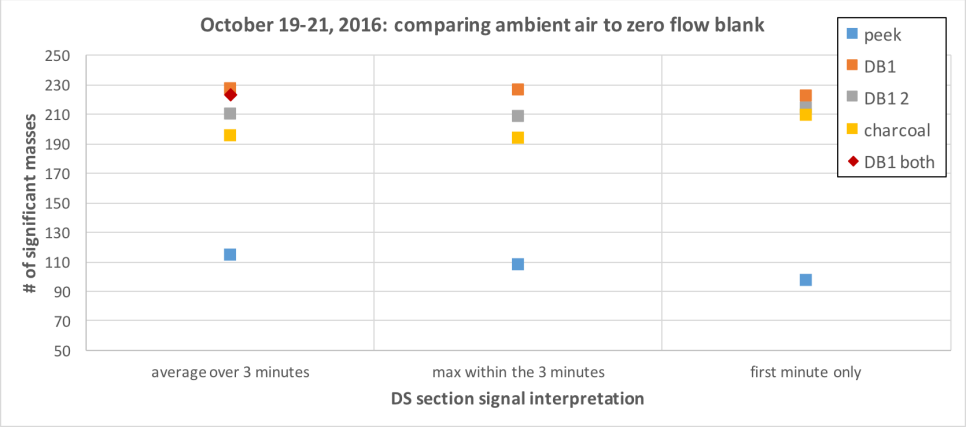

(b)

Figure 11: The different methods for interpreting the DS section peaks are depicted by the number of masses that were determined to be significant in air compared to each blank method using a Student T-test ($p < 0.05$). The total number of masses detected is 239.

Comparing samples to each blank in Figures 11 and 11b, over 170 masses were determined to be significantly different than the blanks. More masses were determined to be significant compared to the zero flow blank which is not surprising considering the shape that the nitrogen blank typically produces (see Figure 12). Regardless, the number of significant masses using each method of interpretation does not vary greatly for the first DB1 denuder section. A large number of masses are detected in the second DB1 section as well. However, considering the first minute in both sections did not present a clear advantage compared to considering the first minute of the first DB1 section alone. This unexpected behavior is investigated more extensively by comparing the total mass concentrations for both denuders (Section 6.2.1). Less masses were detected in the other two DS sections. Significantly less masses are observed in the PEEK section, but the amount is still higher than anticipated. Again, analyzing the mass range and total mass concentration for this section provides further insight (Section 6.2.1). As for the charcoal section, there is a clear difference when only considering the first minute. The larger number of masses detected when only considering the first minute may be due to the fact that the VOCs are collected in this section evaporate easily and quickly. However, this result could also be caused by residual signal from the preceding DB1 section which is exponentially approaching background levels. This behavior can be further investigated by comparing the total mass concentration of the individual minutes and by investigating which compounds (SVOCs or VOCs) contribute to this number. Despite the variation in this section, the different interpretations did not produce significantly different results for the first DB1 denuder section which is the main section of interest. Therefore, the average of the three minutes was selected for the subsequent analysis.

4.4 Accounting for contamination by incorporating blanks

Contamination must be properly addressed so that the results can properly reflect the atmosphere of the rural Netherlands. As described in the methods, two blanks were performed during field measurements to address any contamination in the raw measurements. Contamination from the DS is observed when examining the blanks in Figure 12. Figure 12 displays the raw volume mixing ratios for both blanks and two samples.

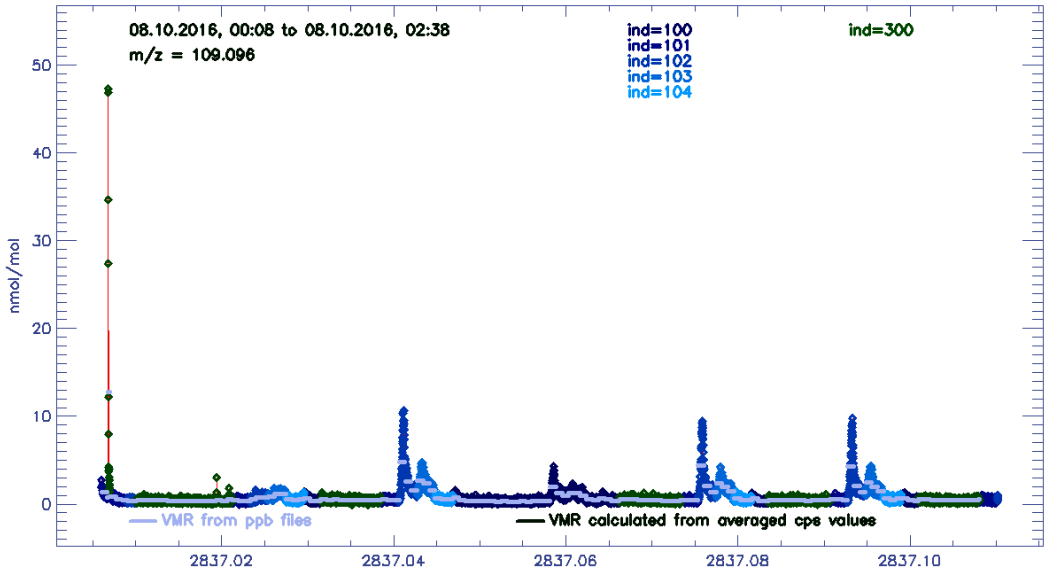

Figure 12: *PTRwid* excerpt for m/z109.096. The x-axis is the Julian Date from 01/01/2009. Index details in Section B.3. A zero flow blank (starting at JD = 2837.0144), followed by ambient air sampling (JD = 2837.0315), a nitrogen blank (JD = 2837.0469), and then two other instances of ambient air sampling (JD = 2837.0662 and JD= 2837.0836) are visible.

A low, but non-negligible signal is observed after the zero flow blank (JD = 2837.0144). An even higher signal results from the nitrogen blank (JD = 2837.0469). The non-zero values observed when no air is sampled suggest that DS contamination is present. The nitrogen blank more accurately reflects the peak shapes that are observed for ambient sampling but the performance of each blank for is explored and compared in Section 6.2.

As mentioned in the previous section, the sample signals are compared to the two blank results using a Student T-test ($p < 0.05$) to distinguish which signals are not caused by contamination. To account for the contamination from the DS materials, the blank averages are subtracted from the sample averages to achieve final result. It is important to consider the fact that complications arise when comparing a sample and a blank executed at different times. The values may be unrealistic due to a sudden peak or lull and the values can easily become negative because the concentrations are as low as $\sim 1ppb$. The effect is minimized by identifying and subtracting the nearest blank, which may occur before or after the ambient air sample. The following function is used to subtract the selected blank. When given the time of the sample DB1 results and an array that contains all of the times that the selected blank occurred, the function finds the nearest time that the blank occurred and returns the time index (idx). Then, the value corresponding to the blank which occurred closest to the air sample is subtracted.

```
def find_nearest(array,value):
    idx = (np.abs(array-value)).argmin()
    return idx
```

Most applications which correct for contamination subtract the zero flow blank because the nitrogen blank was not always available. For instance, nitrogen was not provided at a sufficient flow rate for

the first available nitrogen blanks. The inadequate nitrogen flow rate allowed air to be sampled (see Figure 13) as well, and the results are therefore not a blank. Once amended, the DO7 variable was not available and the nitrogen blank results could not be identified with the current robust index used which is described in Section B.3. The nitrogen blank can applied to measurements during October $17^{th} - 21^{st}$, but after this point other technical issues (details in Section A.1) prevented the data from being incorporated in this analysis.

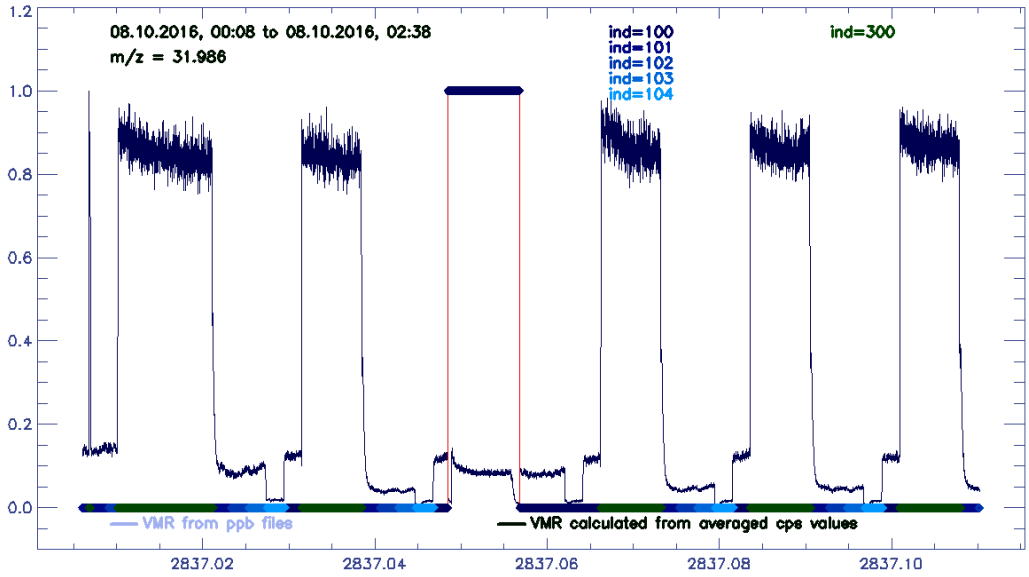

Figure 13: *PTRwid* excerpt for oxygen and DO7 variable.The x-axis is the Julian Date from 01/01/2009. Index details in Section B.3. The secondary nitrogen access is engaged when DO7= 1, but the oxygen signal is not zero as it is for the other nitrogen blanks with sufficient nitrogen flow.

5 Denuder Performance in the Lab Setting

The DS and PTR-ToF-MS were assembled in the lab (February - April 2017) to test the performance of this new SVOC analysis technique in a controlled setting. The denuder performance is tested by sampling solutions containing selected SVOCs of varied volatility and comparing the quantity introduced to the value calculated from the signal. The main three compounds explored throughout the experiments were Decanoic acid (Molar Weight (MW)= $172.260 g/mol$), Pentadecanoic acid (MW= $242.398 g/mol$), and Stearic acid (MW= $284.477 g/mol$), listed in order of decreasing volatility. Solution preparation and a complete list of prepared solutions can be found in the appendix section C. The data produced in each experiment is processed in *PTRwid* and another analysis code (Python environment) was developed to specifically analyze the lab experiment results. This section discusses the results of method development, fragmentation investigation and the denuder recovery.

5.1 Method development

5.1.1 Optimizing the solution insertion method

The setup and method of implementation were modified throughout the project to optimize the results by minimizing lab air intrusion and sample loss. While using the initial setup shown in Figure 6, 'impossible' signals corresponding to compounds that are heavier than the inserted SVOC were detected. These heavier compounds could not be fragments; therefore, these signals must be from contamination, impurities or lab air intrusion. A high oxygen signal during sampling confirmed that lab air was entering the DS despite the fact that sufficient nitrogen was supplied at the entrance. Though nitrogen was being supplied at a sufficient rate, potential turbulence at the entrance may have caused an influx of lab air. Turbulence could have been caused by supplying nitrogen at the junction where the PEEK section has a smaller diameter than the bare DS entrance opening (see Figure 6b).

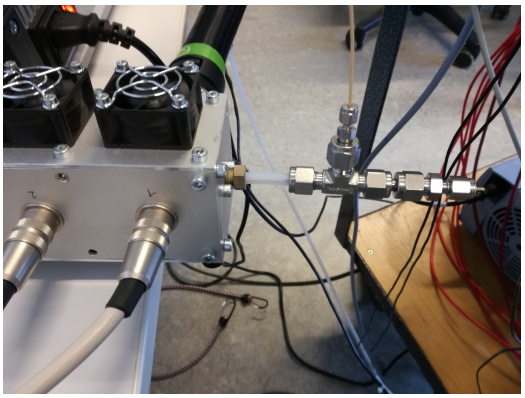

Figure 14: DS setup that supplies nitrogen uniformly and has an end cap to prevent lab air intrusion.

Tubing and connections were attached to the entrance to minimize turbulence by ensuring that nitrogen was supplied uniformly. The second arrangement is pictured in Figure 14. The attachment included a cap at the end that had a small hole for a PEEK material sample stick [10]. Aluminum foil would be placed on the end of the stick each time to apply the liquid solution without cross-contamination. The sample would be inserted and then the cap would be tightened preventing any influx of lab air. This method exhibited a large reduction in oxygen signal as desired. However, the extra attachments for this method increased the likelihood of surface contact, and therefore sample loss, during implementation. Implementation time was also increased, exacerbating sample loss through evaporation before reaching the PEEK section. Sample loss contributed to a lack of consistent and reproducible results.

Finally, a setup was developed to minimize both lab air intrusion and sample loss as best as possible. The final setup is shown in Figure 15. Lab air intrusion was reduced by attaching a bolt with tubing of the same diameter as the PEEK section. The sampling flow rate was also reduced from $800 mL/min$ to $400 mL/min$ to potentially reduce the impact of turbulence or contamination, but no notable difference in signal from heavier compounds was observed. Furthermore, with this setup, the length of the attachment is still short enough to limit surface contact during insertion. Overall, this simple setup yielded the most reproducible results and is used for the DB1 denuder recovery experiments.

[10] It was critical that any hole in a sample stick (tubing) was very small as the oxygen signal increased when tubing with a large diameter was used.

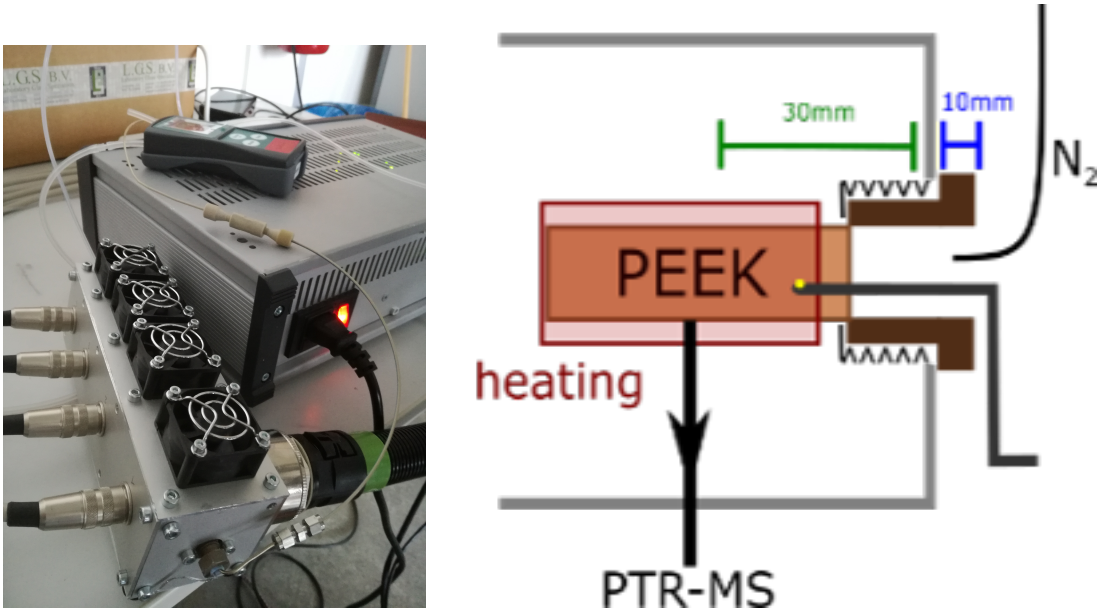

(a) (b) Schematic side-view cross-section

Figure 15: Final DS entrance setup that is used for all experiments used to resolve the recovery of the DS

5.1.2 Determining the optimal insertion length

Throughout the lab experiments different insertion lengths were investigated to determine which placement of the solution produced the highest signal. It was necessary to measure the dimensions of the DS precisely so that the spoon could be positioned in a consistent location. As illustrated in Figure 15b, the sample will not be heated adequately if it is not inserted past the heating element. Also, if inserted too far, the sample will pass the PTR-ToF-MS inlet and cannot be detected during the initial sampling stages (the first six minutes of the automation sequence). The ideal position was evaluated using Decanoic acid and the results are shown in Figures 16a and 16b. The first six minutes of sampling are shaded in yellow and red (PEEK heated) in both figures. The PEEK section remains heated when the DS flow is reversed to ensure that any compounds in this section are transferred and then the first DB1 denuder section is heated and the collected SVOCs are desorbed and transferred.

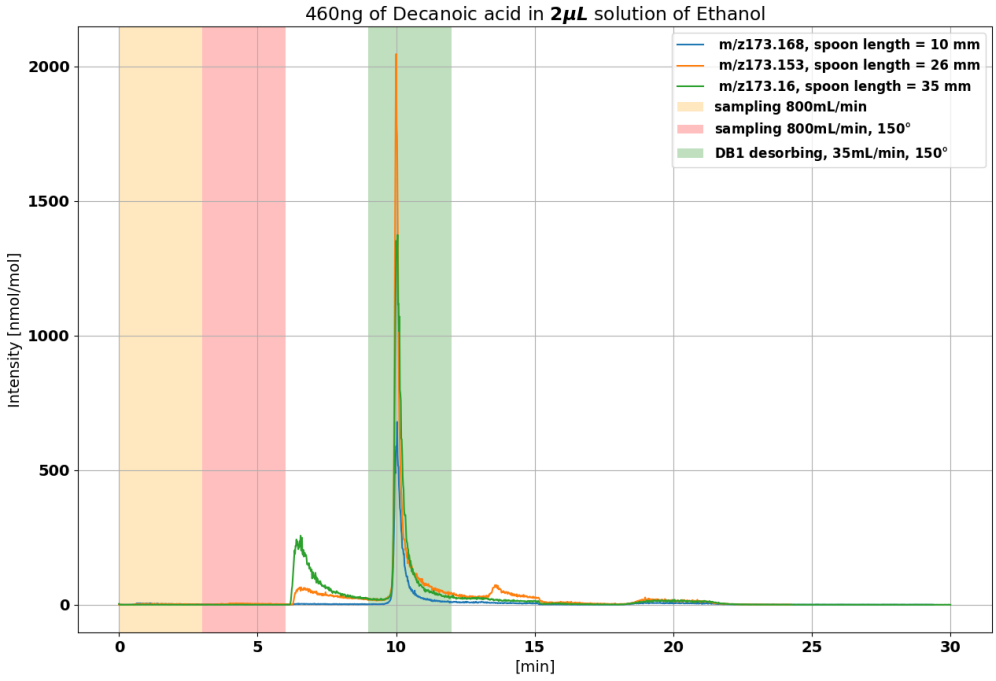

(a) Entire automation sequence

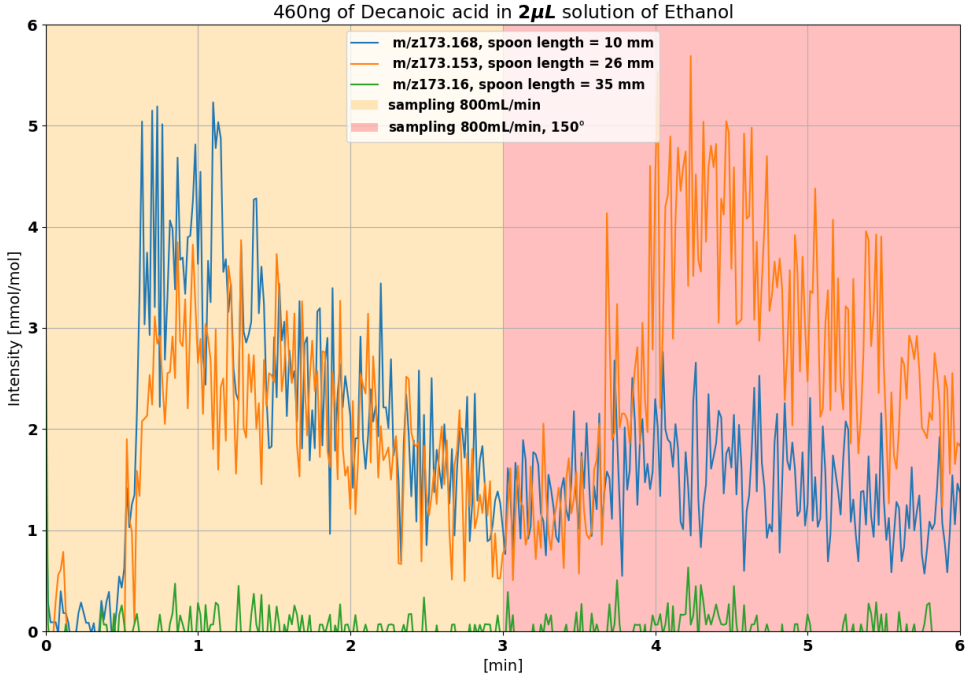

(b) Sampling portion of the automation sequence

Figure 16: March 3^{rd}, 2017: Decanoic acid signal (MW: $m/z173.26$) for three runs (drift tube electric field strength such that E/N = 125Td) employing different insertion lengths. The initial entrance setup was used for this this investigation: Figure 6.

The advantage of the DB1 denuder section is demonstrated in Figure 16: by collecting the SVOC in the DB1 denuder section, the volume mixing ratio is much higher when these compounds are thermally desorbed here (Figure 16a: green shading) compared to direct measurements of the PTR-ToF-MS (at a comparable flow ~ $40mL/min$) during sampling (Figure 16b). The low direct signal during sampling emphasizes the importance of collecting trace SVOCs with a tool such as the DS.

When the DS is sampling at a rate of $800mL/min$ during the first six minutes, a portion of the flow is directed towards the PTR-ToF-MS ($32 - 38mL/min$) and the results are magnified in Figure 16b. As expected, when the spoon is inserted to the position before the heating element ($10mm$), the heating has less influence than the case where the spoon is inserted to $26mm$. Therefore, the solution may not fully evaporate and less SVOCs will be collected, producing a lower signal when the DB1 denuder section is heated and SVOCs are thermally desorbed. However, the shorter insertion length produces a higher signal in the first three minutes, which may be due to turbulence present with the initial DS setup. As mentioned in the previous section, turbulence was likely present because oxygen was detected during the sampling stage. When the insertion length passes the detector inlet ($35mm$), no signal is produced directly during sampling as expected.

In Figure 16a, during the time that the first DB1 denuder section is heating, the largest signal was achieved when inserting the solution $26mm$ past the DS hole. It is also notable that only the $26mm$ case shows a clear signal for the second DB1 section which is heated directly after the first section. This signal could originate from the first DB1 section if a large amount of compounds are collected and not fully desorbed within the three minutes. However, this case is unlikely because the peak is isolated and therefore it is possible that some of the SVOC carried over. The $35mm$ length should produce a similar signal from the DB1 denuder section. The expected result is not observed, but there is a higher signal when only the PEEK section is heated while the nitrogen flow is reversed. This behavior may be due to accidental surface contact when inserting the solution to this length or outer heating of the adjacent DB1 denuder section allowing some of the SVOCs to desorb. The $10mm$ length produced the lowest signal while the first DB1 section is heating. This result may be caused by solution loss due to turbulence, or more likely that the compound was heated adequately to fully evaporate the compound in this case. All following experiments were inserted at a minimum of $26mm$ to yield the best results.

5.2 Investigating fragmentation by changing drift tube electric field strength

The impact of fragmentation was investigated in the lab setting by adjusting the drift tube electric field strength (E) and therefore the energy of the ionizing collisions. E/N was varied from 85 Td to 135 Td[11], where N is the constant number concentration of neutral particles. Other factors, such as flow rate and insertion length, were kept constant. The signal corresponding to the parent ion of the SVOC in the solutions expected decrease as E/N increases due to the increased energy of the ionizing collisions and frequency of fragmentation. This behavior is shown in Figure 17 which shows the results of two experiments with Pentadecanoic acid using different E/N values.

[11] unit Townsends: Td= $10^{-17} V \cdot cm^2$

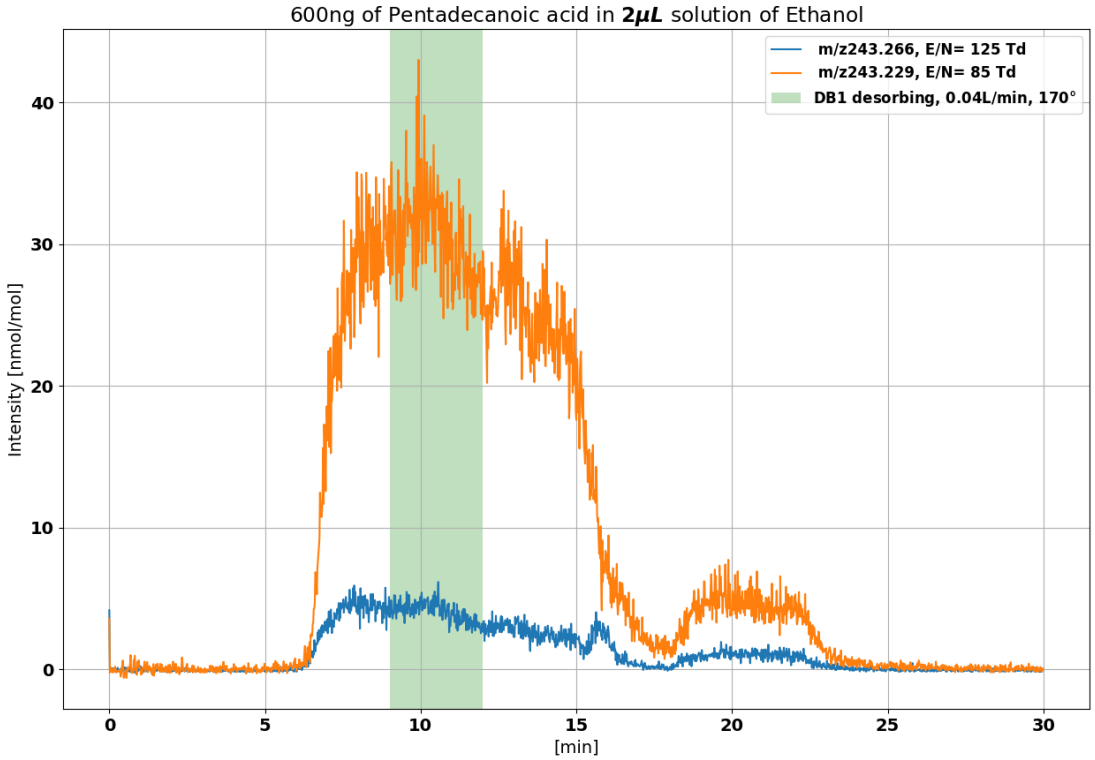

Figure 17: March 27^{th}, 2017: two experiments using the optimal DS entrance setup shown in Figure 15. E/N was varied while the insertion length remained at $40mm$ past the bolt entrance.

The influence of the drift tube electric field strength is obvious in Figure 17: when E is reduced, the amount of signal increases drastically because there is less fragmentation and more parent ions are detected. Though sample loss could also explain a drastic decrease, the drastic decrease was reproducible and a clear increase in signal was observed in all experiments applying a lower E/N. For example, in many cases, the Stearic acid parent ion was not detected when $E/N = 125Td$ but could be detected with low signal when $E/N = 85Td$ (i.e. Figure 18).

Overall, Pentadecanoic acid behaves differently than Decanoic acid as the signal is present when the flow direction is reversed and only the PEEK section is being heated (relative time: $6-9$min). The signal is still visible when the second DB1 denuder section is heated as well. This behavior may be due to contamination or the fact that this compound is less volatile and the six minutes of sampling with three minutes at a temperature of $170°C$ may not be sufficient to fully evaporate the SVOC. If the SVOC is still present on the spoon, this could explain why the SVOC signal extends beyond the three minutes corresponding to the first DB1 section.This theory is supported by the experiment results in Figure 18. Though the shape of the Pentadecanoic acid parent ion signal is different, the signal is drastically reduced at higher E/N and there is a large fraction of the signal in the PEEK section of the DS. In Figure 18, it is also notable that both compounds ($E/N = 85Td$) peak when the charcoal section is heated (relative time: $15-18$min) and the flow rate increases to $300mL/min$. Considering the signal during the entire nine minutes may yield better recovery results for heavier compounds.

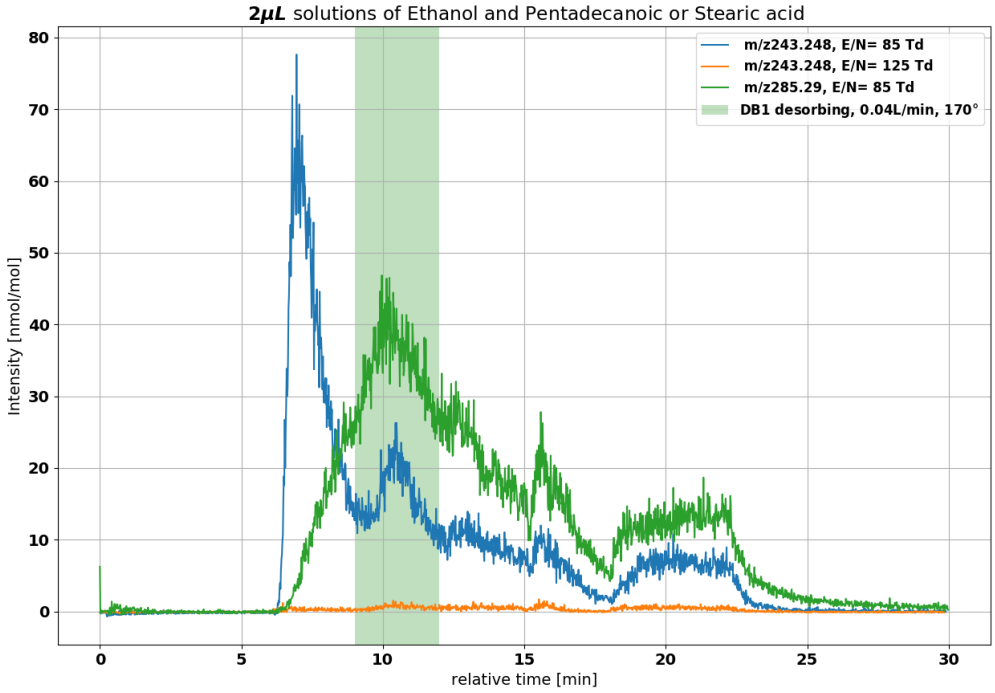

Figure 18: March 29^{th}, 2017: three experiments using the optimal DS entrance setup shown in Figure 15. E/N was varied while the insertion length remained at $40mm$ past the bolt entrance. Pentadecanoic acid (MW= $242.398g/mol$) was detected at both E/N but Stearic acid (MW= $284.477g/mol$) parent ion was only detected when $E/N = 85Td$.

Whenever the Stearic acid parent ion was detected, the signal displayed a peak when the DB1 denuder section was heating. An example is shown in Figure 18. This acid is the least volatile of the three main acids used; therefore, the compound may not fully evaporate during sampling. Unfortunately, the evaporation of the compound during sampling could not be investigated like the case with Decanoic acid (Figure 16b). Longer sampling periods and higher temperatures within the physical limits[12] should be explored in future experiments to accommodate less volatile, semi-volatile organic compounds. Testing slightly higher concentrations is recommended in the future as well. Nonetheless, Decanoic acid was used for further, extensive fragmentation investigation because of the clear signal it exhibited. The Decanoic acid solution was used for six runs with E/N ranging from $85 - 135$ Td. In each experiment, the parent ion was detected (19) as well as lighter ions with similar signal shapes.

[12]The physical limits of the heating elements are discussed in Appendix Section A.1

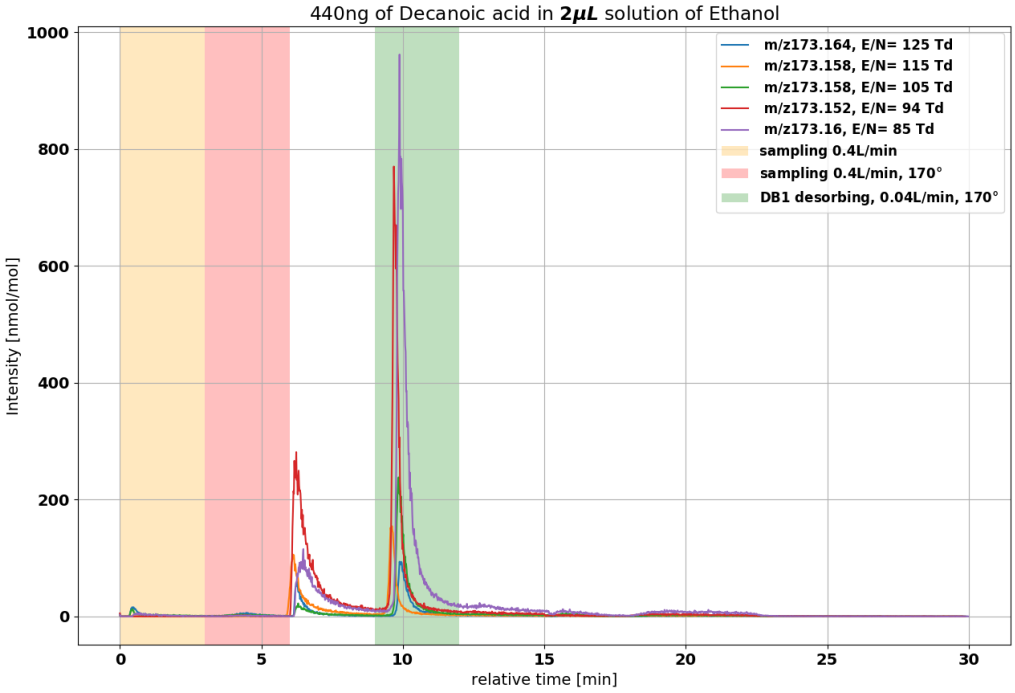

Figure 19: March 28^{th}, 2017: The signal corresponding to mass $m/z173$ for different drift tube electric field strengths. The DS sampling flow rate = $400mL/min$, the insertion length was $40mm$ past the bolt entrance of the final setup shown in figure 15.

For each run in Figure 19, a clear peak is observed when the DB1 denuder section is heating. Therefore, the DB1 coated denuder is performing well because the SVOC is colliding and condensing in this section, to be later desorbed during this time. Parallel to the case with Pentadecanoic acid, as the electric field strength decreases, the amount of fragmentation decreases and the signal of the parent ion is larger. Relatively little signal corresponding to the second DB1 denuder section (relative time: $12-15$min) is observed. However, a relatively large amount of signal is present when only the PEEK section is heated and the flow is reversed (relative time: $6-9$min). No clear trend is observed for this behavior but the signal may be caused by unintentional heating of the first DB1 denuder section when the adjacent PEEK section is heated. The sections may not be insulated well enough and a portion of the denuder section may be heated sufficiently to thermally desorb some of the compounds[13].

So far, a lower E/N yields the largest parent ion signal when the DB1 denuder section is heating. However, applying a lower E/N is not a clear means to improve results because the amount of water clusters ($m/z55.054$ Da) is expected to increase with lower energy collisions. Water clusters complicate detection in the PTR-ToF-MS because they can also react with the organic compounds. Additionally, for each run, lighter compounds were detected with peak shapes similar to that of the parent ion. Therefore, if present in significant amounts, these lighter compounds could potentially be fragments. The influence of electric field strength on fragmentation and water cluster formation is evaluated by comparing the amount detected to the corresponding E/N of each run in Figure 20. The counts are calculated by integrating the counts per second detected over the three minutes that the first DB1 denuder section is heated and collected SVOC parent ions are evaporated and transferred to the PTR-ToF-MS. Integration is done within Python using *scipy.integrate.simp* [10].

[13]The DS casing is removed and the sections are exposed in Figure 50

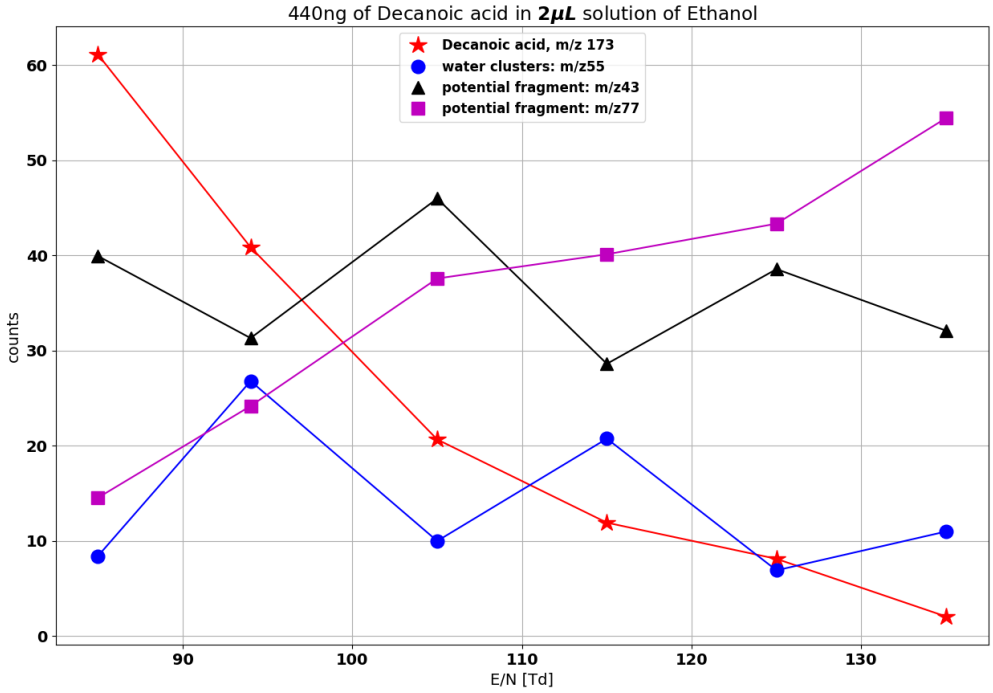

Figure 20: March 28th, 2017: The counts are calculated by integrating the counts per second when the DB1 denuder section is heating over the three minutes ($180s$). Any collected SVOCs are expected to evaporate during this time.

As expected, the parent ion ($m/z173$) decreases as E/N increases because fragmentation occurs more frequently at higher energy ionizing collisions within the drift tube. Potential fragments are expected to reciprocate by occurring more frequently as E/N increases. Two potential fragments were chosen because of their relatively large amount of counts and because of the similar peak shape. Though $m/z77$ appears to increase as E/N increases, as expected, no clear trend is seen for $m/z43$ (suggested match: C_2H_2O). Clearly, not all masses that are detected in large amounts are fragments of the parent ion. It is possible that fragmentation may also occur with Ethanol ($m/z47$), but these lighter compounds are expected to collect in the charcoal section of the DS. The large signal of lighter compounds may also be characteristic of DS contamination, the small amount of lab air present, or impurities within the solution.

The number of water clusters appeared to be unaffected by changing the energy of the collisions. Though this behavior is amicable for selecting a low E/N value, which is unexpected. Furthermore, the behavior of $m/z55$ appears to mirror $m/z43$ at different levels of E/N. Perhaps the signal was affected by other compounds which are not water clusters, such as $C_4H_6H^+$, $m/z55.098$. However, the exact charge-to-mass ratio detected here is $m/z55.055 \pm 2mDa$ which is a much closer match for water clusters ($m/z55.054$).

The results of this section suggest that fragmentation may be an issue when calculating the recovery of the SVOC administered. Fragmentation was further investigated by introducing the solution to a different PTR-MS to exclude the possibility of DS contamination (details in Appendix Section C.4). Similar results were observed so the signals are likely not from DS contamination. However, the possibility of impurities, compounds from lab air, and Ethanol fragmentation cannot be excluded. Therefore, a new method was developed to determine if these lighter compounds originate from the solution.

A series of blanks were developed so that the compounds originating from the solution could be identified. The blank runs involved no solution nor spoon but nitrogen was still provided during sampling. Blanks were executed for 10 consecutive runs where E/N = 125 Td immediately followed by ten runs where E/N = 85 Td. Any compounds that result from fragmentation of the parent ion should not be detected in absence of a sample. The integrated quantity of Decanoic acid for both cases is displayed in Table 1

and the calculations can be found in Appendix Section C.2.

Parent ion signal [ng]	E/N = 85 Td	E/N = 125 Td
Blank average	0.12	0.03
Decanoic acid solution	45.42	4.74

Table 1: This table displays the mass recovered for the Decanoic parent ion during experiments on March 29^{th}, 2017 alongside to the average blank results. The blank average is the average of the mass values corresponding to the 10 runs for each E/N.

There is a clear difference between the experiments which include the SVOC sample and the blanks. The amount of the parent ion that is detected during experiments that involve the solution is substantially greater than the blanks. Comparing the blank averages for each E/N, there appears to be a relative increase of approximately 4× when decreasing the electric field field strength. The decrease is much more substantial for the runs involving SVOC exposure. Potential fragments also exhibited larger signals during the experiments involving the SVOC solution. Caution is advised when extrapolating these results because Ethanol was not present during the blank measurements. Due to the drastic influence of the drift tube electric field strength on fragmentation, both E/N = 85Td and 125 Td will be considered when testing the denuder performance and calculating the recovery.

5.3 Results: recovery

In this section, the recovery is resolved for multiple SVOCs by comparing the mass detected from the first DB1 denuder section to the known quantity. The recovery is calculated for experiments using the optimized method of implementation where the SVOC sample is inserted to $40mm$ with the setup shown in Figure 15. From the previous section, it is predicted that the best recovery will be obtained when setting the drift tube electric field strength such that E/N = 85 Td. Also, an indirect recovery that incorporates the potential impact of fragmentation is calculated using the blanks.

To start, a unified mass list is created in *PTRwid* for each sample run and the 20 blank runs. This list and the corresponding $60s$ average volume mixing ratios are imported to the analysis code. The code sorts through each time (t) and compound (m) and identifies the experimental run using the time (Julian Date, JD), E/N (EN) and DS section heating temperatures (T1, T2, T3, T4). The signal is integrated and stored for each instance. and A section of the code, with comments, is shown below as an example.

```
for t in range(1,len(Data_blank[0])): # for each stored value (time)
    if Data_blank[JD][t] > 3009.45 and Data_blank[JD][t] < 3010.04: #Julian Date is within the
        time the blanks were executed
        if Data_blank[T3][t] < 100.0 and Data_blank[T2][t-1] < 100.0 and Data_blank[T2][t] >
            100.0 and Data_blank[T2][t+1] > 100.0 and Data_blank[T2][t+2] > 100.0: #first DB1
            denuder started heating
            if Data_blank[EN][t]>80.0 and Data_blank[EN][t]<90.0: #E/N = 85Td
                time_85_blank.append(Data_blank[JD][t]) #store the time
                for m in range(mass_start_blank,len(Data_blank)): #for each mass
                    EN_85_blank[m-mass_start_blank][t1]
                            =(scipy.integrate.simps(Data_blank[m][t:t+2],Data_blank[JD][t:t+2]))*(60.0*24.0)
                                # store the integral of the signal in the 3 minutes the DB1 is
                                heating
                t1=t1+1
            elif Data_blank[EN][t]>120.0 and Data_blank[EN][t]<130.0: #E/N = 125Td

...
```

To calculate the recovery, the volume mixing ratio is integrated over the three minutes[14] that the DB1 denuder section is heating [10]. The values are later converted to mass using the calculation shown in

[14] y-axis is in Julian Date, so the value is converted using $(60.0\frac{\text{sec}}{\text{min}} * 24.0\frac{\text{hr}}{\text{day}})$

Appendix Section C.2. For the blank runs, the values are stored for each individual run and then averaged to produce one value which can be compared to the experiment that sampled the SVOC solution. Then, the value corresponding to the parent ion during the blank is subtracted from the mass detected when the solution was inserted and this final result. The direct recovery is then calculated by dividing the mass detected from the DB1 denuder by the SVOC quantity administered (green shading in Tables 2 and 3).

The values corresponding to other detected compounds are also stored and evaluated. Potential fragments are identified by determining whether the mass detected when the SVOC was present is at least three standard deviations above the average value achieved during the ten corresponding blanks. Only compounds with charge-to-mass ratios above Ethanol but below the parent ion were considered. If this condition is satisfied, then the blank value is subtracted from the value detected when the SVOC was present and this final value is stored and sorted.The compounds which satisfy this condition are sorted by quantity and are converted to *ng* considering that the molar weight is that of the parent ion. The molar weight of the parent ion is used to compensate for the neutral compounds produced during fragmentation that cannot be detected. The indirect recovery is finally calculated using the parent ion added to the five highest fragments, divided by the amount administered (blue shading in Tables 2 and 3). Five fragments were chosen because it was considered unlikely to have more than five significantly contributing fragments.

Many compounds were tested and all experiments can be found in the online OneNote log and a complete list of solutions is available in Appendix Section C. However, the recovery was only calculated for five solutions shown in Tables 2 and 3. The experiments that are omitted yielded no signal for the parent ion at both electric field strengths.

Sample Organic Compound (Molar Weight)	Sample amount [ng]	amount during DB1 desorption [ng]	direct sample compound recovery [%]	including five potential fragments [ng]	indirect sample compound recovery [%]
Decanoic acid (172.26 g/mol)	440	9,8	2,2	186,4	42,4
Pentadecanoic acid (242.3975 g/mol)	600	0,4	0,1	55,1	9,2
Stearic acid (284.4772 g/mol)	710	-	-	-	-
Fluoranthene (202.26g/mol)	833	116,2	13,9	149,8	18,0
Aminobutyric acid (103.12g/mol)	260	0,2	0	132,5	50,9

Table 2: **E/N=125Td**. March 28^{th} – 29^{th}, 2017: The direct recovery (green) of the parent ion is determined by calculating the amount detected while the first DB1 denuder section is heated and dividing by the sample amount administered. Then, the mass of the parent ion is added to the mass of the five fragments with the highest quantities and the recovery is calculated indirectly (blue).

Sample Organic Compound (Molar Weight)	Sample amount [ng]	amount during DB1 desorption [ng]	direct sample compound recovery [%]	including five potential fragments [ng]	indirect sample compound recovery [%]
Decanoic acid (172.26 g/mol)	440	81,4	18,5	250,8	57,0
Pentadecanoic acid (242.3975 g/mol)	600	13,9	2,3	247,6	41,3
Stearic acid (284.4772 g/mol) *	710	51,7	7,3	-	-
Fluoranthene (202.26g/mol)	833	254,5	30,6	270,6	32,5
Aminobutyric acid (103.12g/mol)	260	0,1	0,0	17,0	6,5

Table 3: **E/N=85Td**. March 28^{th} – 29^{th}, 2017: The direct recovery (green) of the parent ion is determined by calculating the amount detected while the first DB1 denuder section is heating and dividing by the sample amount administered. Then, the mass of the parent ion is added to the mass of the five fragments with the highest quantities and the recovery is calculated indirectly (blue).
$*$ Stearic acid parent ion was detected when E/N = 85Td, but was not substantial so the compound was no longer present when a unified mass list was created for this run as well as the E/N = 125Td run and the 20 blanks.

Overall, the direct recovery is low for most compounds tested, especially when E/N = 125Td. Potential losses include sample loss during insertion and SVOCs being transferred at times other than when the first DB1 section is heating (i.e. when only the PEEK section is heated and the flow direction is reversed).

As expected, a higher mass of the parent ion was recovered for most compounds when E/N = 85 Td. Aminobutyric acid is an exception, but had near-zero values overall. In fact, Aminobutyric acid had a larger signal corresponding to the charcoal section which suggests that it can be classified as a VOC and the recovery should not be high in the DB1 denuder section. The less volatile, Stearic acid was not detected when E/N = $125Td$ and the mass recovered when E/N = $85Td$ was very small. Pentadecanoic acid was also poorly recovered at both electric field settings and is also less volatile than Decanoic acid. Considering the entire nine minutes that were shown to have a signal in Figure 17 did not yield significant improvement. Again, the low recovery and variation for these SVOCs may be related to the experimental method such that the heat may not have been sufficient to evaporate the entire amount of SVOCs provided. Flouranthene was administered in the highest concentration and has the highest recovery at both E/N settings.

The indirect recovery that includes the five highest contributing fragments performed better in all cases. The experiments with a lower drift tube electric field strength still yielded better results when incorporating the fragments. The best performance was observed when sampling Decanoic acid. However, a red flag is raised because there are limitations to the amount that can be detected by the PTR-MS and the drastic difference when considering the top five fragments would suggest that the fragments account for more mass than the parent ion itself. The highest contributing compounds for the Decanoic acid experiment with E/N = $125Td$, listed from highest to lowest contribution are $m/z75.033, 57.066, 149.056, 55.054, 61.031$. When E/N = $85Td$, the highest contributing fragments were $m/z57.066, 71.083, 85.097, 149.056, 103.079$. Some compounds appear in both cases, but the fact that $m/z77$ was not in this list and that water clusters appear to have occurred with a high contribution is strange[15]. Therefore, this method is not suitable to address potential fragmentation. Methods should be further developed to better resolve the recovery of the DS. For instance, blank methods that involve administering the aluminum spoon with pure Ethanol may help to identify the contribution from the SVOCs because any fragmentation from Ethanol will be present in the blank. [16]. A complete E/N study, similar to that of Materic et. al [**?**], could be developed for SVOCs, but this is beyonf the scope of this project.

5.4 Summary

Optimized and re-producible results were achieved when the setup minimized lab air intrusion (Figure 15) and when the solution was inserted to $30mm$ past the opening of the DS for adequate heating and evaporation. Despite the small recovery, a clear signal corresponding to the first DB1 denuder section was frequently observed after sampling a solution containing a SVOC. However, signal was also observed prior to heating the DB1 denuder sections which may have been caused by the PEEK section element heating the adjacent DB1 section as well. Therefore, residual signal from adjacent sections should be considered in the field measurements. More effectively insulating the sections could increase confidence in signal origin. In cases with less volatile SVOCs, the solution may not have evaporated completely which may have also produced behavior such as this. More extensively incorporating the mass detected in the neighboring sections may improve the SVOC recovery calculations. More experiments which extend the sampling time or increase the temperature within physical limits of the heating element are suggested to better resolve the performance of the denuder. Furthermore, using newly purchased compounds may also help to improve the results by eliminating potential impurities.

Though fragmentation is less common for proton transfer reactions compared to other conventional ionization methods (i.e. electron impact), fragmentation is still a concern for heavier gas-phase compounds such as SVOCs. Parent ion recovery improved when a lower drift tube electric field strength was applied. Quality of measurements did not appear to be sacrificed because water cluster formation was not observed to increase significantly. Applying and investigating lower E/N values is suggested for future field experiments. Accounting for fragmentation by comparing the parent ion recovered to the average of multiple consecutive blanks did not provide realistic results. The total mass of the five highest con-

[15] Water clusters appearing are strange for two reasons: Firstly, the value pertaining to the water clusters must be greater than the average blank value plus 3 standard deviation. Secondly, it is unexpected that the value was so large and significant during the run with a setting of E/N = $125Td$ instead of the E/N = $85Td$ run.

[16] One Ethanol blank was performed (E/N = $125Td$). $m/z75.036, 57.070$ and 149.058 still emerged as some of the highest detected compounds which surpassed the blank values.

tributing masses greatly outweighed the mass of the parent ion. However, incorporating Ethanol blanks or using an inorganic solvent such as water (if possible) in the future may shed more light on what signal can accurately be attributed to the parent ion.

6 Field Measurements at 200m CESAR

The Denuder Sampler and PTR-ToF-MS setup was stationed at the 200m of the Cabauw Experimental Site for Atmospheric Research (CESAR) from September, 2016 to January, 2017. However, only data from September-November is considered in the analysis due to technical difficulties (details in Appendix Sections A.1 and D.2). This section addresses the research objectives by further evaluating the performance of the new DS technique and providing a comprehensive analysis of the atmospheric results from rural Netherlands. An overview of the results is given before divulging into the DS performance and section results. The analysis is embellished by exploring the influence of different meteorological conditions. The partitioning coefficient is calculated to quantify the partitioning of compounds from gas phase to condensed phase.

6.1 Field measurement overview

The DS and PTR-ToF-MS combination produced results for 354 different compounds over the entire period of measurements. As expected, a large range of masses were detected, $m/z18 - m/z503$Da, as shown in Figure 21. Small volume mixing ratios were characteristic of many of these compounds. Figure 21 displays the upper domain of this mass range and corresponding raw volume mixing ratios. These volume mixing ratios are averages for each time the first DB1 denuder section was heated over the entire time period considered, Sept - Nov, 2016. The error bars depict the corresponding standard deviation.

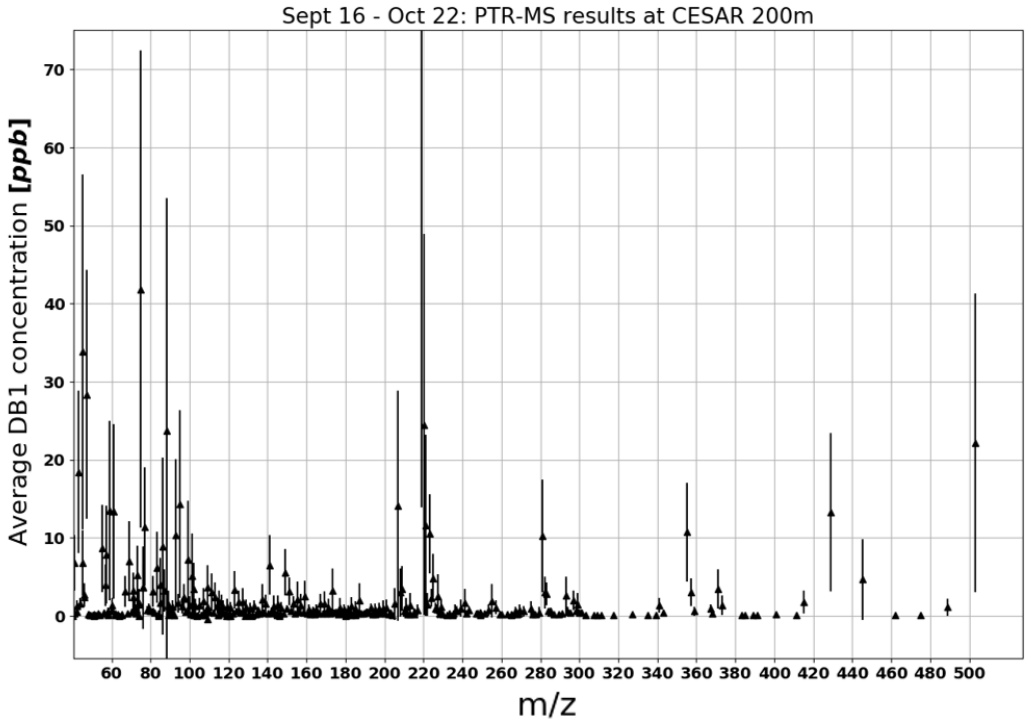

Figure 21: The values depicted here are the average volume mixing ratios detected when the first DB1 denuder section is being heated. These values are the average for all sampling times considered and the error bars correspond to the standard deviation. These volume mixing ratios have not been subjected to any corrections so they are with respect to the DS and not ambient air.

Many heavier compounds, which are likely SVOCs, are detected originating from the denuder, many of which appear in concentrations as low as $1ppb$ which highlights the importance of using a detector as sensitive as the PTR-ToF-MS for investigating SVOCs. Another interesting feature is that many compounds that are present in large concentrations, such as $m/z281$ and $m/z355$ have relatively high

standard deviations. Therefore, these signals may have contributions from alternating contamination or detection in ambient air with significant variation.

As explained in Section 4, the raw output from the PTR-ToF-MS must be corrected to be with respect to ambient air. The blanks are also incorporated to reduce the impact of any contamination. Then, the intensity of each compound is also converted to a mass density. The results are shown in Figure 22, which depicts the total mass concentration collected in the first DB1 denuder section at each time after sampling air. Each value of total mass concentration is the sum of each compound that was detected with the corresponding and nearest zero flow blank subtracted from each compound as well.

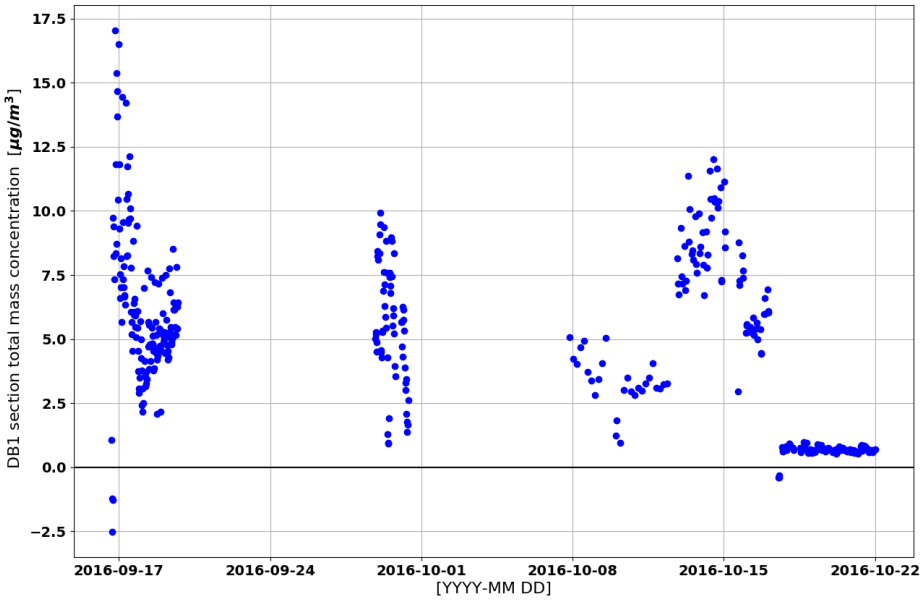

Figure 22: The points depicted here represent the total mass concentration each time the DB1 denuder was heated for three minutes after sampling ambient air. The point in time assigned is the second minute, mid desorption. Each value has been converted to be with respect to ambient air and has been corrected using the zero flow blank.

The total mass concentration detected in the first DB1 denuder section varied greatly over the course of the project. The results of this DS section are expected to represent SVOCs and this will be investigated in Section 6.3. The first values, on September 16^{th}, are much larger which may result from enhanced contamination as this was the first use of the setup. The large variation and potential influence of contamination is investigated next in Section 6.2. However, these results have been corrected using the zero flow blank and therefore the effects of contamination should be minimized. If the behavior is an accurate representation, and contamination is effectively removed, then the results suggest that less mass was collected in the SVOC catching section of the DS at most times in October. For example, a drastic and sudden decrease is observed during the time period of October $18^{th} - 22^{nd}$. The data collected after this period were within a similar range but in this case the first DS heating element is broken. However, the DS appeared to be functional at all points in this analysis; therefore, the result may be due to a drastic change in emissions or boundary layer conditions.

6.1.1 Ion subgroups

Compounds contributing to the total mass concentration in the DB1 denuder sections are expected to be SVOCs. Examining which ion groups are detected provides further information about what compounds exist in air and can be detected with this new collection technique. As described in Section 4, *PTRwid*

has the capability of assigning potential formula matches to the compounds. Potential matches for the 354 compounds were analyzed and the most suitable chemical formulae were attributed as described in Section 4.2. Some compounds had no suggested matches and are likely other groups such as metals or halogenated compounds so they were categorized as unidentified. Most compounds could be identified and categorized and a summary of the findings is shown in Figure 4.

Total ions detected (Sept-Nov):		354
Hydrocarbons (CH):		40
Oxygenated Organics (CHO):		213
N-compounds	(CHN):	4
	(CHON):	19
Unidentified (UN):		33

Table 4: The number of compounds that were found to be in each of the five ion groups

The clear majority are oxygenated compounds. nitrogen-compounds are less abundant, but this is partially due to deprioritizing matches that contained nitrogen when attributing the chemical formulas. However, the relative mass concentration of each ion group provides more information about the quantity of each ion group found in rural air. Figure 23 shows the relative contribution of each ion group considering the sum of the average mass densities of each of the compounds within that group. In Figure 23b, the average zero flow blank concentration for each compound is subtracted before adding to the total average mass concentration of that ion group.

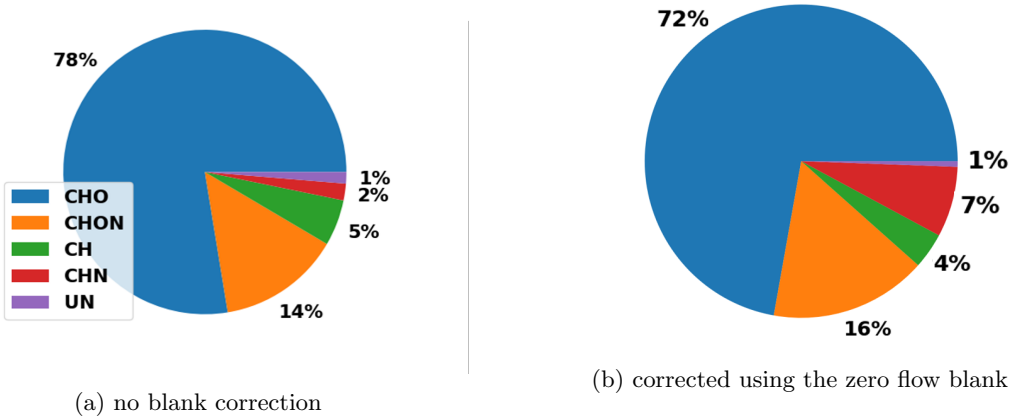

(a) no blank correction

(b) corrected using the zero flow blank

Figure 23: September 16^{th} - October 22^{nd}, 2016, shown in these pie charts is the relative average mass contribution by compound type for the DB1 denuder section. Ion group abbreviations are listed in Table 4

From Figure 23, it is clear that oxygenated compounds accounted for a large percentage of the total average mass concentration found in the first DB1 denuder section. Though a large number of the compounds were identified as hydrocarbons (CH), their relative contribution to the total average mass concentration is minimal. To investigate the potential variation of oxygenated compounds over time, the atomic ratio of oxygen to carbon is calculated. The hydrogen to carbon ratio was also calculated and the two ratios are compared using a Van Krevelen Diagram shown in Figure 24. The atomic ratios are calculated as follows:

$$\frac{O}{C} = \frac{\sum_i \frac{n_i N_{O_i}}{\mathrm{MW}_i}}{\sum_i \frac{n_i N_{C_i}}{\mathrm{MW}_i}}, \frac{H}{C} = \frac{\sum_i \frac{n_i N_{H_i}}{\mathrm{MW}_i}}{\sum_i \frac{n_i N_{C_i}}{\mathrm{MW}_i}}, \frac{N}{C} = \frac{\sum_i \frac{n_i N_{N_i}}{\mathrm{MW}_i}}{\sum_i \frac{n_i N_{C_i}}{\mathrm{MW}_i}} \tag{5}$$

where n_i is the mass density ($\mu g/m^3$) of compound species i and N_{O_i} , N_{C_i}, N_{H_i}, and N_{N_i} are the number of oxygen, carbon, hydrogen, or nitrogen atoms, respectively. MW_i is the molar mass of the compound. Each point, in Figures 24 and 56, pertains to one sample during the entire period of measurements. Initially, all detected compounds were considered and no blank correction was applied. In Figure 24b , only compounds with $m/z > 100$Da are considered to eliminate inorganic contributions and VOC compounds. Finally, in Figures 24c and 56b, the nearest zero flow blank is subtracted from each concentration prior to calculating the atomic ratios [17]. Clusters were visible and grouping different time periods (by color) effectively represented the clusters with some outliers.

In Figure 24a, a trend reflecting the change in season is observed but this result may be related to contributions of contamination or inorganic compounds. The trend became more clear in Figure 24b once lighter compounds were omitted (unlikely SVOC candidates). In addition to excluding lighter compounds, addressing potential contamination by subtracting the zero flow blank had an even greater impact on the atomic ratios and the visible trend. Overall, Figure 24 shows that compounds are more oxygenated in October than in September. This behavior suggests that compounds have been subjected to more oxidizing reactions and are relatively less volatile later in the fall. Typically, colder temperatures in October would facilitate the condensation of less volatile compounds, so detecting a large portion of these compounds was unexpected. However, SVOCs originate from VOCs which have been subjected to oxidizing air chemistry and VOCs are more abundant in the summer which may explain the 'aging' of the air as time progresses [18].

The results of Grannas et al. [13], suggest that a trend along this line in a Van Krevelen diagram signifies methylation, demethylation, or alkyl chain elongation depending on the direction. In this case, demethylation is likely such that the compounds have relatively less hydrogen over time. The DB1 coating is a polydimethylsiloxane and siloxanes are identified as potential containments that have many CH_3 groupings. Siloxanes were present in large amounts (addressed in Section 6.2.2) and therefore if proper background correction is not applied, the H/C atomic ratio can be distorted. However, siloxanes are also present in ambient air and the demthylation may be related to these highly contributing compounds. The nitrogen atomic ratio comparison was also calculated and the results are shown in Section D.1.

[17] Subtracting the nitrogen blank may be interesting in the future but this blank was not available at all times during these field measurements.

[18] Note that time scales of many SVOCs are less than the period of measurements

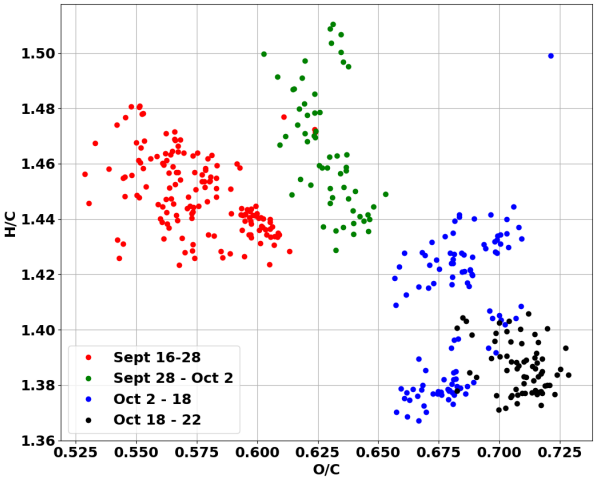

(a) All compounds are considered and no blank correction is applied

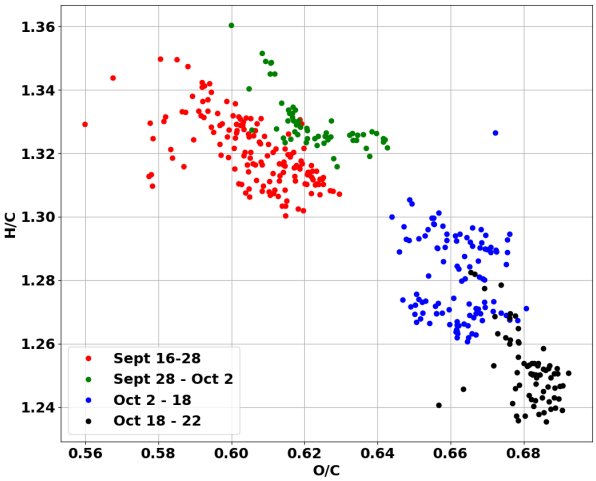

(b) $m/z > 100$Da but no blank correction is applied

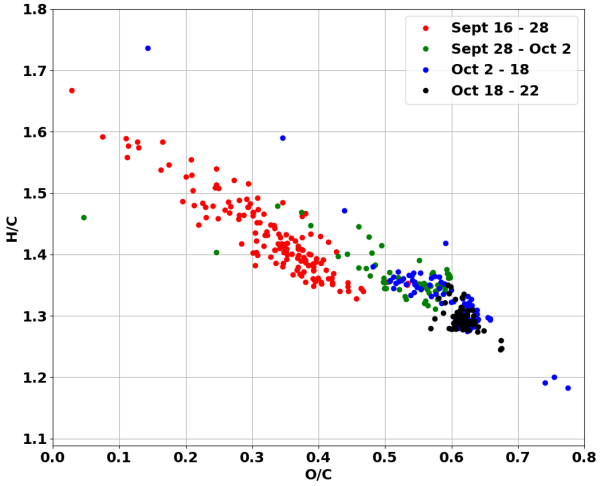

(c) $m/z > 100$Da and zero flow blank corrected

Figure 24: Van Krevelen diagram for all data points from September 16^{th} - October 22^{nd}, 2016

6.2 DS Contamination and Performance

6.2.1 DB1 denuder performance comparing both blank methods

Early in the project, the performance of each DB1 denuder section was compared quantitatively while also evaluating the performance of each blank method. Proper blank correction is an important consideration for this new SVOC collecting tool. The carryover between the two DB1 denuder sections was evaluated while considering the different blank corrections. The data used was collected during October $19^{th} - 21^{st}$, which is a time period that both blanks were executed properly. Data from actual DS cycles where ambient air was actually sampled was compared to each blank using a student T-test (details in Appendix Section B.2). The compounds which passed the T-test (p-value < 0.05) were considered to be veritably present in ambient air. The average concentration for each significant compound was summed after subtracting each corresponding average blank concentration. Compounds in the range $m/z < 40$Da are excluded because they are likely non-organic. The results are shown in Table 5.

	m/z >40		m/z >100	
	ambient - N_2	ambient - 0 flow	ambient - N_2	ambient - 0 flow
DB1 total $[\mu g/m^3]$	0.309	0.694	0.135	0.496
DB1 (2) total $[\mu g/m^3]$	0.266	0.345	-0.003	0.062
% in first DB1	**54**	**67**	**103**	**89**

Table 5: Considering October $19^{th} - 21^{st}$, 2016, these values are the sum of the average concentrations of all SVOCs above m/z40 Da or m/z100 Da, after subtracting the two blank methods. Only masses that were determined to be significant in ambient air were included. The criteria for significance was a student T-test ($p < 0.05$) which compares the measurements during $800mL/min$ sampling of ambient air to the two blank types.

The two blank methods compared reasonably in the range $m/z > 40$ which means that masses between $m/z40 - 100$Da are well captured by both blank methods. The zero flow blank produced higher signals than the nitrogen blank considering both mass ranges. This behavior was potentially due to siloxanes from the denuder column. Most potential siloxane matches exhibited a large average signal prior to blank correction in Figure 21. This theory is supported by the raw signal of a potential siloxane match shown in Figure 25.

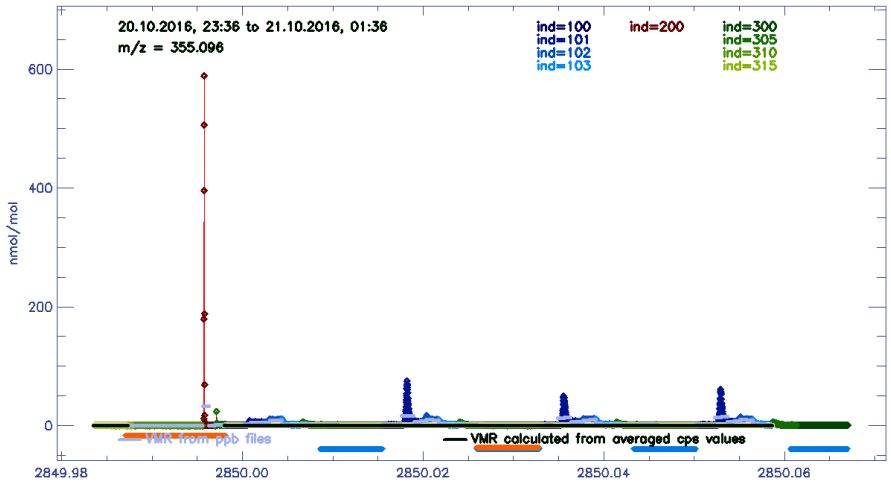

Figure 25: A *PTRwid* excerpt from the time period considered for the blank comparison is shown here for m/z355.096 Da (Potential match: $C_9H_{26}O_5Si_5$). The x-axis is the Julian Date from 01/01/2009. Index details in Section B.3. A zero flow blank (starting at JD = 2849.9873), followed by ambient air sampling (JD = 2850.0092), a nitrogen blank (JD = 2850.0266), and then another instance of ambient air sampling (JD = 2850.0440) are visible.

Figure 25 shows that this SVOC is largely detected in the first DB1 denuder section (ind = 101) compared to the second DB1 denuder section (ind = 102) as expected from the results in Table 5. In Figure 25, the signal results for the zero flow blank (Julian date = 2850.0440) are much lower than the result from the nitrogen blank (JD ~ 2850.035). Additionally, the nitrogen blank results have a similar shape compared to the ambient air results before and after this blank. Despite the similar shape, the peak corresponding to the time when the first DB1 denuder section is heated during the nitrogen blank is smaller compared to the two cases where air is sampled and more compounds are transfered to the PTR-ToF-MS. Nonetheless, a large reduction in signal is expected when subtracting the nitrogen blank.

The nitrogen blank also appears to produce more realistic results when considering compounds with m/z > 100Da in Table 5. This mass range excludes more VOCs and inorganics to better represent SVOCs. There is minimal carryover in the denuder sections for this mass range showing that most of the mass is collected in the first denuder section, as expected. The negative value is possible because, at such low concentrations, a small fluctuation in air can have a significant impact when subtracting a blank. The nitrogen blank method is suggested for future field measurements involving the DS. Further improvements can be made by executing the blank more frequently or developing a setup to implement the blank simultaneously with air sampling so that the blank results more accurately reflect the compared ambient air mass.

The performance of each DB1 denuder section over time is compared in Figure 26. Each point represents the total mass concentration found in that section after sampling ambient air. Blank corrections are applied as per the methods described in Section 4.4. Figure 26 shows that subtracting the zero flow blank yields higher values in the both first and second DB1 section. Both denuder sections suffer ~ 75% reduction in signal when subtracting the nitrogen blank compared to the zero flow blank. This behavior was also seen in Table 5 and is illustrated for a specific, high concentration, compound in Figure 27. The concentration of $m/z503$ detected in both sections while sampling air is shown alongside the blank results. The zero flow blank is more constant over time than the nitrogen blank and has consistently lower values. Therefore, by subtracting the nitrogen blank, the mass concentration is drastically reduced and the total mass in the DB1 section is also reduced. If $m/z503$ is purely from contamination, then the nitrogen blank provides the most realistic correction.

The total mass concentration for each denuder section in Figures 26a and 26b is also quite variable. A pattern appears in the variation such that the air sample following the zero flow blank is relatively higher. The blank concentrations for highly contributing individual ions were investigated but it was determined that there was no excessive variation to cause such a pattern (Example: red lines in Figure 27). In Figure 27, the nitrogen blank shows more variation, but the pattern is in fact largely caused by a pattern in the sample results. The highly contributing compounds, such as $m/z355.096$ (Figure 25), were further scrutinized and the pattern appears to be caused by a higher signal for the air sample executed after the zero flow blank relative to other sample results. The higher peak is observed in Figure 25 and this behavior was not limited to potential siloxanes nor October $19^{th} - 21^{st}$. Many compounds exhibited this behavior across the entire mass range. The impact of the relatively high peak is exacerbated for nitrogen blank corrections. Further examination also revealed that the variability and lower values observed when incorporating the nitrogen blank are likely caused by some key compounds (i.e. $m/z119.085$, Figure 28) which have higher signals during nitrogen blank desorption. Other compounds which exhibited this behavior were $m/z161.104, 177.136,$ and 179.12. More experimentation is required because the nitrogen blank was only implemented for a small period of the available data.

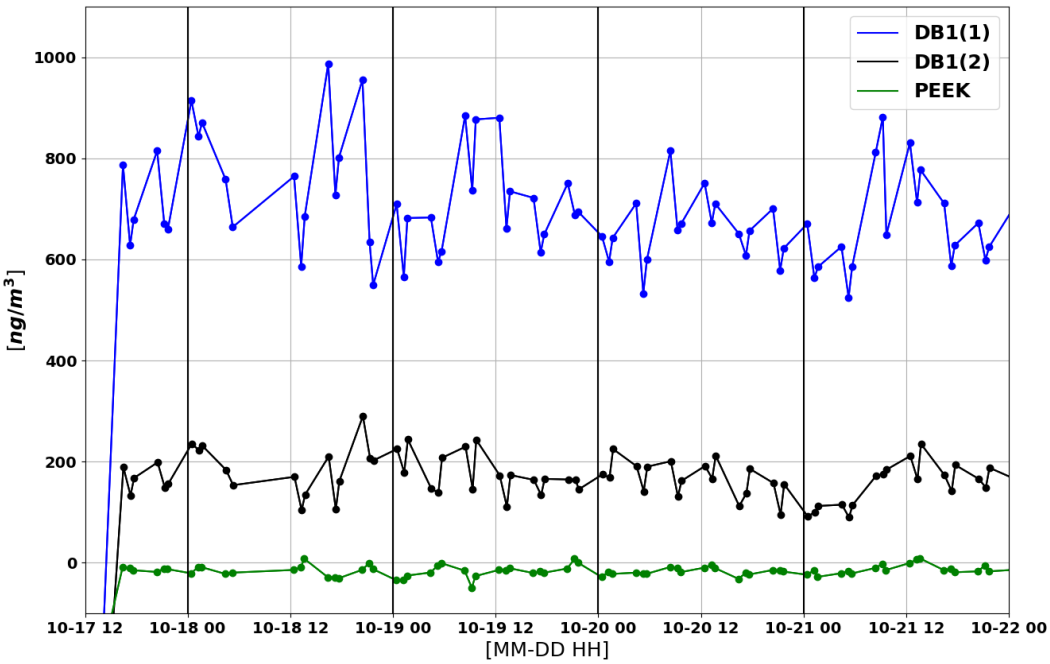

(a) **zero flow blank**

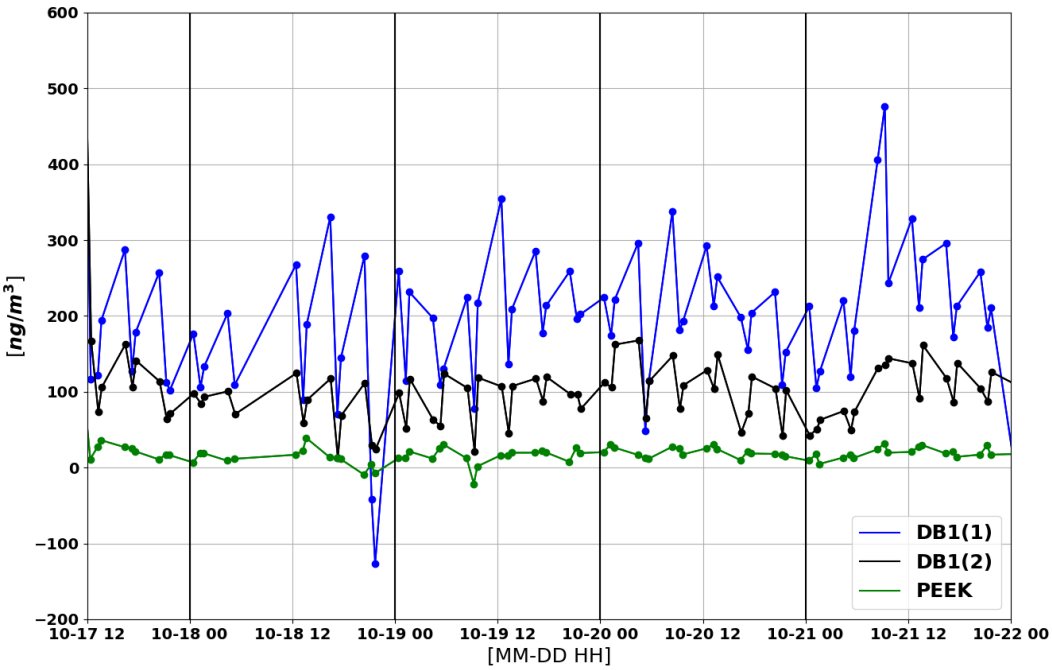

(b) **nitrogen blank**

Figure 26: Each point represents a time that a DS section is heating after sampling ambient air. The value is the sum of the concentration corresponding to each significant compound with $m/z > 100$ Da subtracting the nearest blank of interest.

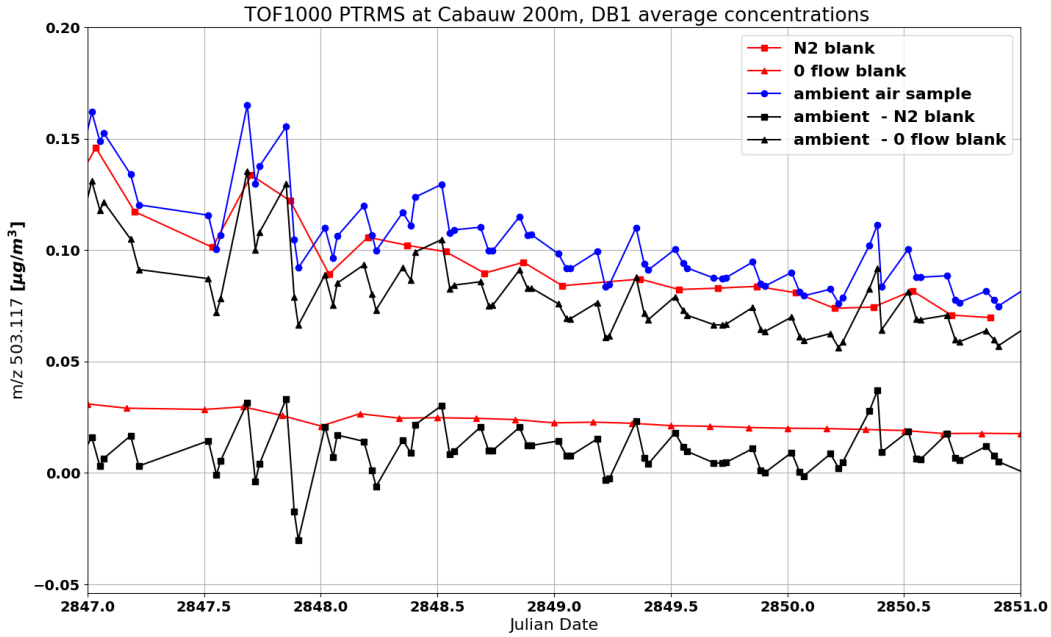

Figure 27: The average mass concentration detected while the first DB1 denuder section is heated for multiple samples is plotted here. The DB1 section results for each blank are pictured in addition to the corrected ambient air results.

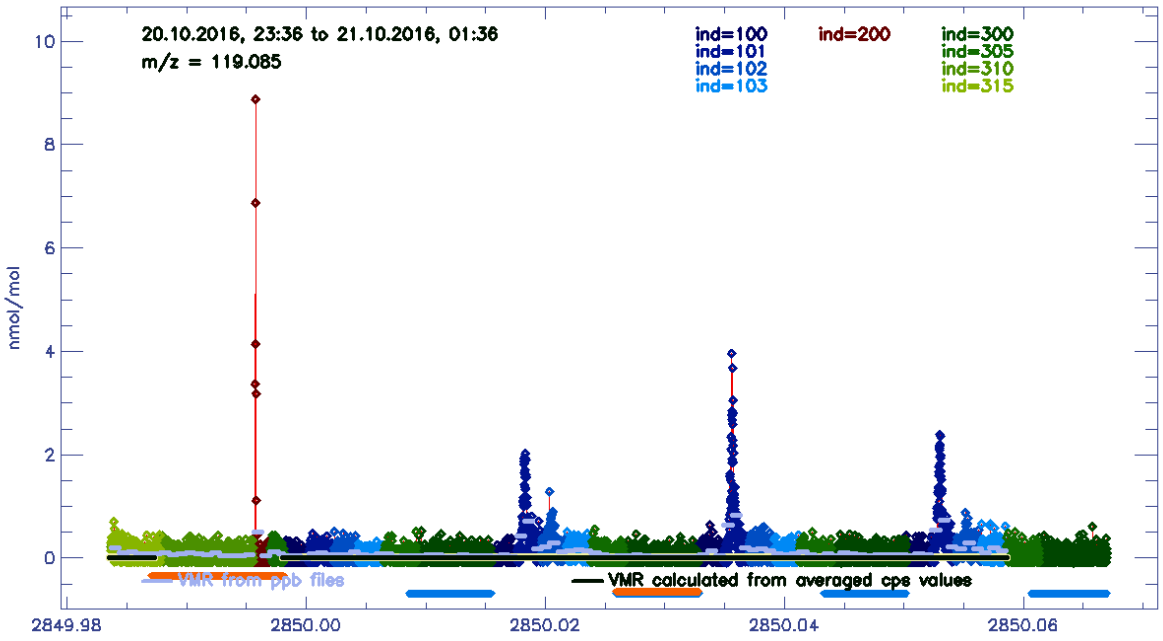

Figure 28: A *PTRwid* excerpt from the time period considered for the blank comparison is shown here for m/z119.085 Da. The x-axis is the Julian Date from 01/01/2009. Index details in Section B.3. A zero flow blank (starting at JD = 2849.9873), followed by ambient air sampling (JD = 2850.0092), a nitrogen blank (JD = 2850.0266), and then another instance of ambient air sampling (JD = 2850.0440) are visible.

6.2.2 Siloxanes

As concluded in the previous section, many individual compounds have a large and questionable relative influence on the total concentration detected in each section. In this section, siloxanes are investigated because these ion signals are expected to be partially due to contamination. This contamination, is predicted to accrue from the DB1 denuder section coating which is made of a polydimethylsiloxane. Siloxanes are compounds which have silicon-oxygen chains (Figure 29) which can connect in a ring. CH_3 compounds occupy the free bonds, but other variations of the siloxane can be present as listed below [19]:

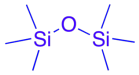

Figure 29

- Dodecamethylcyclo-hexasiloxane (D6): $m/z445.120$ ($C_{12}H_{36}O_6Si_6$), $m/z429.089$ ($C_{11}H_{32}O_6Si_6$)
- Decamethylcyclo-pentasiloxane (D5): $m/z371.101$ ($C_{10}H_{30}O_5Si_5$), $m/z355.070$ ($C_9H_{26}O_5Si_5$)
- Octamethylcyclo-tetrasiloxane (D4): $m/z297.082$ ($C_8H_{24}O_4Si_4$), $m/z281.051$ ($C_7H_{20}O_4Si_4$)
- Hexamethylcyclo-trisiloxane (D3): $m/z223.064$ ($C_6H_{18}O_3Si_3$), $m/z207.032$ ($C_5H_{14}O_3Si_3$)

Schematics and extensive details such as the vapor pressure, boiling point, and logP, are available for each compound in The Danish Ministry of the Environment's Environmental Project No. 1531 [14]. All of the listed compounds were detected throughout the field measurements. For example, raw signal excerpts for $m/z429$ from September and October are shown in Figure 30. Despite the fact that the total mass concentration in the first DB1 section was higher in September than October, this specific compound was present in larger quantities during this period in October. Furthermore, the results of the zero flow background are drastically different for both cases where the blank appears to exhibit higher signals in September. This result may be due to an increased about of contamination present when the experiment is started using the new DS causing higher values during the blank compared to actual samples. Other compounds, such as $m/z419$, 427, and 445 exhibited similar behavior. The cause is likely due to a large amount of contamination during the initial period of the field measurements, because $m/z419$ and 427 were only detected in September. $m/z503$ also showed signs of contamination in September. In Figure 31, it is the second DB1 denuder section which detects a higher signal during the zero flow blank. The same cannot be said for the first denuder section and the difference may be caused by a portion of the signal originating from compounds in the air. Clearly, this signal is influenced by contamination.

[19] These charge-to-mass ratios were calculated using *isotope list.xls*

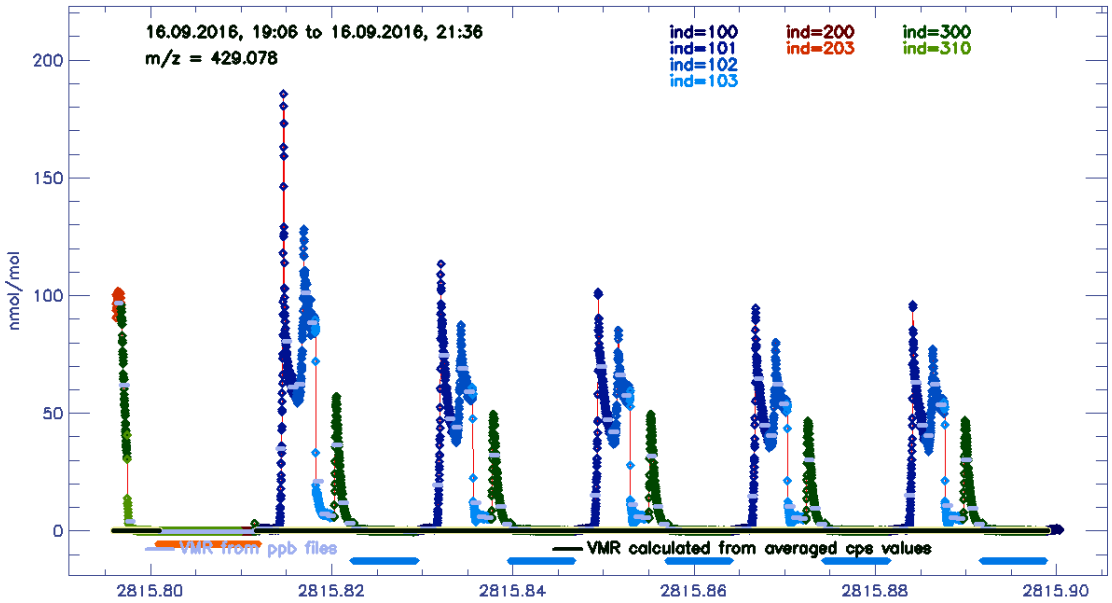

(a) A zero flow blank, starting at JD = 2815.801, is displayed. The nitrogen blank was not yet employed, so all following data picture is ambient air sampling.

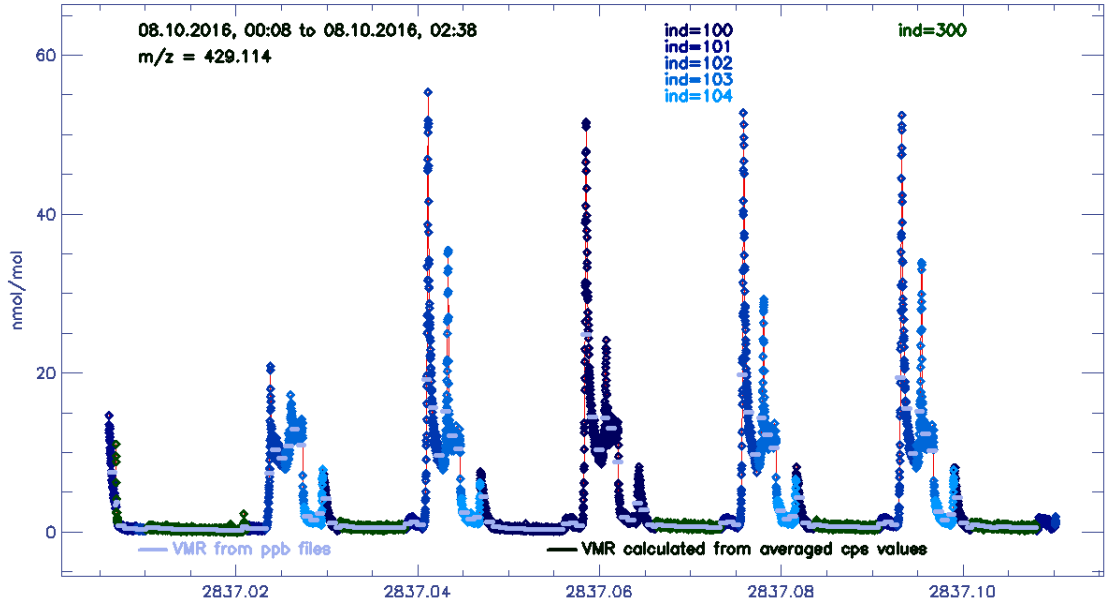

(b) A zero flow blank (starting at JD = 2837.0144), followed by ambient air sampling (JD = 2837.0315), a nitrogen blank (JD = 2837.0469), and then two other instances of ambient air sampling (JD = 2837.0662 and JD= 2837.0836) are visible.

Figure 30: *PTRwid* excerpt where the number indexes are applied using the robust October categorization listed in Appendix Section B.3. The x-axis is the Julian Date from 01/01/2009. Index details in Section B.3.

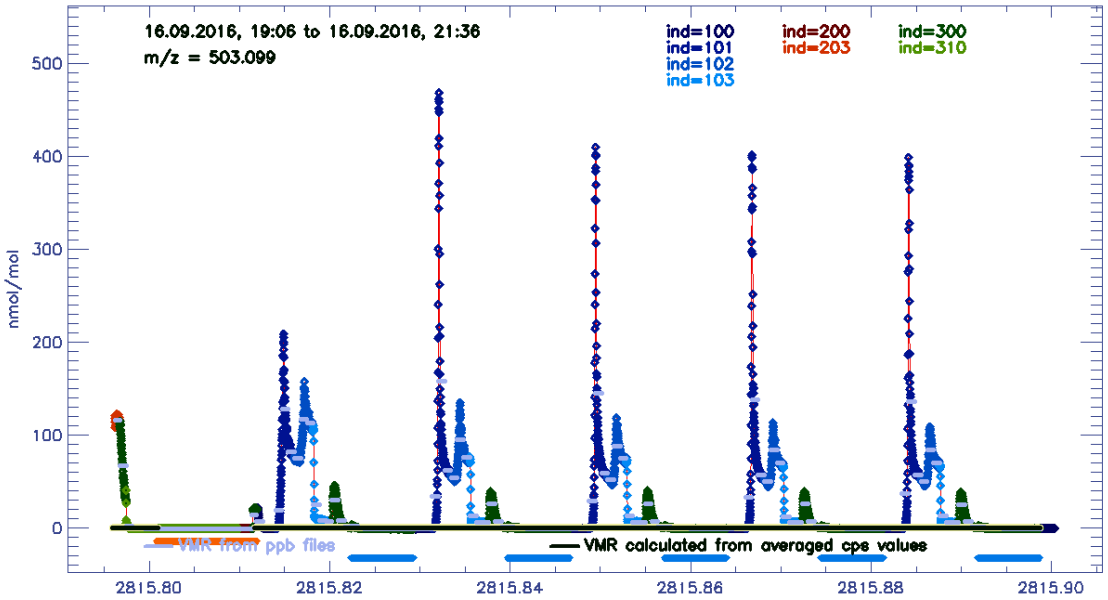

Figure 31: A *PTRwid* excerpt from the time period considered for the blank comparison is shown here for $m/z503.099$ Da. The x-axis is the Julian Date from 01/01/2009. Index details in Section B.3. A zero flow blank, starting at JD = 2815.801, is displayed. The nitrogen blank was not yet employed, so all following data picture is ambient air sampling.

The detected signal of siloxanes may not be solely from contamination. Siloxanes are a common pollutant that are used in familiar projects such as cosmetics, polishes, waxes and hair conditioners. For example, roughly 200 siloxanes and their derivatives are listed in the inventory of ingredients used in cosmetic products compiled by the European Commission INCI [14]. Once released in the atmosphere, these siloxanes may make their eventual way into the aquatic food chain or react with hydroxyl radicals. The Half-life in air for D4 is 16 days and 10 days for D5 which makes long term evolution of these compounds such as in the data available from our field measurements especially interesting [14]. Meteorological conditions were investigated to explore any relationship that could be found relating siloxanes in the atmosphere and not from contamination. The meteorological data such as mean temperature and wind speed at $200m$, precipitation, cloud cover fraction, cloud cover height and surface pressure from CESAR were available. The siloxanes which were detected in the highest quantities are shown in Figure 32 compared to the mean temperature and wind speed.

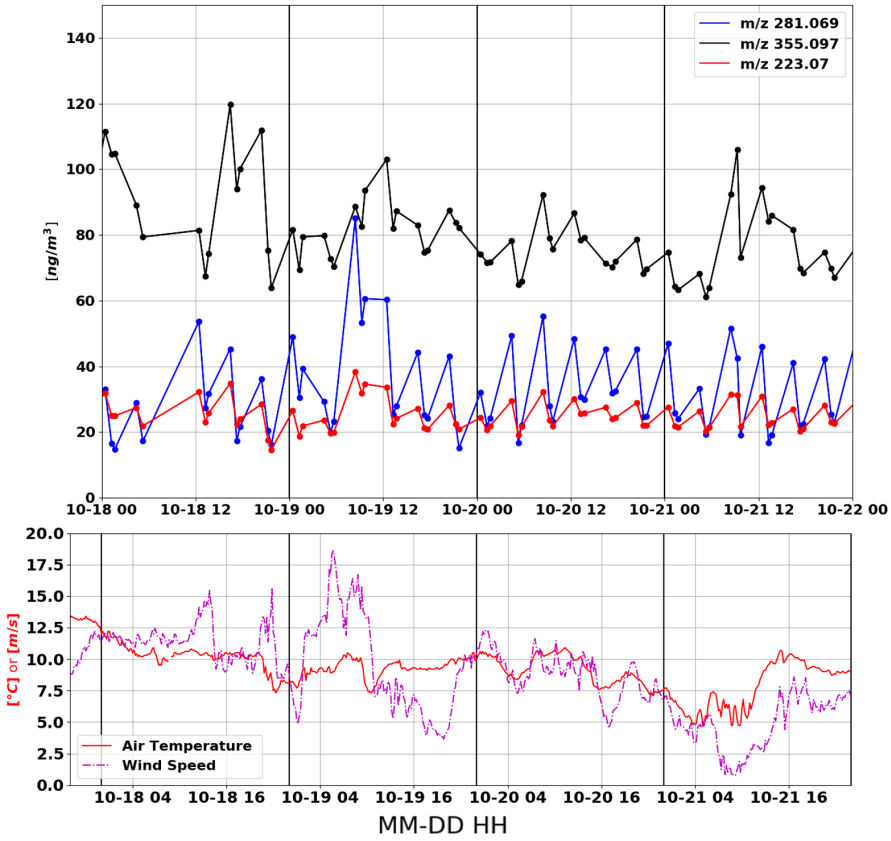

Figure 32: D3, D4, and D5 siloxane variation's mass concentrations corrected using the zero flow blank.

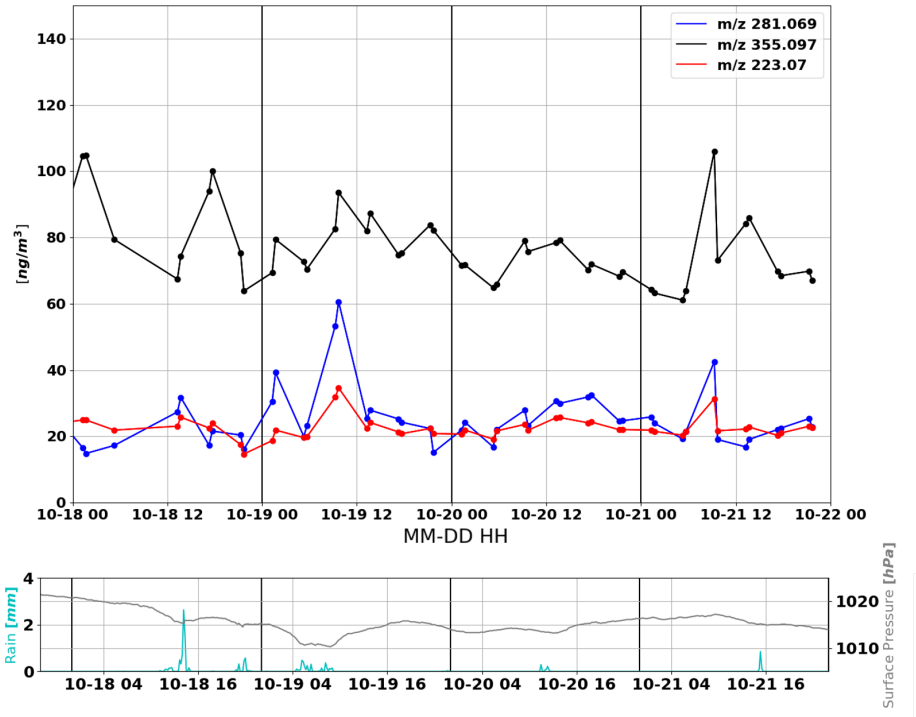

Figure 33: D3, D4, and D5 siloxane variation's corrected using the zero flow blank but the ambient air sampling directly after the zero flow blank is removed.

The values in Figure 32 have been corrected for contamination, so it is expected that what remains is found in air; however, this claim is questionable using the zero flow blank. A clear pattern is observed such that the value corresponding to air sample directly after the zero flow blank is relatively higher. These points are removed to give a clearer picture of the actual variation of the compounds and the results are shown in Figure 33. The increase in $m/z355$ just before October 19^{th} and the increase in $m/z281$ around noon may be related to sudden relative increases in wind speed which facilitates boundary layer mixing. An increase in SVOCs is expected in this case with an increase in mixing of the boundary layer transporting emitted siloxanes to the $200m$ height and therefore, these siloxane measurements may in fact represent what is in the atmosphere and not contamination after correction. However, these increases as well as the increase in each compound just before noon on October 21^{st} seem to occur around rain events as well, though the latter compound increase is just before the rain event. Field measurements in four locations in Denmark[20] produced average air concentration measurements of D4 and D5 in the range $0.26-2.4\mu g/m^3$, $0.19-1.3\mu g/m^3$, respectively [14]. The D5 range compares reasonably to our the mass concentrations detected during our field measurements. The mass concentration for D5 was slightly lower than the Danish field measurements, as the concentration varied between $0.6-1.1\mu g/m^3$ in Figure 33. The range observed for D4 was approximately ten times lower than the Danish field measurements' range. Perhaps the blank correction in our field measurements overcompensates or these compounds may simply be less abundant in air at this time. Despite the fact that these compounds are clearly present in ambient air, siloxanes may still be produced as contamination from the DS.

6.2.3 Reducing the sampling rate to limit DS contamination

The sampling flow rate was altered to explore the impact of potential siloxanes originating from the DB1 material. Decreasing the sampling flow rate was hypothesized to reduce the amount of contamination from the DS materials though sacrificing the total amount and thus trace gases sampled in the same time. The four hour cycle was changed so that after the zero flow blank, air sampling at $800mL/min$, the nitrogen blank, and two more air sampling cycles at $800mL/min$, the following air sampling cycles employ flow rates of $700mL/min, 600mL/min, 500mL/min$, and $400mL/min$. The results are shown in Figures 34 and 35. In Figure 34, raw data for two D5 siloxane species are shown for one full four-hour sequence. A large fraction of the uncorrected signal from these compounds is assumed to be contamination from the DB1 coating and the amount may be significantly reduced at lower flow rates. The horizontal lines denote the maximum values of the peaks that occur when the first DB1 section is heated.

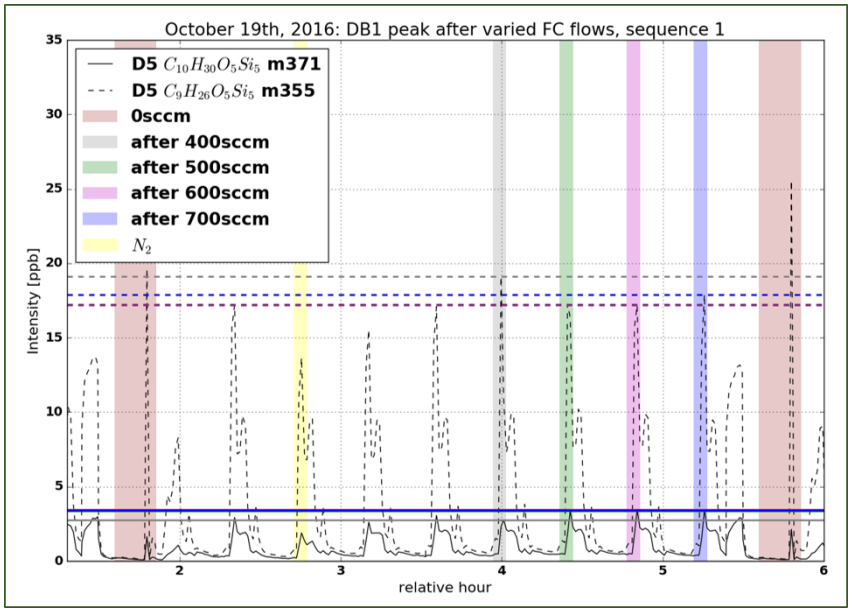

Figure 34: The maximum raw volume mixing ratio corresponding to the three minutes when the first DB1 denuder section is denoted by a horizontal line for the four cases where the sampling flow was reduced for two siloxanes.

[20] Three measurements were executed outdoors and one was taken inside a sewage treatment plant.

Clearly, when the flow is reduced, i.e. 400sccm = $400mL/min$ at standard conditions ($0°C$, seal level pressure), there is no significant reduction in the peak. Therefore, contamination is likely not alleviated significantly by using lower sampling flow rates. Four compounds with large raw signals are investigated by calculating the average values corresponding to the six four-hour sequences that day for the different sampling rates. The results are shown in Figure 35. No corrections are made for contamination because the objective is to observe potentially changing contamination contributions. These compound signals must be largely due to contamination because the raw signal for a compound that is actually in ambient air will decrease if the sampling flow is decreased. Furthermore, no clear trend suggests that by reducing the sampling flow rate, the contamination can be decreased either. A comprehensive analysis of all compounds detected during this time may reveal which compounds were detected in ambient. In fact, the relative contribution of contamination seems quite constant for these rates. The same conclusion was made during the controlled lab experiments. Implementing and testing even lower flow rates may be useful in future field measurements.

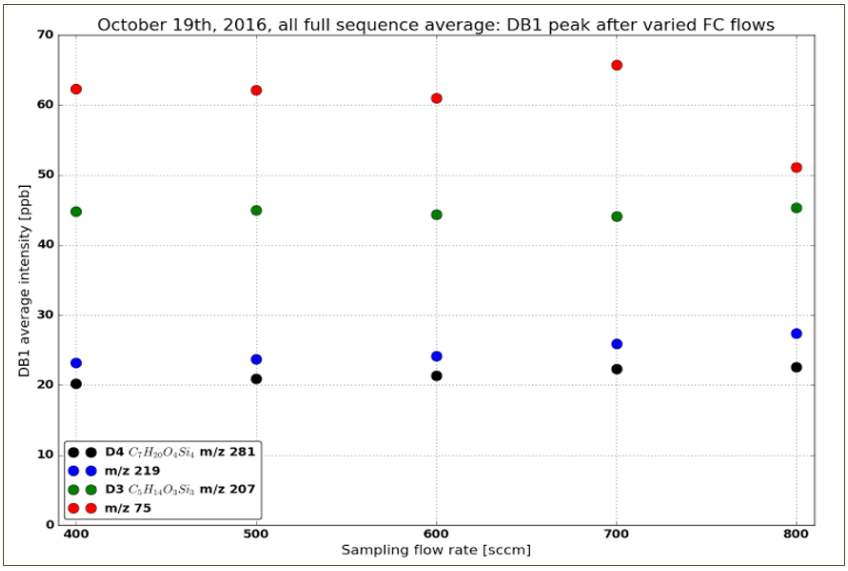

Figure 35: The average raw volume mixing ratio is stored and averaged for the six four hour cycles on October 19th, 2016 for four compounds with the highest concentrations.

6.2.4 Highly contributing compounds

Multiple compounds, aside from the siloxanes, also contributed to contamination or exhibited unexpected behavior that strongly influenced the results. For instance, in Figure 28, the contribution from the second DB1 denuder section is relatively low compared to the same compound in September shown in Figure 36. Other compounds such as $m/z120$ and 133 also exhibit this behavior in September. This suggests that the results from these compounds may have been enhanced by contamination present at the beginning of the field measurements.

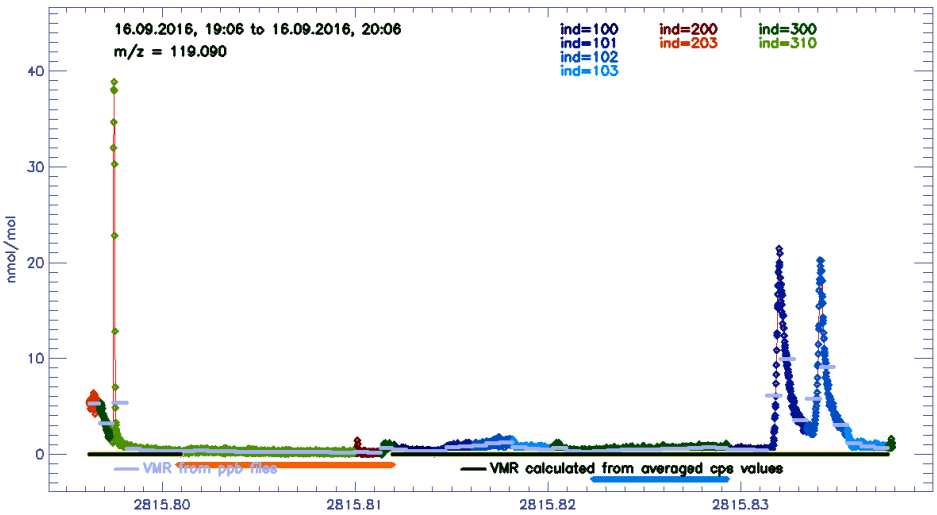

Figure 36: A *PTRwid* excerpt from the time period considered for the blank comparison is shown here for $m/z119.090$ Da. The x-axis is the Julian Date from 01/01/2009. Index details in Section B.3. A zero flow blank, starting at JD = 2815.801, is depicted, followed by air sample results.

Other unexpected behavior is seen for some compounds, such as $m/z231$, which display a signal during the zero flow sampling stage of the zero flow blank in September. More importantly, many compounds such as $m/z141, 219, 275, 276, 293$, and 294 show an elevated signal that is not characteristic of most compounds and may not be adequately handled by the current method of incorporating the zero flow blank. Examples are shown for $m/z219$ (Figure 37) which contributed largely to the total concentration in each of the DS sections (PEEK included) even after blank corrections. Upon investigation, (Figures 37a, 37b, and 37c), it was observed that the compound had high amounts of signal at all times, including while sampling ambient air.

The best match for this specific compound is $C_8H_{10}O_7$. The expected separate peaks when the different DS sections are heated was not observed. A broad contamination peak is present when both of the DB1 denuder sections are heated which suggests that the results do not necessarily represent compounds collected in each section individually. It is clear from these Figures that the raw volume mixing ratio only reaches zero during the zero flow 'sampling'. The PTR-ToF-MS inlet constantly has a flow of $32-38mL/min$ at all times the signal is elevated. It appears that this compound is not from ambient air but contributes contamination whenever a flow is going through the DS. The large, raw signal above the base decreases from September to October which is consistent with the decrease of total mass contribution in the DB1 denuder section.

Despite blank corrections, certain compounds contributed highly to the total mass concentration in every section of the DS. It is possible that compounds are detected in ambient air, but heavy compounds should not appear to originate in the PEEK section. The mass concentration of compounds are expected to be zero in the PEEK section. However, in October, the following compounds had the highest mass contributions corresponding to the PEEK section: $m/z219.050, 355.097, 371.123, 429.117, 445.133$, and 503.117. Other compounds, such as $m/z207.053$ and 223.07 had the lowest, negative mass concentrations. Therefore, these specific compounds are not corrected properly by the zero flow blank. Most of these compounds have potential siloxane matches. These results suggest that the zero flow blank under or over corrects for certain siloxanes. Specifically D5 and D6, the heavier siloxane variations, may be better compensated with the nitrogen blank. Meanwhile the D3 variation is clearly over-corrected by the zero flow blank. In October, the compounds with the highest concentration that are detected from the first DB1 section are $m/z219.050, 281.069, 355.097, 429.117$, and 503.117. Over-corrected negative contributions come from compounds $m/z207-210$. Similar excesses or deficits were repeatedly seen for these compounds in all DS sections. Therefore, different correction methods should be developed to manage these compounds so that the amount detected in the denuder sections represents the amount in ambient air.

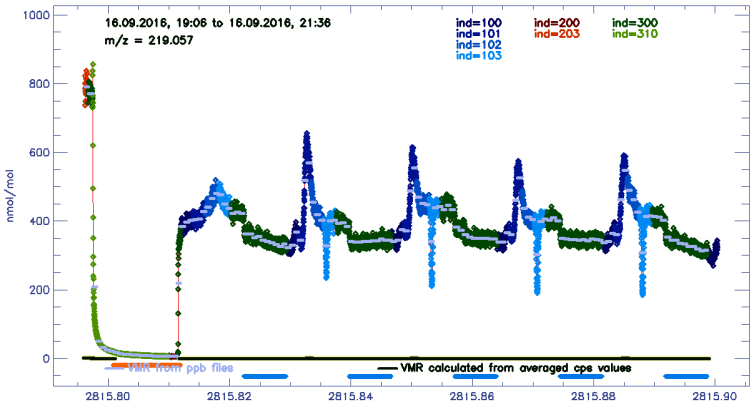

(a) A zero flow blank, starting at JD = 2815.801, is displayed. The nitrogen blank was not yet employed, so all following data picture is ambient air sampling.

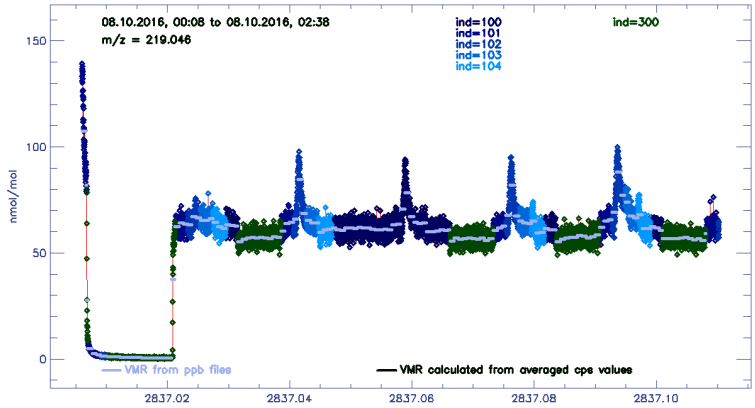

(b) A zero flow blank (starting at JD = 2837.0144), followed by ambient air sampling (JD = 2837.0315), a nitrogen blank (JD = 2837.0469), and then two other instances of ambient air sampling (JD = 2837.0662 and JD= 2837.0836) are visible.

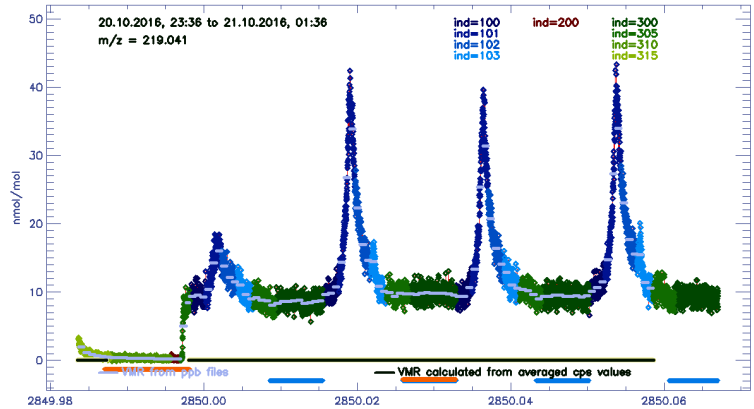

(c) A zero flow blank (starting at JD = 2849.9873), followed by ambient air sampling (JD = 2850.0092), a nitrogen blank (JD = 2850.0266), and then another instance of ambient air sampling (JD = 2850.0440) are visible.

Figure 37: *219* excerpt where the x-axis is the Julian Date from 01/01/2009. Index details in Section B.3.

6.3 DS results

6.3.1 Average total mass concentration

The average total mass concentration found in each DS section is shown below in Table 6. The value is calculated by summing the average total mass concentration of all compounds with $m/z > 100$Da that were determined to be significant in air using a student T-test ($p < 0.05$). Most masses passed the student T-test for comparing the data sets of samples and each blank for the entire time period. Due to the high amount of compounds detected in the PEEK section, the p-value limit was made more exclusive. The limiting p-value was reduced to 0.01 but this did not drastically influence the number of masses which passed. This result may be due to the large amount of variation over the entire time period. Other methods for determining significance should be developed for future analysis of this data. For instance, perhaps the volume mixing ratio from the air sample should be three standard deviation above the average value corresponding to the nearest blank volume mixing ratio. For this analysis, the data set was also modified, removing flagged, highly contributing compounds. The results for the modified mass list is shown in Table 6 as well.

	all compounds $m/z > 100$	flagged ions removed
DB1 $[\mu g/m^3]$	8.86	1.1896
DB1 (2) $[\mu g/m^3]$	4.37	-0.0666
% in first DB1	**70**	~ **100**
Charcoal $[\mu g/m^3]$	2.78	-0.6167
PEEK $[\mu g/m^3]$	1.88	-0.1788

Table 6: September 16^{th} - October 22^{nd} and $m/z > 100$ Da. These values are the sum of the average concentrations of all SVOCs subtracting the average zero flow blank. Only masses that were significant in ambient air were included. The criteria for significance was a student T-test ($p < 0.05$) which compares the measurements during $800mL/min$ sampling of ambient air to the zero flow blank. A modified dataset which omitted flagged compounds was also evaluated. Flagged compounds: m/z 207.053 – 210.039, 219.050, 220.051, 223.070, 275.114, 276.120, 293.102, 294.110, 355.097, 371.123, 429.117, 445.133, and 503.117.

As expected, when considering compounds with $m/z > 100$ Da, the highest mass concentration is found in the first DB1 denuder section. The lowest concentration is found in the PEEK section but there is still a higher concentration than expected which is likely due to contamination. The concentration is reduced drastically when the highly contributing compounds are removed. When the flagged compounds are removed, all of the mass concentration from SVOCs is collected in the first denuder section. The total average concentration of compounds in the charcoal section is low for both data sets because the VOCs that collect in this section are typically $m/z < 100$Da. To confirm that heavier compounds are responsible for the large mass concentration in the DB1 section, the relative contribution from different mass ranges are investigated. SVOCs are expected to appear as heavier compounds and the results are shown in Figure 38.

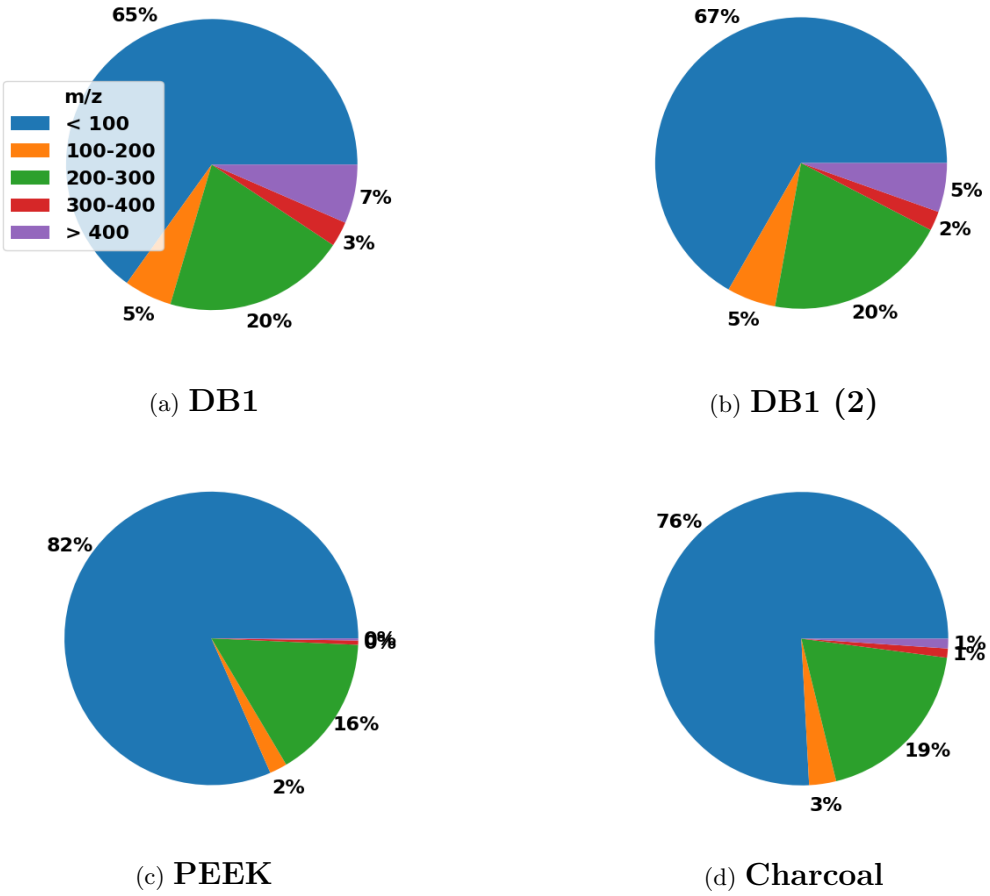

(a) **DB1** (b) **DB1 (2)**

(c) **PEEK** (d) **Charcoal**

Figure 38: Average mass concentration for each DS considering relative contributions from different mass ranges. No blank corrections are applied.

The relative amount of mass contribution from compounds with $m/z > 200$ Da is higher in the DB1 denuder sections, shown in Figure 38a and 38b, than the PEEK and Charcoal sections in Figures 38c and 38d. This result suggests that these sections are, in fact, catching SVOCS. Some SVOCs may also be present in the $m/z 40 - 100$ range, but these compounds are more likely to be VOCs.

The unanticipated amount of mass contributed by lighter mass ranges may be due to the fact that all masses were considered including the compounds which are likely inorganic. In the PEEK section in Figure 38c, most compounds that were detected had charge-to-mass ratios which were below 100 Da. The relative total mass concentration of these compounds in total compared to that of the denuder sections is minimal as shown in Table 6. A similar mass range is observed in the charcoal denuder section which is expected because the VOCs which collide and condense there typically have charge-to-mass ratios below 100 Da. Near-zero amounts of heavier masses above 300 Da are seen in both of these sections. Nonetheless, the relative contributions will likely be more accurately represented if the inorganic compounds are excluded and if the mass concentrations are blank corrected.

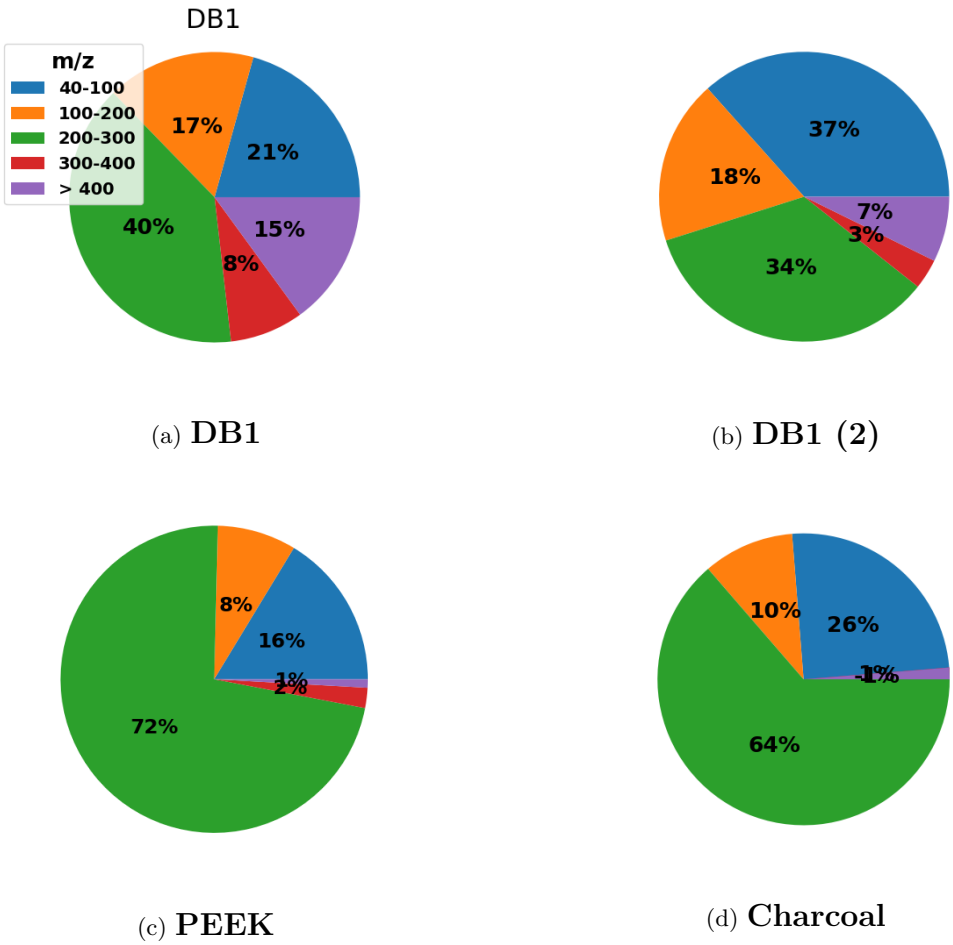

(a) **DB1** (b) **DB1 (2)**

(c) **PEEK** (d) **Charcoal**

Figure 39: Average mass concentration for each DS considering relative contributions from different mass ranges. Here, compounds with $m/z < 40$ are excluded and the average zero flow blank has been subtracted from each compound's average mass concentration.

The total average concentration for each section was recalculated omitting the inorganic compounds and subtracting the zero flow blank. The results, shown in Figure 39, are drastically different with much less relative mass concentration found in the range $m/z40 - 100$ Da. Again, little to no mass is detected corresponding to $m/z > 300$ in both the PEEK and charcoal sections. Compounds with $m/z > 300$ were mostly detected in the DB1 sections. Overall, the relative contribution from the $m/z200 - 300$ range increased for all DS sections. It is important to note that compounds with the highest mass concentrations, such as $m/z219$ typically occupy this higher mass range as well. These compounds were not effectively reduced using the zero flow blank and therefore the large relative contribution of this mass range, i.e. in the PEEK section, may result from these compounds.

6.3.2 Temporal evolution DS section results

The total mass concentration found in each section was calculated for the entire period. The results for the two DB1 denuder sections are plotted in Figure 40 in addition to the PEEK section for comparison.

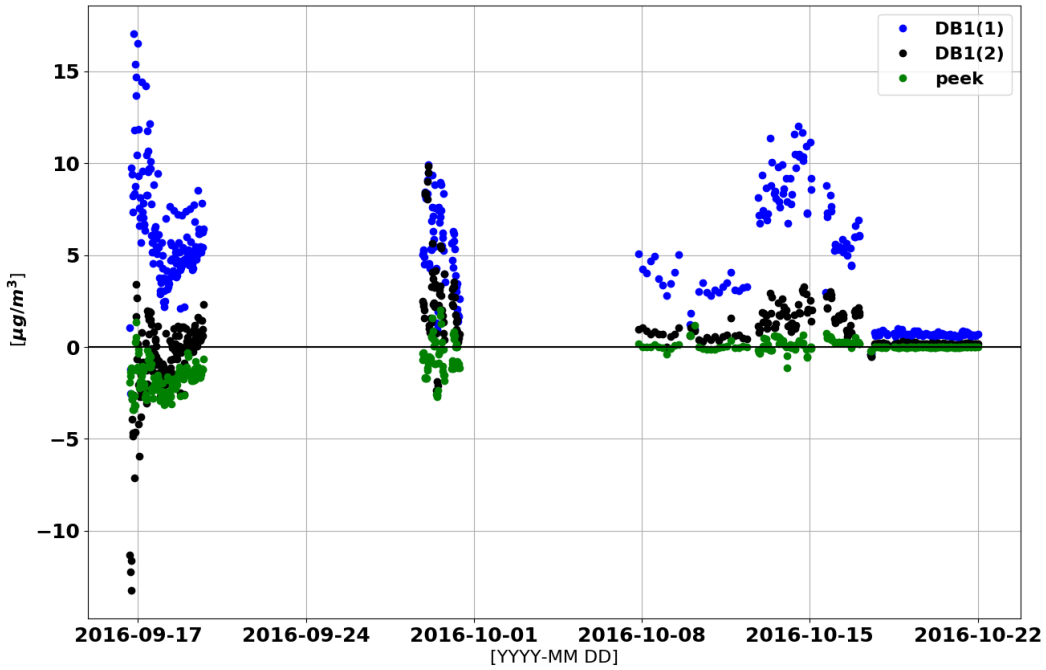

Figure 40: The points depicted here represent each time that the selected DS section was heated after sampling ambient air. The values are the total mass concentration for each compound detected in the corresponding section. Each value has been converted to be with respect to ambient air and has been corrected using the zero flow blank.

As expected, though a large amount of variation is observed, the first DB1 denuder section almost consistently has a total mass concentration higher than the second DB1 section. The high amount of variation was investigated and drastic variations in the raw volume mixing ratios were responsible. Therefore, the meteorological conditions were investigated and a weather overview is shown in Figure 41.

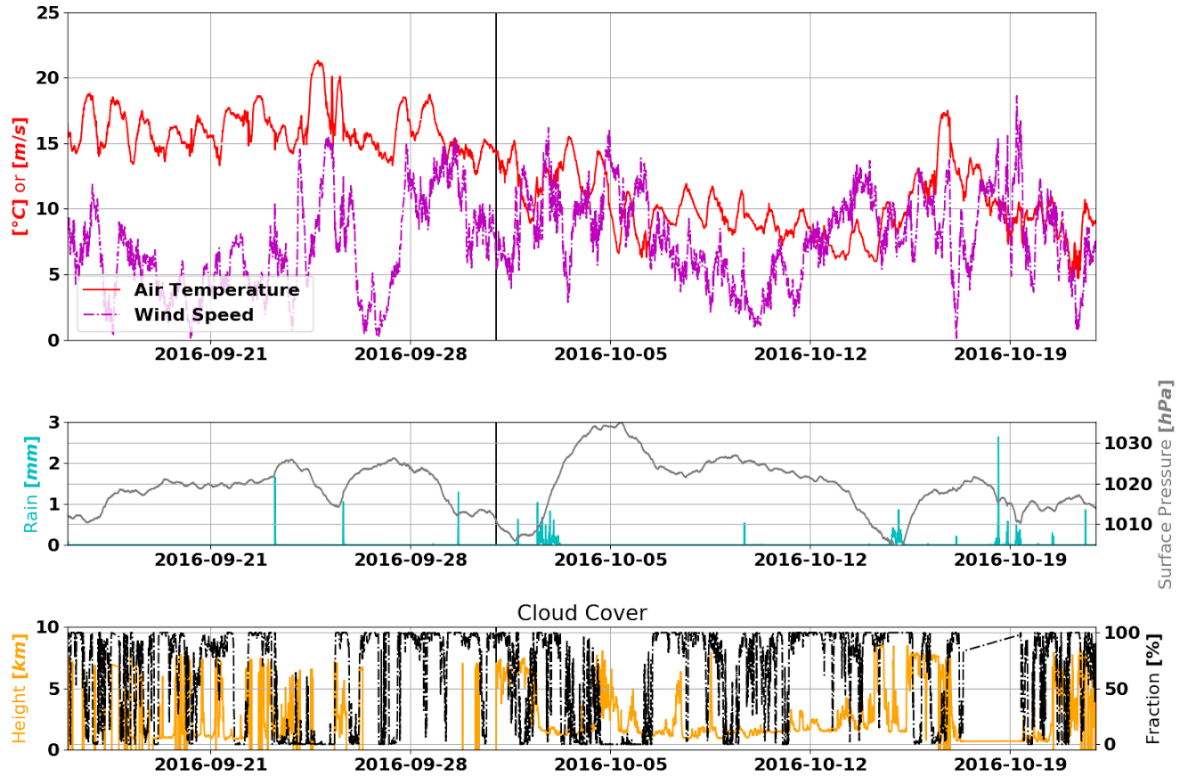

Figure 41: Data retrieved from KNMI Cesar Database [5]. The mean air temperature and wind speed are for the $200m$ height and it is important to note that the cloud cover data has not yet been validated or gap-filled.

The total mass concentration in each DS section is highest at the beginning of the field measurements in September. These high values may be caused by initial contamination. During September $16^{th} - 22^{nd}$ there is a slight dip that may be induced by the relative decrease in wind speed at $200m$ on the 18^{th}. Higher wind speeds help to mix the air in the boundary later which is an important consideration for detecting atmospheric compounds at such a high altitude. Overall, the temperature at $200m$ was high during this period and displayed clear diurnal variation. Diurnal variation alludes to thermal instability during the day time which also contributes to mixing and air chemistry. No major rain events occurred and the cloud cover fraction varied. Similar DB1 concentrations are seen at the end of the month when there is a period of relatively high wind speed following a period with no wind speed. This time period precedes a large rain event with low surface pressure. Low pressure systems entail a lot of mixing and lifting air, so an increase in SVOCs at $200m$ is expected. It is important to note that overheating was common for the setup until ventilation was properly managed by October. High temperatures such as this could have affected the starting temperatures of the DS which could explain the large amount of contamination seen in September.

The concentrations in October start low, become higher and more variable and then drastically decrease after the 17^{th}. During the high period, there is a rain event and a very low surface pressure. The cloud cover height is relatively high which suggests that there is a tall boundary layer and more access to SVOCs which come from oxidation reactions with VOCs emitted at the surface. The cause for the sudden decrease is still quite ambiguous. However, this period is characterized by a very large rain event and increase in wind after a period with no wind. The temperature is also relatively low at this time, all of which may have facilitated condensation and deposition. However, it is unlikely that these meteorological conditions justify the sudden decrease and other information, such as OA data should be explored to determine if the pollution was really low at this point.

6.4 Compound partitioning

SVOCs can exist in both the gaseous and the condensed phase. In this section the partitioning between the two phases is investigated by comparing gas phase measurements from $200m$ and condensed phase measurements from $5m$. Organic Aerosol (OA) data provided at the $5m$ level is collected using a TOF8000 PTR-MS detector that employs an aerosol inlet (Collection-Thermal-Desorption, CTD). Two time periods in which both setups were collecting data are available for comparison. To compare the data sets, the air is assumed to be the same at both heights, but this is not always realistic, especially at night when the boundary layer is stable. A summary of the comparison is given and then the partitioning coefficient is calculated to give insight to the preferred phase of the compounds.

The analysis code loops through both the gas phase and condensed phase data sets and finds instances in which both setups were sampling simultaneously. When a time match is found, the mass concentrations for both phases of any matching compound is stored to be later compared. To determine whether the masses in the separate data sets could be considered equal, different deviation restraints were applied because heavier compounds had a larger peak width in the mass spectrum. Therefore, the restraints were less strict for higher masses [21] From September 16^{th} – 18^{th}, 2016, 13 sampling times coincided and 51 compound matches were stored. During October 8^{th} – 13^{th}, 2016, there were 7 sampling time coincidences and 31 compound matches. The range of masses was smaller in the OA phase such that there were very few masses above 200 Da.

The phase of each compound is initially explored by determining what percentage was typically found in the condensed phase:

$$\frac{c_{aer}}{c_{aer} + c_{gas}} \tag{6}$$

where c_{aer} and c_{gas} are the mass concentrations (ng/m^3) of the aerosol phase at $5m$ and gas phase at $200m$, respectively. The gas phase value from this project is the amount that was detected while the first DB1 denuder section is heated because the SVOCs collided and condensed in this part of the DS. The percentage is calculated for each time that sampling took place for both detectors and the average values are shown in Figures 42a and 42b.

[21] If $m/z < 100$Da then a match is withing ±0.0025Da, $m/z100 - 125$: ±0.004Da, $m/z125 - 200$: ±0.005Da, $m/z200 - 300$: ±0.01Da, $m/z > 300$: ±0.02 Da.

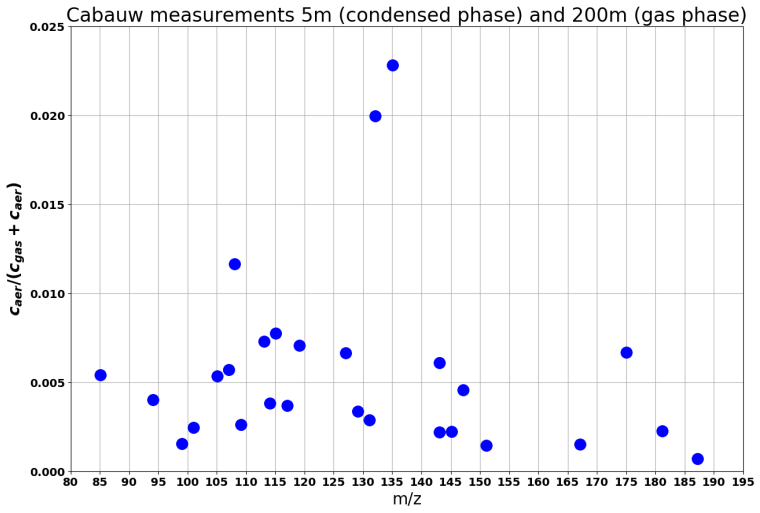

(a) Averages for September $16^{th} - 18^{th}, 2016$

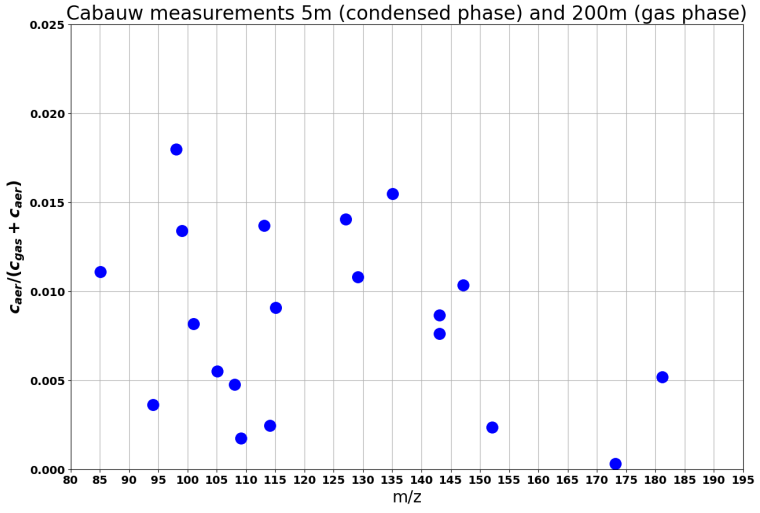

(b) Averages for October $8^{th} - 13^{th}, 2016$

Figure 42

All compounds had larger mass concentrations in the gas phase for both time periods. The values are much lower than expected where every compound has less than 2.5% of the total mass detected in the condensed phase. In September, the highest value corresponds to the compound $m/z135.052$ where the best match is $C_6H_{14}O_3$. There are many variations of this species, one of which is 2-(2-Ethoxyethoxy) ethanol which is used in textiles and varnishes. This compound is selected for analysis when looking at the temporal evolution. Aside from the outliers, in general, more compounds had relatively larger fractions found in the condensed phase in October. This result may be due to the decrease in temperature or perhaps the compounds are less volatile as autumn advances. The results of the Van Krevelen diagram showed that the compounds became more oxidized over time which also supports this conclusion.

6.4.1 Partitioning coefficient

The amount of each compound that existed in each phase differed greatly in the previous section. Therefore, it is interesting to investigate the preferred phase of the compounds by calculating the partitioning coefficient using these concentrations. The partitioning coefficient (K_p) is an indicator of the amount a compound will be found in either phase. Given the total ambient mass of aerosol at a time (M_T), the ratio between the condensed and gas phase can be calculated. The partitioning coefficient is calculated as follows:

$$K_p = \frac{c_{aer}}{c_{gas} \times M_T} \tag{7}$$

where M_T is the total ambient aerosol mass concentration in $\mu g/m^3$ [17]. Data for M_T is retrieved from a GRIMM aerosol detector at CESAR from TNO. The partitioning coefficient for each temporal match was plotted for each compound. Two examples are shown in Figures 43, 44, and 45.

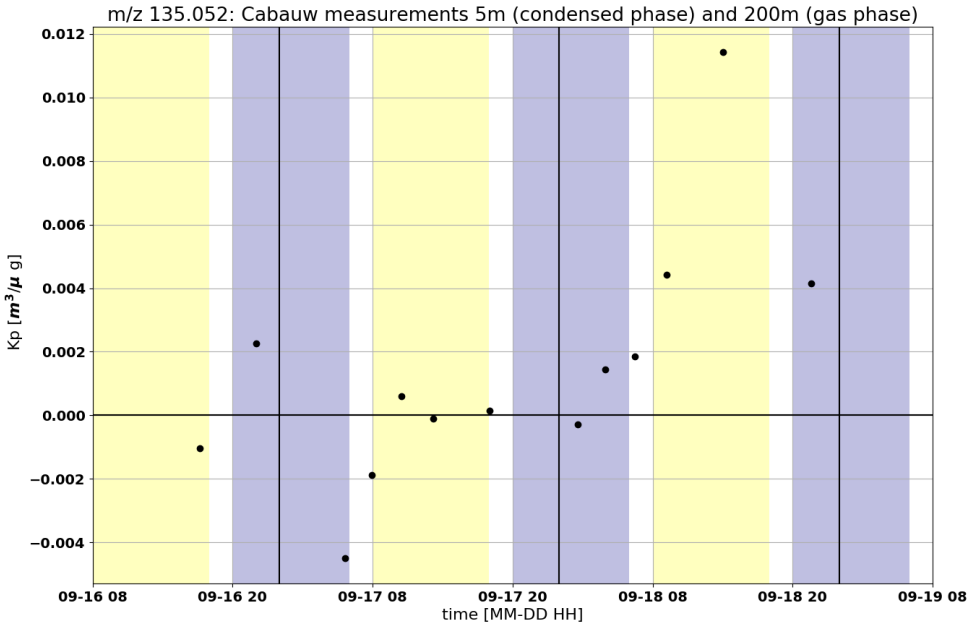

Figure 43: The calculated partitioning coefficient of compound $C_6H_{14}O_3$ for different conditions at each time that was both setups sampled simultaneously in September.

The partitioning coefficient varies greatly over time which may be related to diurnal boundary layer variation, changes in emission, or different meteorological conditions which will effect the variables in Equation 7 . When K_p is high, the compound would be found more in the condensed phase. When K_p is near-zero, the compound prefers to occupy the gas phase which is expected for more volatile compounds. The temporal variation seen when calculating K_p likely due changing conditions and therefore the meteorological conditions are included in the analysis. In general, lower concentrations in the gas phase are expected at lower temperatures and lower wind speeds which should yield a low partitioning value.

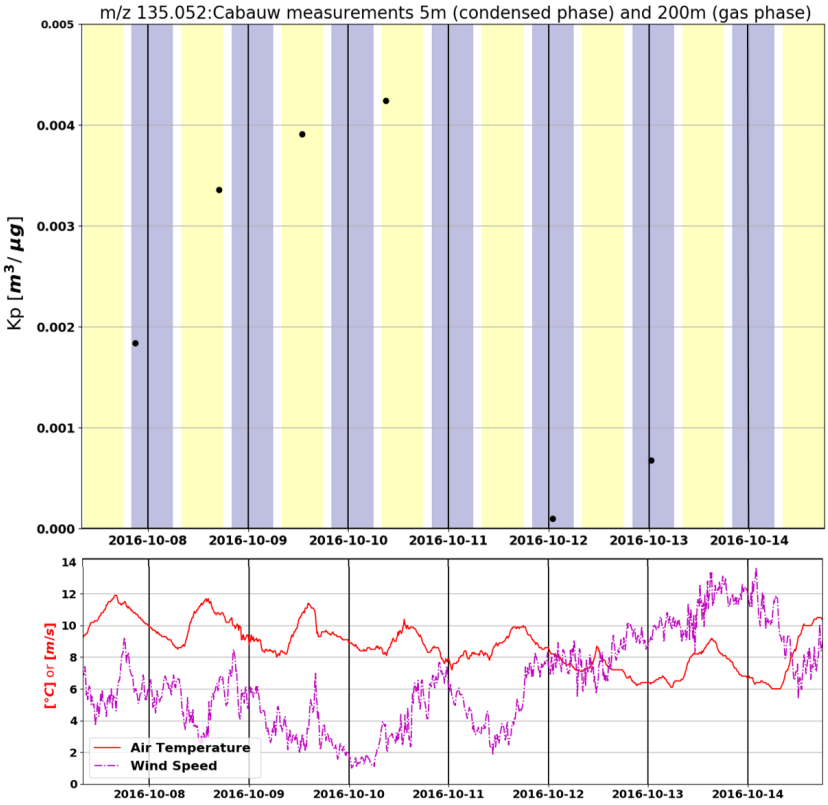

Figure 44: The calculated partitioning coefficient of compound $C_6H_{14}O_3$ for different conditions at each time that was both setups sampled simultaneously in October. The mean temperature and wind speed at $200m$ are obtained from the CESAR Database [5].

The same compound exhibits different behavior and a large range in partitioning coefficients in October as well. From October 8^{th}–11^{th}, the calculated partitioning coefficient increases and does not appear to be related to temperature but perhaps the wind speed is more influential. In the later days, when the values are lower, the wind speed increases which results in more mixing and an increase in c_{gas} is expected. However, these two points occur at night which supports a temperature dependence because SVOCs are more likely to condense at lower temperatures which occur at night, decreasing c_{gas}. However, these values may not be reliable because the boundary layer is typically stable at night and the assumption that both heights have the same air mass may crumble. The relatively high wind may ensure that air within a stable air mass may be mixed. Other compounds, such as $m/z105.069$, detected at this exact time, showed different behavior.

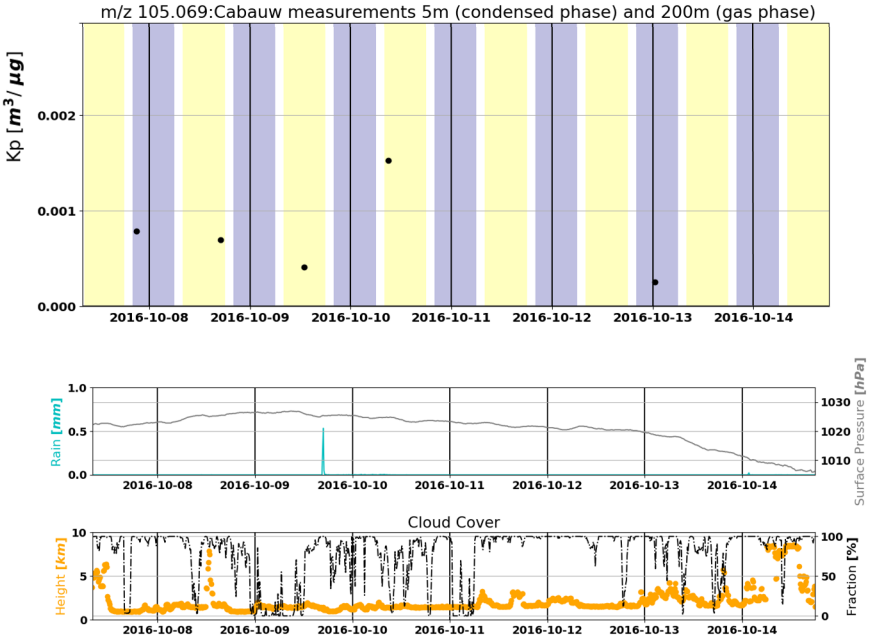

Figure 45: The calculated partitioning coefficient of compound C_8H_8 for different conditions at each time that was both setups sampled simultaneously in October. Meteorological data is obtained from the CESAR Database [5].

The best match for $m/z105.069$ is a hydrocarbon, C_8H_8, which exhibits different partitioning behavior despite the fact it is detected at the same times as $m/z135.052$ and is subjected to the same meteorological conditions. For instance, though the values for $m/z135.052$ are initially increasing, the values for $m/z105.069$ decrease with a sudden increase at noon on October 10^{th}. This behavior could be influenced by the rain event which could deposit the compound if it is soluble, decreasing the amount detected at $5m$. However, this is not likely the case. Also, prior to this period when the value is decreasing, there is a low amount of cloud cover. Low cloud cover facilitates air chemistry because hydroxyl ions are more abundant and insolation causes thermal instability and mixing of the boundary layer. The compound would exist in higher gas-phase concentrations at $200m$ but the sudden increase in cloud cover also occurs before the partitioning coefficient increases around noon. These theories are very speculative, but nonetheless, there is clearly a large variation in the calculated partitioning coefficient over time. The diurnal variation and average K_p value is explored in the following section.

6.4.2 Average partitioning coefficients

The average partitioning coefficient of each compound can be used to calculate the expected ratio of a compound in the condensed phase relative to the gas phase if the total ambient aerosol is known. Additionally, these average partitioning coefficients can be compared to other reference values from different locations and be used to test numerical calculations. Theoretically, K_p should be a constant property of the compound assuming aerosol burden and temperature are constant. The average partitioning coefficient, $K_{p,av}$, is calculated by considering all non-zero values of K_p for each compound. October has only six true matches because M_T was not available for one of the temporal matches. The low number of matches should be questioned when considering the validity of the results. The diurnal variation is also investigated by calculating day and night averages. Day and night averages are categorized by storing the points which occurred within 08:00-18:00 as day values and sample times within 20:00-06:00 were categorized as night values. The results are shown in Figures 46 and 47.

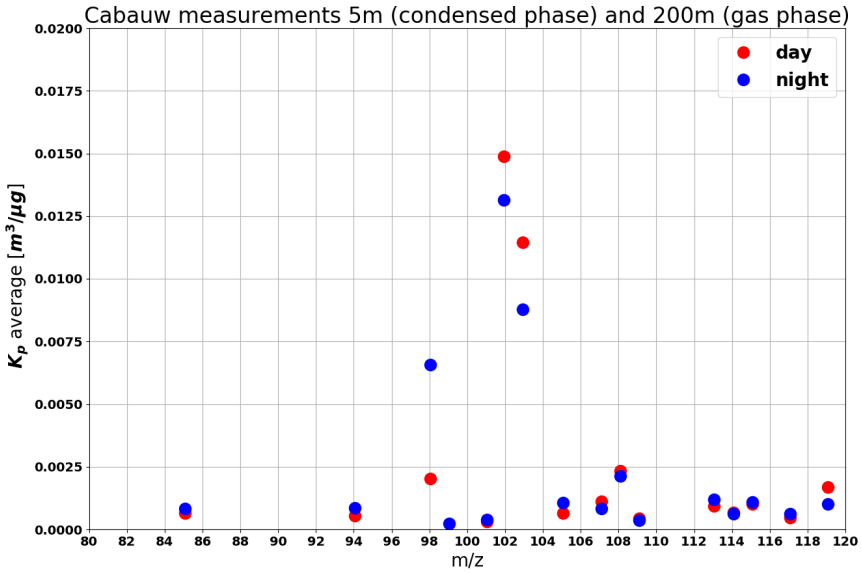

(a) September $16^{th} - 18^{th}, 2016$

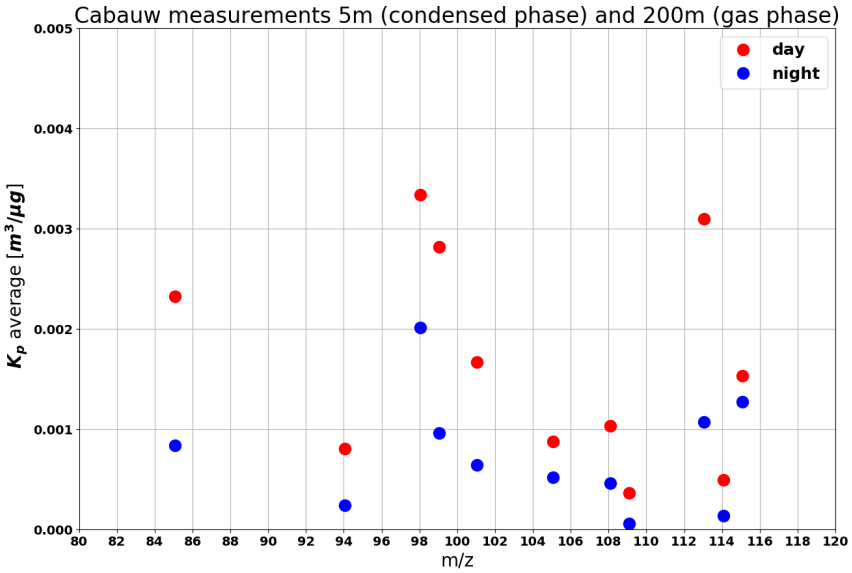

(b) October $8^{th} - 13^{th}, 2016$

Figure 46

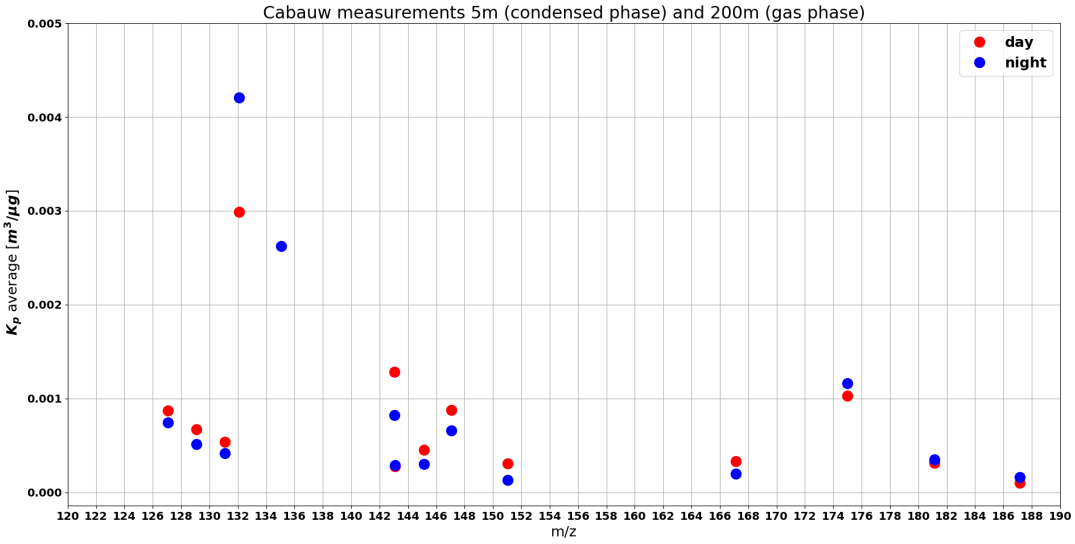

(a) September 16^{th} – 18^{th}, 2016

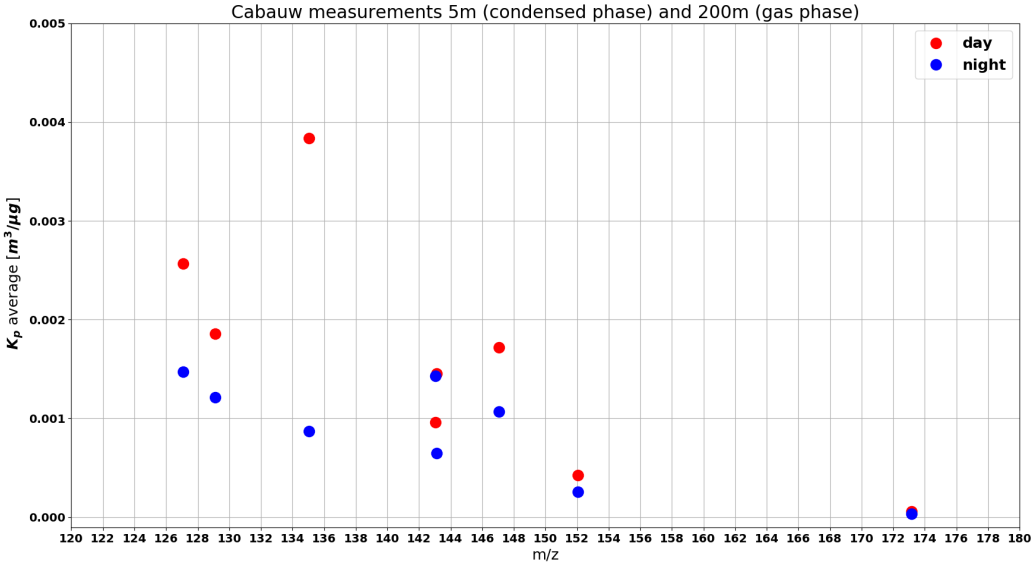

(b) October 8^{th} – 13^{th}, 2016

Figure 47

Figures 46 and 47 show different mass ranges. As mentioned, fewer heavier compounds were available from the detector at $5m$ which limits the domain. Typically, it is expected that more volatile organic compounds will have lower average partitioning coefficients because the gas phase concentration will be higher. However, there was no clear trend observed as the mass range increased. Furthermore, the lighter compounds which are not pictured here are perhaps better reflected if the c_{gas} value assigned is the result of the charcoal denuder section which is designed to collect VOCs instead of the DB1 denuder section. It is interesting to note that $m/z173$, in Figure 47b, is almost completely found in the gas phase. This compound was one of the best resolved during the lab setting experiments.

Most compounds exhibit higher partitioning in October compared to the same compounds in September (i.e $m/z105.069$). This result suggests that compounds are more likely to occupy the condensed phase in October relative to September which is supported by the previous conclusion that less volatile compounds may be more abundant in October. However, SVOCs readily condense on surfaces when the temperature decreases. Therefore, the lower temperatures in October may be responsible for the relatively higher condensed phase mass concentrations.

When considering the diurnal discrepancy of the coefficients, night values were initially expected to be higher than day values because the temperature is lower and more SVOCs would be in the condensed phase. Also, the boundary layer is typically more mixed during the day because of the thermal instability of the boundary layer. Therefore, during the day time, the air chemistry is more active which would increase the concentration detected at $200m$, producing a lower partitioning coefficient. However, in Figure 46, the daily value is generally higher for most compounds. This result shows that the different detectors are likely sampling from different air masses at night because the boundary layer is stable. In this case, deposition of the condensed phase occurs at $5m$, while the $200m$ air mass still has relatively more SVOCs detected in the gas phase causing the partitioning coefficients to be lower at night. Therefore, meteorological conditions within the boundary layer may influence this value and longer time periods are required to improve the analysis.

6.5 Summary

This exploratory project investigated many different aspects of the performance of a new technique for measuring gas phase SVOCs while also analyzing what is found in the atmosphere in rural Netherlands. 354 different compounds were detected using the DS combined with a PTR-ToF-MS. A large range of masses were detected, including heavier SVOCs. The raw volume mixing ratios were converted to mass concentrations found in ambient air and further analyzed using an analysis code developed in Python. A student T-test was used to compare air samples to two blank methods, but most compounds passed and other methods for determining which compounds are significant in air should be tested and compared in the future. Blank measurements were subtracted to reduce the effects of contamination and the nitrogen blank performed better, producing more realistic results than the zero flow blank and should be implemented more frequently in future, similar projects. The blanks could also be further improved by executing them simultaneously with air sampling.

Many compounds, especially siloxane species, were not corrected well by the current blank methods. It is notable that the siloxanes were also present during the lab setting experiments, confirming that a fraction of the signal must be DS contamination. The lab experiments were controlled and the siloxane results could be quantified and potentially used to properly address contamination in the field. Reference contamination values would be an asset for determining what fraction of signal from field measurements is actually present in ambient air.

A large amount of heavier compounds were found in the first DB1 denuder section which showed that the DS is an effective technique for collecting SVOCs. The charcoal section is designed to collect VOCs which is an economical asset to this new tool. The results from this section were not intensively investigated nor discussed in this project but the data is available for further analysis and the analysis code is designed to do so. The time evolution of the atomic ratios revealed that the compounds are more oxygenated and therefore less volatile in October compared to September. However, the temperature is also lower in October which increases the likelihood of condensation and a lower amount of SVOCs detected in the gas phase. $200m$ is an interesting height to detect compounds because the meteorological conditions and boundary layer status has an influence on the mass concentration results. Longer time series during different seasons would be interesting for future field measurements.

The DS is a new technique that provided gas phase SVOC information, and the partitioning of the compounds was explored by incorporating condensed phase measurements from a PTR-MS setup at the $5m$ level. Results showed that most compounds were present in higher concentrations in the gas phase with less than 2.5% of the total amount collected in the gas phase. These values can be compared to urban areas and numerical calculations to further the properties of air in rural Netherlands. Partitioning coefficients were calculated and shed light on the phase in which a compound is likely to be present in. The vapor pressure is available for certain compounds (such as the siloxanes), and could be used to compare the empirical coefficients to numerically calculated values [18]. However, the OA data is questionable because heavier masses were not detected with the setup at $5m$. The current calculations can be improved by including an aerosol inlet at $200m$ which would give a better comparison because both phase concentrations come from the same air mass. Though there is also an outlook for future field measurements, there is still much to be explored within the large amount of data available from this completed campaign.

Appendices

A Denuder Sampler Maintenance

A.1 Broken DS heating element

The heating elements are a critical component of the DS because the heat converts the collected SVOCs back into the gas phase for detection. Unfortunately, on November 30^{th}, sometime between 13:24 and 13:54, the heating element in the PEEK section of the DS could no longer reach the set temperature of 150° as seen in Figure 48. Though the three denuder sections could still be heated, this relatively cold section is connected to the PTR-ToF-MS inlet and compounds will enter this section during transfer. Therefore, measurements may suffer due to re-condensation of the thermally-desorbed compounds. The issue remained until the setup was removed from the tower on January 19^{th} and any data after this point should be analyzed with this in mind or omitted.

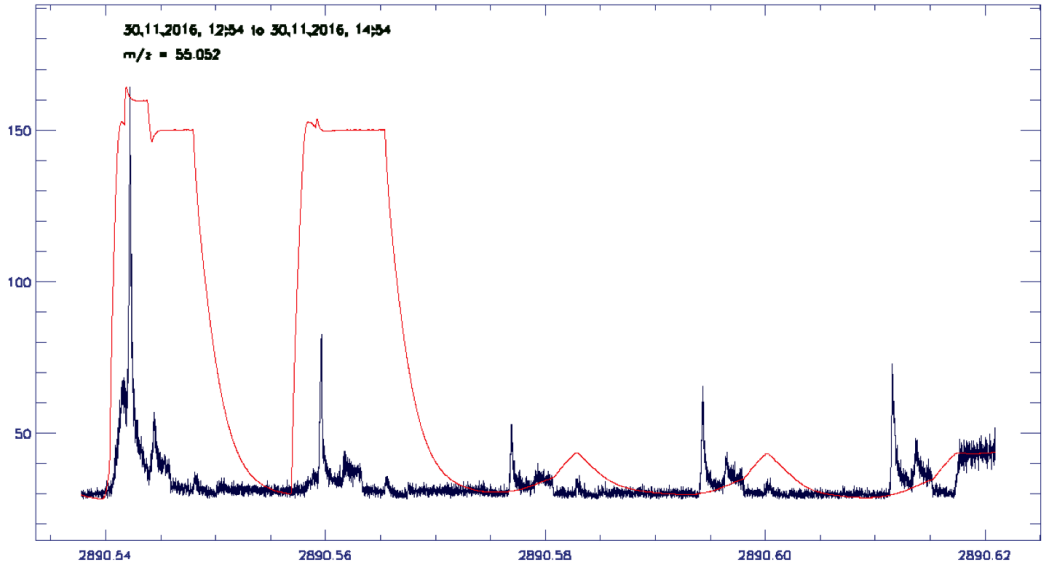

Figure 48: In blue: concentration of compound $m/z55$ in nmol/mol vs. Julian Date, In red: Temperature of PEEK section of DS vs. Julian Date. During this time period, a clear problem is visible as the temperature assigned is no longer reached in the PEEK section.

After relocating the setup to the lab, the problem could be investigated by taking the DS casing apart. The heating element was clearly broken and appeared to have overheated as seen in Figure 54. There is no manual threshold/limit to prevent overheating; however, there is no spike in temperature seen prior to the sudden decrease in Figure 48. The element was replaced and after installation, the ability to achieve the assigned temperature was tested and confirmed. The displayed temperature in the *TOF2.3* software matched the assigned temperature within 1 degree and the reading was confirmed using a Fluke t3000FC k-type thermometer (°C). Onward, maintaining a temperature below 200° is recommended.

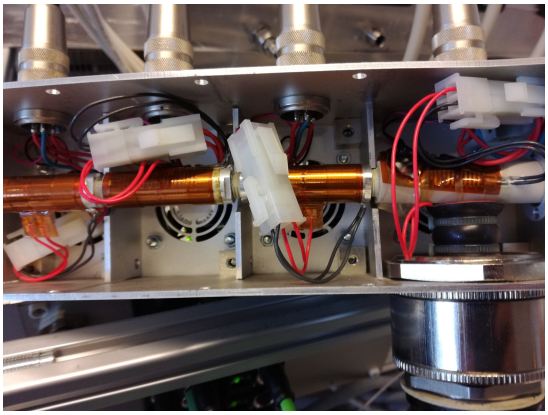

(a) Denuder Sampler (DS) with casing removed. The damaged heating element in the PEEK section is visible prior to removal

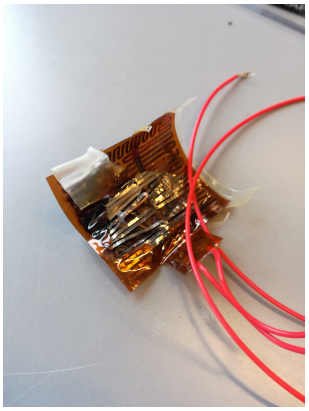

(b) Broken heating element after removal

Figure 49

A.2 Denuder flow confirmation

The flow rate at the exit (connected to the N_2 source and pump) and entrance (where sampled air will enter) of the DS was confirmed when testing the DS performance in the lab setting (see figure 7). Different values were assigned and the direction of flow was changed. The flow rate was measured using a flow meter and the results are shown in Figure 50. The discrepancy between the assigned value and the flow meter reading is plotted in Figure 51.

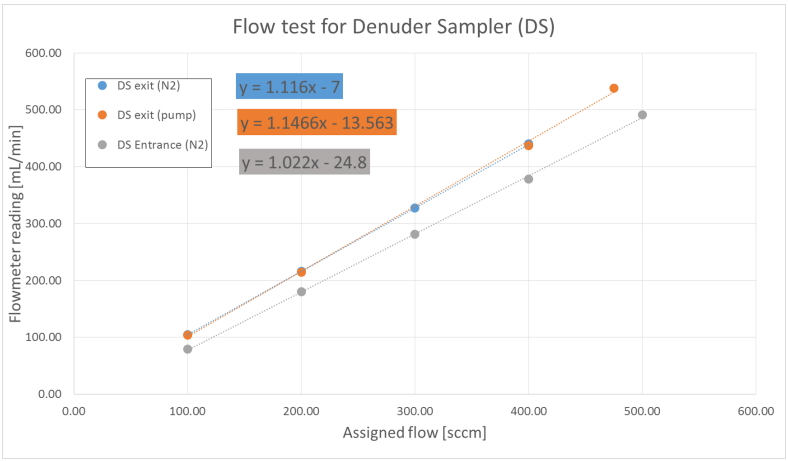

Figure 50: Flow rate measured at the entrance of the DS (where sampling occurs) and exit of the DS with the direction of the flow set to pump (sampling: from entrance to exit) or N_2 (transferring towards PTR-MS: from exit to entrance)

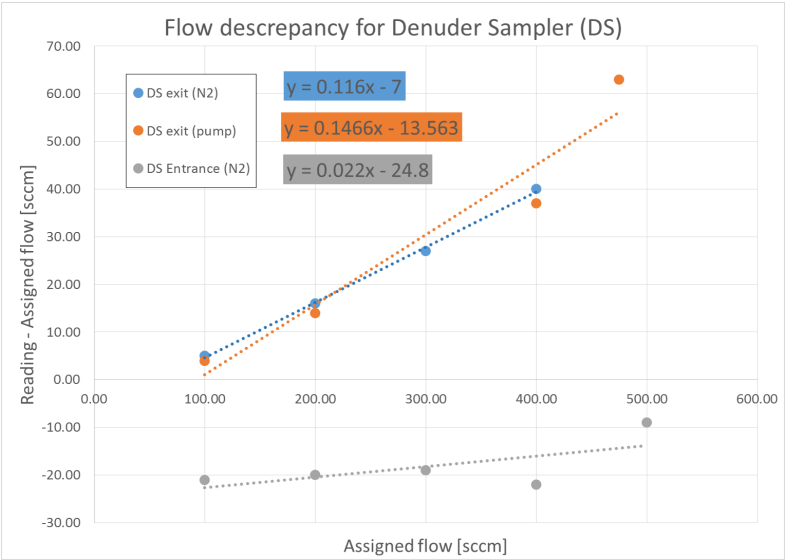

Figure 51: the discrepancy between what was assigned and the results of the flow meter

The behavior in both figures revealed corrections that must be made in order to test for leaking. Figure 50 illustrates that at the exit of the DS, the measured value tends to be above the flow rate that is assigned, regardless of flow direction. The discrepancy appears to increase as the flow rate increases and this is confirmed in figure 51. This behavior is related to the fact that the flow controller (FC) sets the flow for standard conditions (assuming 0°, sea level pressure). The setup is at room temperature and this will cause a discrepancy of roughly 10% which is seen as the difference increases at higher flow rates. Therefore, this correction should be considered when analyzing results that involve calculations with high flowrates (assigned in *sccm*).

In contrast, at the entrance of the DS, both figures depict that the value is consistently underestimated. This constant discrepancy is due to the pull from the PTR-ToF-MS which was between $32 - 38$mL/min. This flow rate towards the PTR-ToF-MS was measured by connecting the flow meter to the PTR-ToF-MS inlet which was removed from the PEEK portion of the DS in the lab setting. A range of values is stated because the tubing of the PTR-MS inlet had a slight twist/kink in it which may have occurred while disconnecting it from the DS. After replacing the tubing, the flow increased from 32.5mL/min to 37.6mL/min.

B Data Treatment

B.1 Converting raw data

B.1.1 Converting with respect to ambient air

The raw volume mixing ratios corresponding to each DS section are initially with respect to the nitrogen flow ($35mL/min$) during desorption. These values need to be converted to be with respect to the ambient air ($10min$ of sampling at $800mL/min$). To convert these values, C_{N_2}, which are $60s$ averages in parts per billion ($ppb = nmol/mol$) to be with respect to ambient air C_{ambient}, the amount with respect to the nitrogen flow is compared to the amount of air that is actually sampled:

- amount with respect to that nitrogen flow during desorption ($60s$ average): $(C_{N_2}[nmol/mol] \times FC_{N_2}[L/min] \times 1[min])/22.4[L/mol]$
- amount of air sampled: $(0.8[L/min] \times 10[min])/22.4[L/mol]$

where FC is the denuder flow which is typically $0.035 - 0.04L/min$ for each section, but for the case where the charcoal section is desorbing the flow rate is $0.3L/min$. The value $22.4[L/mol]$ is the molar volume of nitrogen gas at room temperature [15]. Then, by dividing the first argument by the second argument, the calculation that can be applied to the average concentrations to convert them to be with respect to air is achieved:

$$C_{\text{ambient}} = \frac{(C_{N_2}[nmol/mol] \times FC[L/min] \times 1[min])/\cancel{22.4[L/mol]}}{(0.8[L/min] \times 10[min])/\cancel{22.4[L/mol]}}$$

This calculation is done in the Python analysis code by a defining function, with a variation for the charcoal section.

```
def convert_to_air(array): # convert wrt ambient air
    new_array=np.zeros((len(array),len(array[0])))
    for t in range(0,len(time_amb_JD)-1): # changed from len(array)
        if time_amb_JD[t]>2880.0:
            Flow_rate=35.0 #mL/min
        else:
            Flow_rate=30.0
        for i in range(0,len(array)):
            new_array[i]=array[i]*(Flow_rate*10**(-3)/22.4)/(800.0*10**(-3.0)*10.0/22.4)
    return new_array #returns ppb
```

B.1.2 Converting the volume mixing ratio to mass density

Next, to convert the corrected volume mixing ratios to mass concentrations in air, $MC[\mu g/m^3]$, the following calculation is done:

$$MC = C_{\text{ambient}}[nmol/mol] \times MW[g/mol]/22.4[L/mol]$$

This conversion is executed using a defined function that can be applied to either a 1D list (one overall average for each compound) or 2D list (each sample value corresponding to each compound) of values.

```
def convert_to_density(array): # convert to micrograms/m^3
    if array.ndim== 1: # 1D, i.e list of average for each mass
        new_array=np.zeros(len(array))
        for i in range(0,len(array)):
```

```
            new_array[i]=array[i]*mass_list[i]/(22.4)
        return new_array
    else: # 2D, i.e. multiple values stored for each mass over time
        new_array2=np.zeros((len(array),len(array[0])))
        for i in range(0,len(array)-1):
            new_array2[i]=array[i]*mass_list[i]/(22.4)
        return new_array2
```

B.2 Student T-test

There are two different blank methods executed during the field measurements at Cabauw. Blank measurements are used to analyze and determine which compounds veritably appear in ambient air during the non-blank sampling runs. In the Python analysis code, the statistical function *scipy.stats.ttest_ind* is used to compare sample arrays to blank arrays. This function performs a Student T-test for the two independent samples (blank and non-blank in this case) assuming that the samples have identical variances [16]:

```
from scipy.stats import ttest_ind
...
for i in range(0,len(Data)-mass_start): # for each mass
    p_a_n.append(ttest_ind(DB1_amb800_no0[i],DB1_N_no0[i])[1])
    # ttest for first DB1 section averages of ambient sampling and N2 blank
```

This operation returns the calculated t-statistic and the two-tailed p-value which is used in this project to establish significance. The p-value is a two-sided test for the null hypothesis that two independent samples have identical expected values. Therefore, the p-value can gauge whether the average expected value differs between the samples. Specifically, for large p-values ($p > 0.05$), the null hypothesis cannot be rejected. However, if the p-value is smaller than the threshold ($p < 0.05$), the null hypothesis is rejected and the samples are statistically different. Therefore, when comparing the concentrations of an air sample to blank concentrations, if the p-value is below the threshold, then the mass is considered significant in ambient air.

B.3 PTRwid index files

Engineering data available:

- September $16^{th}, 2016$– October $8^{th}, 2016$
- October $17^{th}, 2016$– October $21^{st}, 2016$

Measurement Indexes

- index 100, 101, 102, 103: heating PEEK, DB1, DB1 (2), and Charcoal sections, respectively. $\sum_{n=1}^{4} \text{Fans} < 4.5 - n$, then $index = 99 + n$
- index 200: background with standard gas addition. Digital Output 2 ($DO2$) = 1
- index 203: cleaning stage. DS section Temperature > $160°C$
- index 300, 305: Sampling air, all fans are on, index 100 is null and no others are assigned. The first 360 points where this is true are marked with a different index, 305, because higher contamination is expected in the first 4 minutes.

- index 310, 315: cooling after cleaning stage. Digital Output 1 ($DO1$) = 1 to start standard gas background addition. First 360 points marked as 315 because contamination may be higher and this would period be nice to distinguish.

Sample Indexes

- blue (100) = 10: sampling . Flow rate > $100mL/min$
- orange (200) = 10 and blue (100) = 10 : sampling nitrogen. Flow rate > $100mL/min$ and $DO7$ = 1
- orange (200) = 2: 0 flow sampling. Flow rate = $0mL/min$

*Engineering data **not** available:*

- October 8^{th}, 2016– October 16^{th}, 2016

Measurement Indexes When the signal for mass m/z 32 < 1000 (oxygen signal is low when nitrogen is supplied for the desorption process):

- index 101: the first three minutes when this condition is satisfied correspond to the **PEEK** section
- index 102: the next three minutes when this condition is satisfied correspond to the first **DB1** denuder section
- index 103: the next three minutes when this condition is satisfied correspond to the second **DB1 (2)** denuder section
- index 104: the final three minutes when this condition is satisfied correspond to the **Charcoal** denuder section
- index = 300: m/z 32 > 1000
- Otherwise index = 100

Digital Output variables (DO) are used to identify the blanks in Python. However, The DO engineering was not available for the entire period.

C Lab Experiment Solutions

C.1 Solution preparation

A known solution is inserted into the DS entrance so that the recovery of the sample can be calculated and the performance of the denuder is tested. For these experiments, a variety of solutions were created containing compounds ranging in volatility. The complete list of prepared solutions is available. In each experiment used in this analysis, the compound of interest was mixed with pure Ethanol as a solvent to create a liquid solution. $2\mu L$ of the final solution is placed on a 'spoon' constructed from aluminum foil using a μL syringe that is flushed before each deposit. Only a small quantity of the solution was required so the amount of solute required was very minimal. The amount required was roughly calculated expecting to see a signal of $\sim 5ppm$. First, the sample flow rate is multiplied by one minute (time for the SVOC to evaporate):

$$\sim 1L/min \times 1min \sim 1L$$

Then, this volume is multiplied by the desired signal: $5ppb = 5nL/L$

$$1L \times 5nL/L = 5nL$$

Then, the amount required, in L, is converted to mol which will depend on the molar weight of the selected compound:

$$\frac{5nL}{22.4L/mol} \sim 0.25nmol$$

$$0.25nmol \times 172g/mol = 43ng$$

which is what needs to be administered to yield $5ppb$.

Next, the calculated amount of the SVOC to be mixed with Ethanol as a solvent in order to get $43ng$ of solute in the $2\mu L$ which is inserted into the DS:

$$(43ng \text{ in } 2\mu L) \times 10^3$$

$$(43\mu g \text{ in } 2mL) \times 5$$

$$415\mu g = 0.415mg \text{ Decanoic acid in } 10mL \text{ Ethanol}$$

Due to the limitations of the scale shown in figure 52, an initial solution was created with roughly $\times 10$ the amount required, and then $1mL$ of this solution was diluted with $9mL$ of Ethanol to achieve the desired amount when inserting $2\mu L$ of the solution.

Figure 52: Shown here is the scale used to select the amount of solid semi-volatile organic compound for the lab experiments. The bottle in which each solution is contained and the spatula tool used are also pictured.

C.2 Converting volume mixing ratio signal to mass

The process of converting an intensity signal to a mass begins with integration. The Python package *scipy.integrate* with the *simps* function is used to integrate over the three minutes in which the DB1 denuder section is heating. The *simps* function uses Simpson's rule to compute the integral from samples [10]. This will give the amount, I, in ppb = $[nmol/mol]$ multiplied by minutes. Next, the amount of mass detected, X, is calculated as follows:

$$X[ng] = \frac{I[nmol/mol \cdot min] \times Mw[g/mol] \times FC_{N_2}[L/mol]}{22.4[L/mol]}$$

C.3 Solution list

Solutions are listed alphabetically but are also listed in the online log by date. Note that impure ethanol was meant for cleaning. Distilled water could be used as a solvent for some solutes and using this solvent in the future may be beneficial because the organic nature of Ethanol proved to be a complication. Acetone, even when combined with Ethanol as a solute, produced very noisy results. Most solutes were a minimum of four years old.

- P67 – Aminobutyric Acid 2.8mg in 10mL pure Ethanol - didn't dissolve, maybe in water
- P11 – Decanoic Acid 2.3mg in 10mL impure Ethanol
- P10 – Decanoic Acid 0.23mg in 10mL impure Ethanol
- P27 – Decanoic Acid 2.2mg in 10mL pure Ethanol
- P92 – Decanoic Acid 0.022mg in 1mL pure Ethanol
- P83 – Decanoic Acid 2.2mg in 10mL pure Acetone

- P19 – Decanoic Acid 0.022mg in 1mL pure Ethanol + acetone. 100 microlitres of P83 added to 900microL of ethanol

- P2 – Pentadecanoic Acid 3.0mg in 10mL impure Ethanol
- P25 – Pentadecanoic Acid 0.30mg in 10mL impure Ethanol
- P42 – Pentadecanoic Acid 3.0mg in 10mL pure Ethanol
- P57 – Pentadecanoic Acid 0.030mg in 1mL pure Ethanol
- P94 – Pentadecanoic Acid 3.0mg in 11mL pure Acetone - 11 was an accident - confirmed by comparing to bottles certainly filled with 10mL
- P84 – Pentadecanoic Acid 0.030mg in 1mL pure Ethanol + acetone. 110 microlitres of P94 was added to 890microlitres of ethanol

- P1 – Stearic Acid 3.6mg in 10mL impure Ethanol
- P9 – Stearic Acid 0.36mg in 10mL impure Ethanol
- P93 – Stearic Acid 3.5mg in 10mL pure Ethanol
- P58 – Stearic Acid 0.035mg in 1mL pure Ethanol

- P49 – Pipet tip in vile filled with impure Ethanol - I let the bottle sit from 11:57 - 13:45 and then the tip was removed
- P100 – Pure ethanol
- P34 – mistake, flushed with ethanol, will be used for flushing syringe
- A40 – Pure acetone

Trouble dissolving, seems dissolved now:

- P76 - polydimethlysiloxane (liquid) 0.2213 g in 10, then a total of 20 mL of ethanol
- P35 - Flouranthene 0.0026g in 10, then a total of 20mL of ethanol
- P33 -Luperox 0.0125g in 10, then a total of 30mL of ethanol

C.4 Fragmentation investigation using PTR-MS with TOF8000

The inlet of a TOF8000 PTR-ToF-MS was exposed to the sample directly to determine if lighter compounds were also detected using this detector or if they were characteristic of the DS. If the solution was placed too close to the inlet, the signal was very noisy, but with multiple, careful attempts and investigation in *PTRwid*, a resulting parent ion signal is shown in Figure 53. The PTR-MS was constantly detecting and at first the solution was held too close to the inlet, but near the end of this recording, I held the open bottle away from the inlet.

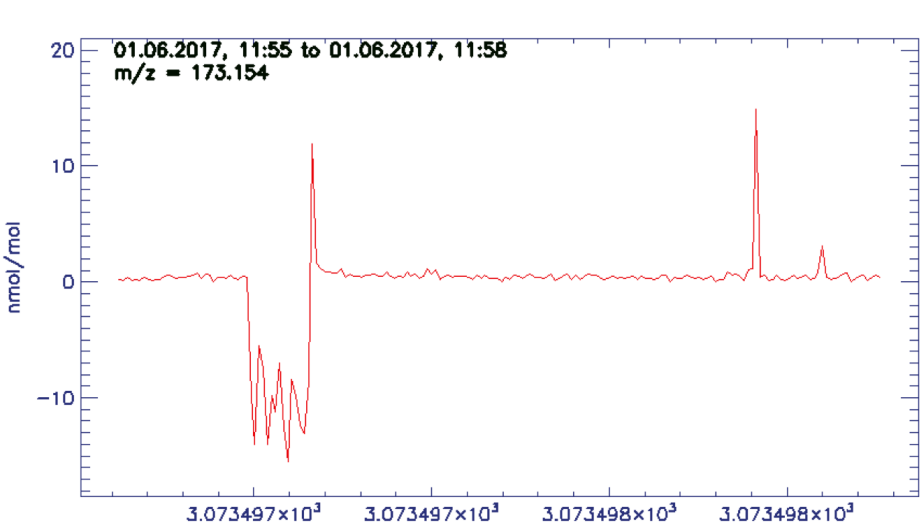

Figure 53: Repeatedly bringing the open bottle of the Decanoic acid solution (P92) close to the inlet of the PTR-MS TOF8000

A large Ethanol signal was detected simultaneously (Figure 54a) as well as many other light compounds with high counts in the experiments with the TOF1000 detector (Figures 54b and 54c). The shape of the peaks are similar to that of the parent ion. However, the intensity of the Ethanol signal is very high, as expected, and the intensity of the two lighter compounds is also relatively high compared to the intensity of the parent ion.

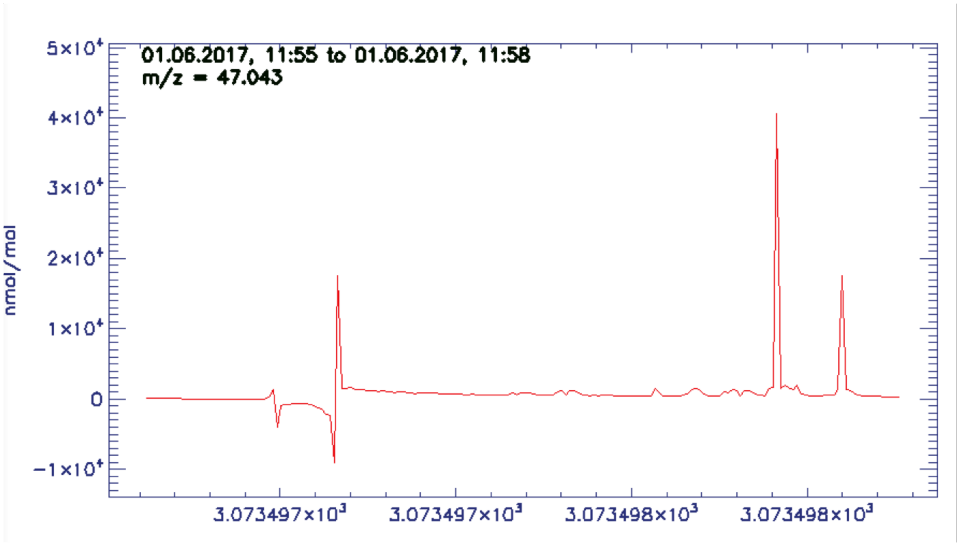

(a)

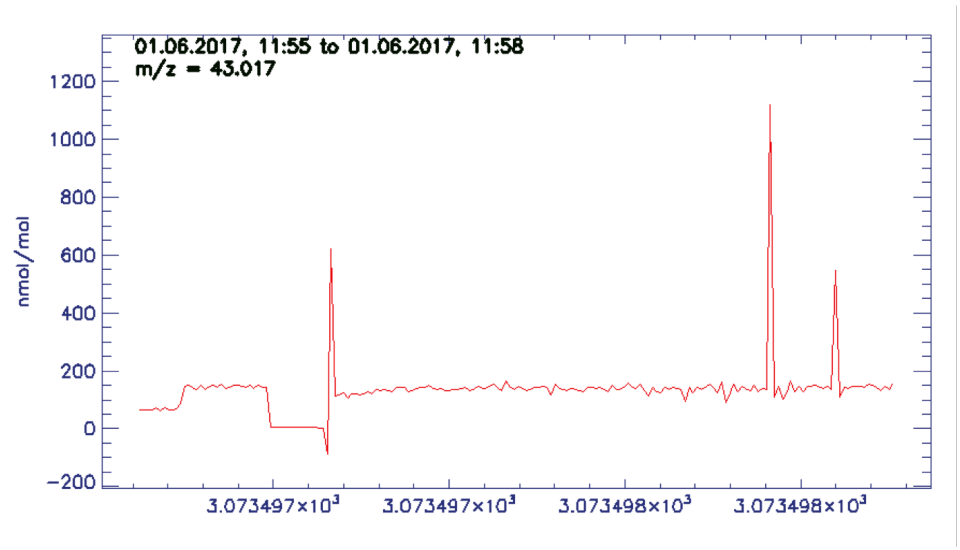

(b)

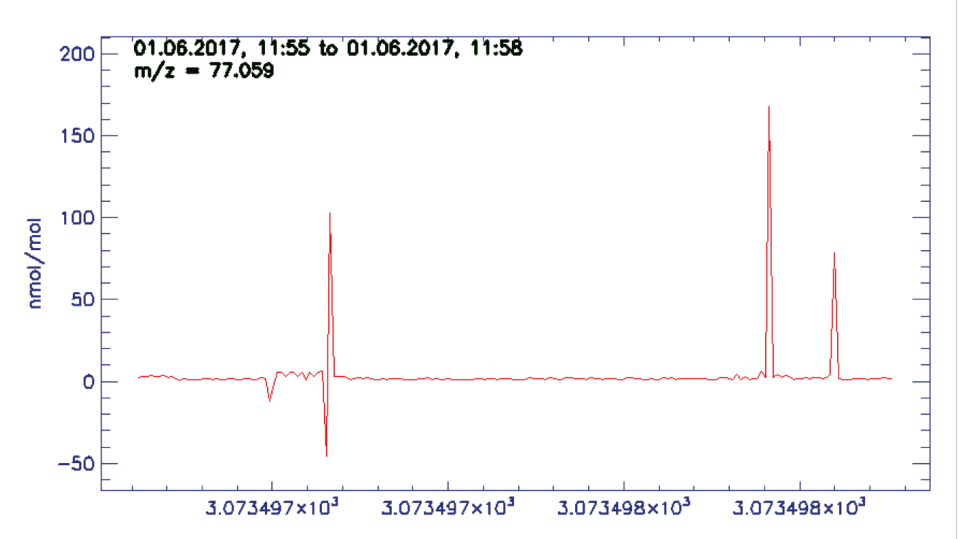

(c)

Figure 54: Repeatedly bringing the open bottle of the Decanoic acid solution (P92) close to the inlet of the PTR-MS TOF8000

Heavier compounds ($m/z > 173$) were also detected which may be due to impurities in the solution or, more likely, are detected in the lab air because the inlet is exposed. Furthermore, some of the heaver compounds were present at higher intensities than the parent ion (i.e. $m/z231$ in Figure 55).

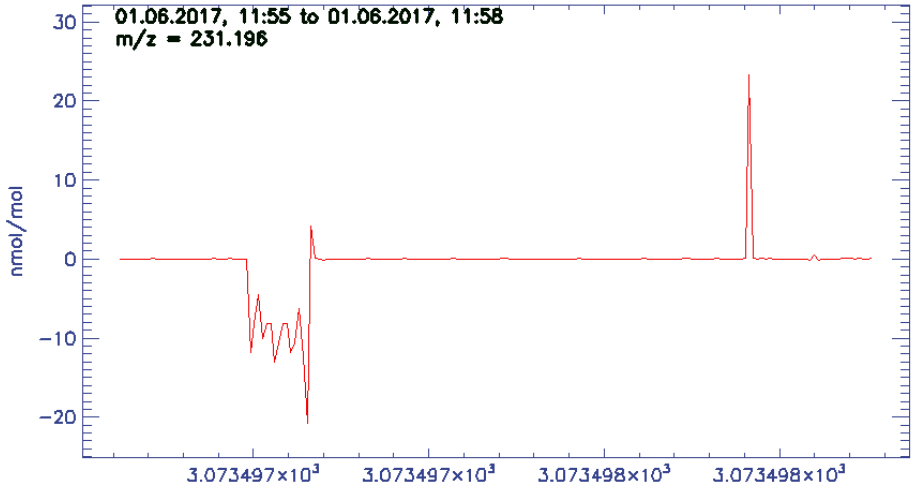

Figure 55: Repeatedly bringing the open bottle of the Decanoic acid solution (P92) close to the inlet of the PTR-MS TOF8000

I attempted to reduce the influence of lab air by inserting the inlet into the penetrable top of the closed bottle but then the signal was too strong. This method can be further developed by flushing a bottle so that there is only nitrogen inside. Then, a small amount of the solution can be inserted into the capped bottle with the μL syringe, and then the PTR-ToF-MS inlet can be inserted. This test did not eliminate the possibility that these signals could be produced by lab air or Ethanol. The pure SVOC substance should be applied in this experiment to eliminate the possibility of impurities in the solution. Ultimately, this test produces similar results to that of the initial lab experiments (Setup shown in Figure 6) which showed signs of lab air intrusion. Therefore, the lighter compounds are require further investigation.

D Field Measurements

D.1 N/C atomic ratio

$$\frac{N}{C} = \frac{\sum_i \frac{n_i N_{N_i}}{\mathrm{MW}_i}}{\sum_i \frac{n_i N_{C_i}}{\mathrm{MW}_i}}, \frac{O}{C} = \frac{\sum_i \frac{n_i N_{O_i}}{\mathrm{MW}_i}}{\sum_i \frac{n_i N_{C_i}}{\mathrm{MW}_i}} \tag{8}$$

where n_i is the mass density ($\mu g/m^3$) of compound species i and N_{O_i} , N_{C_i}, and N_{N_i} are the number of oxygen, carbon, hydrogen, or nitrogen atoms, respectively. MW_i is the molar mass of the compound. Each point, in Figure56, pertains to one sample during the entire period of measurements. Initially, all detected compounds were considered and no blank correction was applied. In Figure 56b, the nearest zero flow blank is subtracted from each concentration prior to calculating the atomic ratios. Clusters were visible and grouping different time periods (by color) effectively represented the clusters with some outliers.

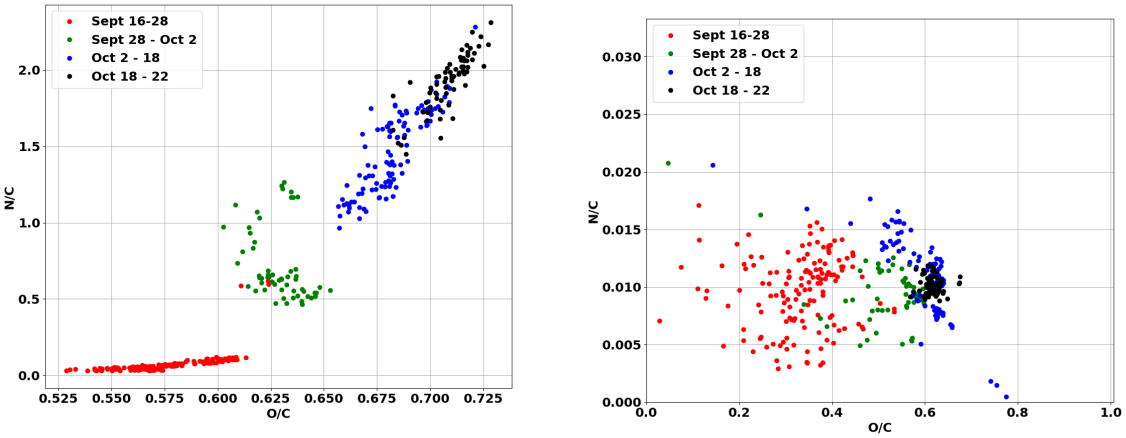

(a) All compounds are considered and no blank correction is applied

(b) $m/z > 100$Da and zero flow blank corrected

Figure 56: nitrogen and oxygen atomic ratios comparing to carbon September 16 - October 22

The nitrogen ratio was also investigated and the N/C ratio values are very high. This result is probably caused by including inorganic compounds. To address this, only compounds with $m/z100$ are considered in Figure 56b. When the zero flow blank is incorporated and inorganic compounds are excluded, the N/C ratio decreases drastically. Overall, a clear discrepancy between September and October is observed which was also seen considering H/C and O/C. In this case, a trend is less obvious. Additionally, subtracting the nitrogen blank may be more realistic for this case in the future but this blank was not available at all times during these field measurements.

D.2 Diurnal activity

Diurnal variation was considered for the entire time series available: Sept $16^{th}, 2016$–$Jan4^{th}, 2017$. Mass concentrations corresponding to compounds ($m/z > 100$ Da) were stored as day values if the sampling time was between $10:00$ and $16:00$ and stored as night values if the sampling time was between $22:00$ and $04:00$. These times were selected because they have avoid sunrise and sunset for the entire period. Once categorized, the day and night data sets were compared to each other using a student t-test. 47 masses yielded a p-value < 0.05 suggesting that the day and night data sets were statistically different. The difference between day and night concentrations was positive for all compounds such that each compound reached higher concentrations during the day time, which is expected due to increased mixing and active air chemistry which produces SVOCs. VOCs are emitted naturally and anthropogenically during the day and will be become subject to oxidizing reactions which will produce less volatile SVOCs. However, this result could also be the result of contamination that is higher in the daytime because the starting temperature of the denuder is higher. The largest diurnal concentration discrepancy was observed for compounds that were likely contamination (siloxanes). Siloxanes occur in nature, but are also a potential contaminant because the DB1 coating is a polydimetylsiloxane.

The compounds were sorted using their p-value to try to exclude the compounds which had higher absolute concentrations due to contamination. Siloxanes still appeared as the some of the most statistically different between day and night. The data was further analyzed and due to the peek section heating element breaking, the data after Nov $30^{th}, 2016$, was omitted from the analysis. When omitted, the amount of masses which had day and night data sets that were determined to be statistically different was reduced drastically. This result suggests that no obvious diurnal variation is present from September to October, but perhaps this is not the case when looking at smaller scales or looking at the relative concentration change between day and night instead of using the t-test. The results when considering the entire period of measurements available were likely caused by the diurnal change in temperature effecting the compounds because of the faulty heating element. This conclusion is supported by the

behavior observed in Figure 57

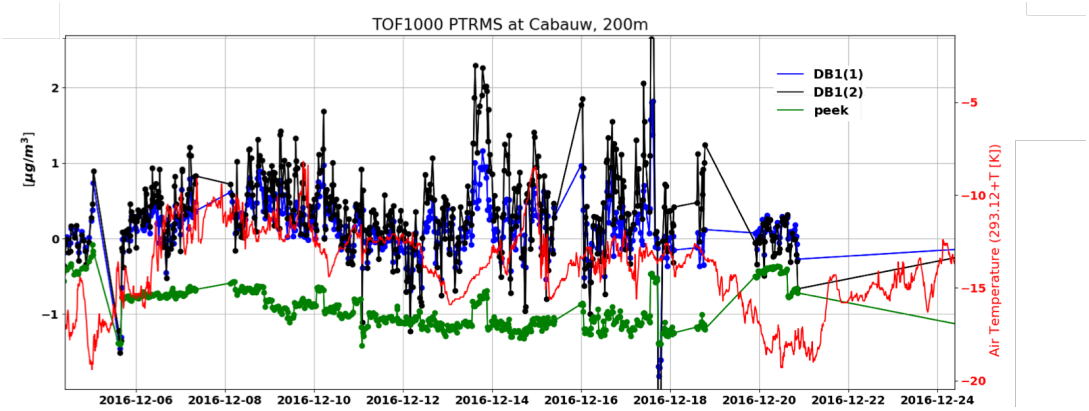

Figure 57: The total mass concentration detected from the DS sections during the time period that the PEEK section heating element was broken. Mean air temperature data for the $200m$ height is obtained from the CESAR database [5].

References

[1] G. Myhre, D. Shindell, F.-M. Bréon, W. Collins, J. Fuglestvedt, J. Huang, D. Koch, J.-F. Lamarque, D. Lee, B. Mendoza, T. Nakajima, A. Robock, G. Stephens, T. Takemura and H. Zhang, 2013: Anthropogenic and Natural Radiative Forcing. In: Climate Change 2013: The Physical Science Basis. Contribution of Working Group I to the Fifth Assessment Report of the Intergovernmental Panel on Climate Change [Stocker, T.F., D. Qin, G.-K. Plattner, M. Tignor, S.K. Allen, J. Boschung, A. Nauels, Y. Xia, V. Bex and P.M. Midgley (eds.)]. Cambridge University Press, Cambridge, United Kingdom and New York, NY, USA

[2] A. H. Goldstern, I. E. Galbally (2007) Known and unexplored organic constituents in the Earth's Atmosphere. *Environmental Science and Technology*

[3] M. Hallquist, J. C. Wenger, U. Baltensperger, Y. Rudich, D. Simpson, M. Claeys, ... J. Wildt (2009) The formation, properties and impact of secondary organic aerosol: current and emerging issues. *Atmos. Chem. Phys., 9*, 5155-5236. doi:10.5194/acp-9-5155-2009

[4] Y. Xu, J. Zhang (2011) Understanding SVOCs, *ASHRAE Journal* 53(12),121-125

[5] `http://www.cesar-observatory.nl/` accessed June, 2017

[6] A. Hansel, A. Jordan, R. Holzinger, P. Prazeller W. Vogel, W. Lindinger (1995) Proton transfer reaction mass spectrometry: on-line trace gas analysis at ppb level, *Int. J. of Mass Spectrom. and Ion Proc.*, 149/150, 609-619.

[7] A. Jordan, S. Haidacher, G. Hanel, E. Hartungen, L. Märk, H. Seehauser, R. Schottkowsky, P. S ulzer, T.D. Märk (2009) A high resolution and high sensitivity proton-transfer-reaction time-of-flight mass spectrometer (PTR-TOF-MS), *International Journal of Mass Spectrometry, 286*, 122-128, http://doi.org/10.1016/j.ijms.2009.07.005.

[8] scipy.stats.linregress page of Scipy.org Reference Guide sponsered by *Enthought* `https://docs.scipy.org/doc/scipy-0.19.0/reference/generated/scipy.stats.linregress.html`. accessed June, 2017.

[9] R. Holzinger (2015) PTRwid: A new widget tool for processing PTR-TOF-MS data. *Atmos. Meas. Tech., 8,* 3903–3922. doi:10.5194/amt-8-3903-2015

[10] scipy.integrate page of Scipy.org Reference Guide sponsered by *Enthought* `https://scipy.github.io/devdocs/tutorial/integrate.html`. accessed June, 2017.

[11] R. Holzinger, S. Dusanter , S. Sauvag, and T. Wright (2016) Development of a measurement standard and a data submission protocol for organics based on PTR-MS.

[12] D. Materić, M. Lanza, P. Sulzer, J. Herbig, D. Bruhn, V. Gauci, N. Mason, C. Turner (2017, article in press) Selective reagent ion-time of flight-mass spectrometry study of six common monoterpenes, *International Journal of Mass Spectrometry,* -(-).

[13] A. M. Grannas, W. C. Hockaday, P. G. Hatcher, L. G. Thompson, and E. Mosley-Thompson (2006) New revelations on the nature of organic matter in ice cores. Journal of Geophysical Research 111, doi:10.1029/2005JD006251

[14] The Danish Ministry of Environment (2014) *Siloxanes (D3, D4, D5, D6, HMDS)* Evaluation of health hazards and proposal of a health-based quality criterion for ambient air. Environmental Project No. 1531.

[15] R. Mortimer (2000) *Physical Chemistry.* Elsevier Inc. ISBN: 978-0-12-508345-4

[16] stats.ttest_ind page of Scipy.org Reference Guide sponsered by *Enthought* `https://docs.scipy.org/doc/scipy-0.14.0/reference/generated/scipy.stats.ttest_ind.html`. accessed June, 2017.

[17] M. Hallquist, J. C. Wenger, U. Baltensperger, Y. Rudich, D. Simpson, M. Claeys, J. Dommen, N. M. Donahue, C. George, A. H. Goldstein, J. F. Hamilton12, H. Herrmann, T. Hoffmann, Y. Iinuma, M. Jang, M. E. Jenkin16, J. L. Jimenez17, A. Kiendler-Scharr, W. Maenhaut, G. McFiggans, Th. F. Mentel, A. Monod, A. S. H. Prevot, J. H. Seinfeld22, J. D. Surratt23, R. Szmigielski, and J. Wildt (2009) The formation, properties and impact of secondary organic aerosol: current and emerging issues. *Atmos. Chem. Phys., 9,* 5155–5236

[18] J. F. Pankow and W. E. Asher (2008) SIMPOL.1: a simple group contribution method for predicting vapor pressures and enthalpies of vaporization of multifunctional organic compounds. *Atmos. Chem. Phys., 8,* 2773–2796.

[19] R. Holzinger, A. Khan1, A.Klinger and J. Herbig (2016) Semivolatile organic compounds measured by thermal desorption denuder sampling. *Applications in Environmental Science*

[20] W. Lindinger, A. Hansel (1996) Analysis of Trace Gases at ppb Levels by Proton-Transfer-Reaction Mass Spectrometry (PTR-MS), *Plasma Sources Science and Technology, 6*(2).